Received: 2 May 2022 | Revised: 6 June 2022 | Accepted: 28 June 2022

DOI: 10.1002/inf2.12357

REVIEW ARTICLE

WILEY

Recent progress on the long-term stability of hydrogen evolution reaction electrocatalysts

Wenfang Zhai[1,2] | **Yuanyuan Ma**[1] | **Dong Chen**[3,4] | **Johnny C. Ho**[3,4] | **Zhengfei Dai**[2] | **Yongquan Qu**[1]

[1]Key Laboratory of Special Functional and Smart Polymer Materials of Ministry of Industry and Information Technology, School of Chemistry and Chemical Engineering, Northwestern Polytechnical University, Xi'an, China

[2]State Key Laboratory for Mechanical Behavior of Materials, Xi'an Jiaotong University, Xi'an, China

[3]Department of Materials Science and Engineering, City University of Hong Kong, Hong Kong, China

[4]Shenzhen Research Institute, City University of Hong Kong, Shenzhen, China

Correspondence

Johnny C. Ho, Department of Materials Science and Engineering, City University of Hong Kong, 83 Tat Chee Avenue, Hong Kong, China.
Email: johnnyho@cityu.edu.hk

Zhengfei Dai, State Key Laboratory for Mechanical Behavior of Materials, Xi'an Jiaotong University, Xi'an 710049, China.
Email: sensdai@mail.xjtu.edu.cn

Yongquan Qu, Key Laboratory of Special Functional and Smart Polymer Materials of Ministry of Industry and Information Technology, School of Chemistry and Chemical Engineering, Northwestern Polytechnical University, Xi'an 710072, China.
Email: yongquan@nwpu.edu.cn

Funding information

National Natural Science Foundation of China, Grant/Award Number: 21872109; Fundamental Research Funds for the Central Universities, Grant/Award Numbers: D5000210829, D5000210601; Environment and Conservation Fund of Hong Kong SAR, China, Grant/Award Number: ECF 2020-13

Abstract

Developing new methodologies to produce clean and renewable energy resources is pivotal for carbon-neutral initiatives. Hydrogen (H_2) is considered as an ideal energy resource due to its nontoxic, pollution-free, high utilization rate, and high calorific combustion value. Electrolysis of water driven by the electricity generated from renewable and clean energy sources (e.g., solar energy, wind energy) to produce hydrogen attracts great efforts for hydrogen production with high purity. Recently, the breakthrough of the catalyst activity limit for the hydrogen evolution reaction (HER) catalysts has received extensive attention. Comparatively, fewer reviews have focused on the long-term stability of HER catalysts, which is indeed decisive for large-scale electrolytic industrialization. Therefore, a systematic summary concentrated on the durability of HER electrocatalysts would provide a fundamental understanding of the electrocatalytic performance for practical applications and offer new opportunities for the rational design of the highly performed HER electrocatalysts. This review summarizes the research progress toward the HER stability of precious metals, transition metals, and metal-free electrocatalysts in the past few years. It discusses the challenges in the stability of HER electrocatalysts and the future perspectives. We anticipate that it would provide a valuable basis for designing robust HER electrocatalysts.

KEYWORDS

electrocatalysis, heterogeneous catalysts, hydrogen evolution reaction, stability, water splitting

Wenfang Zhai and Yuanyuan Ma authors contributed equally to this work.

This is an open access article under the terms of the Creative Commons Attribution License, which permits use, distribution and reproduction in any medium, provided the original work is properly cited.
© 2022 The Authors. *InfoMat* published by UESTC and John Wiley & Sons Australia, Ltd.

1 | INTRODUCTION

The gradual depletion of fossil fuels and the accompanying environmental and climate problems have stimulated the development and usage of clean and renewable energy resources.[1,2] Among various clean energy carriers, hydrogen (H_2), with a high energy density, has been recognized as one of the promising energy resources for a sustainable society.[3] Generally, there are three approaches for industrial hydrogen production: methane steam reforming, coal gasification, and water electrolysis. Methane reforming and coal gasification are the main methods to produce hydrogen in China, accounting for more than 95% of the total hydrogen. However, it is not only heavily dependent on fossil fuels, but also makes a large amount of carbon dioxide and carbon monoxide by-products, thus aggravating environmental problems. Residual CO in hydrogen is also toxic for a majority of downstream catalytic processes. Comparatively, hydrogen evolution reaction (HER) with the earth-abundant water as the raw material is thus the most promising methodology for hydrogen production, which has many advantages, including environmental friendliness, high purity of hydrogen production, and low carbon emissions.[4] Besides, it can be easily combined with other renewable energy systems such as hydropower, photovoltaic energy, wind energy, tidal energy, and so on, which are greatly limited by climate and seasonal height changes and the alternation of day and night. Integrating HER and the intermittent electricity generated from those renewable energy resources represents a promising future for energy storage of renewable energies in the form of chemical energy.[5,6] Thus, many efforts have been devoted to developing highly performed water electrolysis and satisfying the demands for carbon-neutral initiatives.[7–10]

Generally, excellent HER activity will occur on the dedicatedly designed electrocatalysts. Since the electrocatalysts go through extra voltage to overcome the energy barrier for HER, it is crucial to develop novel electrocatalysts with small overpotentials to reduce energy consumption and improve energy conversion efficiency.[11,12] Besides, low production cost, high chemical, and electrochemical stability, and supports for large-scale electrode fabrication are also significant for an excellent electrocatalyst.[13] At present, the best state-of-the-art electrocatalysts for HER are Pt-based metals, which have the optimal adsorption of hydrogen that benefits both the adsorption of active hydrogen species and the desorption of hydrogen molecules.[3,14–16] However, precious-metal-based catalysts suffer from high cost and low catalytic stability in highly acidic and alkaline electrolytes. Recently, many cost-effective electrocatalysts based on cheap transition metals and metal-free electrocatalysts as the alternatives have been rationally designed and synthesized with a high catalytic activity for HER, which are comparable to or even better than the Pt-based HER electrocatalysts. Those investigations have been well summarized and illustrated in many previous review articles.[17–22]

In comparison with the intensive investigations on the activity of HER electrocatalysts, another important criterion for practical applications, catalytic durability, is proverbially known as the critical parameter of HER electrocatalysts to determine whether it can be commercialized, but much less research has been done in this area. Many factors can significantly limit the catalytic durability of HER electrocatalysts, including the leaching due to the poor chemical/electrochemical stability of the electroactive components under operation, the aggregation of electrocatalysts, poor mechanical stability, and so on.[23–26] Therefore, the summary of recent progress on the stability of HER electrocatalysts lays a foundation for the subsequent design of high-activity and high-stability catalysts that are more in line with the industrial needs.

Here, we highlight the recent advances in the robust heterogeneous electrocatalysts for HER in various electrolytes. Generally, heterogeneous HER catalysts are classified into three categories (Figure 1): noble metal-based (NMB), transition metal-based (TMB), and metal-free catalysts (MFC).[27–50] This review addresses the current progress of catalytic stability of the heterogeneous HER electrocatalysts. Remarkably, it discusses the understanding of the deactivation mechanisms and the illustration of the existing strategies to improve the durability of those three types of HER electrocatalysts. Finally, the challenges and perspectives for developing robust HER electrocatalysts under various catalytic environments are discussed and proposed.

2 | THE MECHANISM OF HER

HER is a half-reaction of overall water splitting, a multistep process occurring on the surface of the electrode. A catalytic intermediate in the reaction process is H* (where * represents the active site).[51] As shown in Figure 2A, under acidic solution, the source of protons is H_3O^+, which combines with an electron at the active site to form chemisorbed protons in the Volmer step (Equation 1). The adsorbed H* can be converted to H_2 in two ways: one is the Heyrovsky step, in which H_2 is formed by binding electron, H*, and H_3O^+ (Equation 2), and another is the Tafel step, in which two adjacent

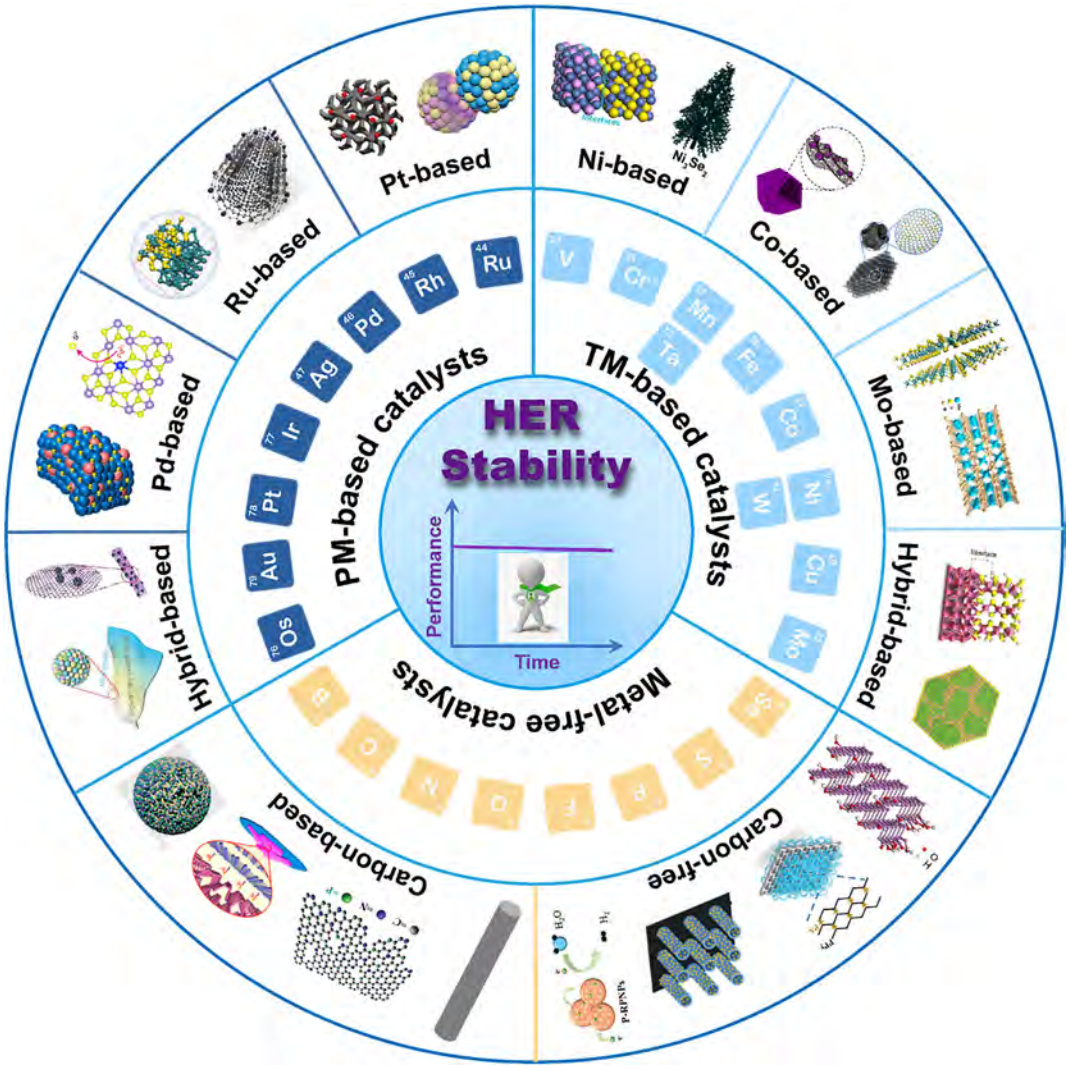

FIGURE 1 Recent advances in the stability of PM-based, TM-based and Metal-free HER catalysts. Reproduced with permission.[27] Copyright 2021, Wiley-VCH. Reproduced with permission.[28] Copyright 2019, Wiley-VCH. Reproduced with permission.[29] Copyright 2020, Springer Nature. Reproduced with permission.[30] Copyright 2021, Wiley-VCH. Reproduced with permission.[31] Copyright 2018, Springer Nature. Reproduced with permission.[32] Copyright 2022, American Chemical Society. Reproduced with permission.[33] Copyright 2022, Elsevier. Reproduced with permission.[34] Copyright 2021, Wiley-VCH. Reproduced with permission.[35] Copyright 2017, The Royal Society of Chemistry. Reproduced with permission.[36] Copyright 2019, American Chemical Society. Reproduced with permission.[37] Copyright 2015, The Royal Society of Chemistry. Reproduced with permission.[38] Copyright 2018, Springer Nature. Reproduced with permission.[39] Copyright 2020, The Royal Society of Chemistry. Reproduced with permission.[40] Copyright 2017, Wiley-VCH. Reproduced with permission.[41] Copyright 2019, Wiley-VCH. Reproduced with permission.[42] Copyright 2017, Wiley-VCH. Reproduced with permission.[43] Copyright 2018, Wiley-VCH. Reproduced with permission.[44] Copyright 2021, Springer Nature. Reproduced with permission.[45] Copyright 2017, American Chemical Society. Reproduced with permission.[46] Copyright 2016, Wiley-VCH. Reproduced with permission.[47] Copyright 2018, National Academy of Sciences. Reproduced with permission.[48] Copyright 2019, Elsevier. Reproduced with permission.[49] Copyright 2016, Elsevier. Reproduced with permission from Reference.[50] Copyright 2018, Elsevier

H* are directly combined to form H_2 (Equation 3).[12] The research of the HER process in acid solution has been systematically studied. The Tafel slope obtained from the linear sweep voltammetry (LSV) polarization curve is usually used to distinguish which HER mechanism is mainly carried out. According to the slope of the Tafel curve, the reaction mechanism can be divided into Volmer–Heyrovsky or Volmer–Tafel mechanisms according to the Butler–Volmer formula (Equations 4–6).[2]

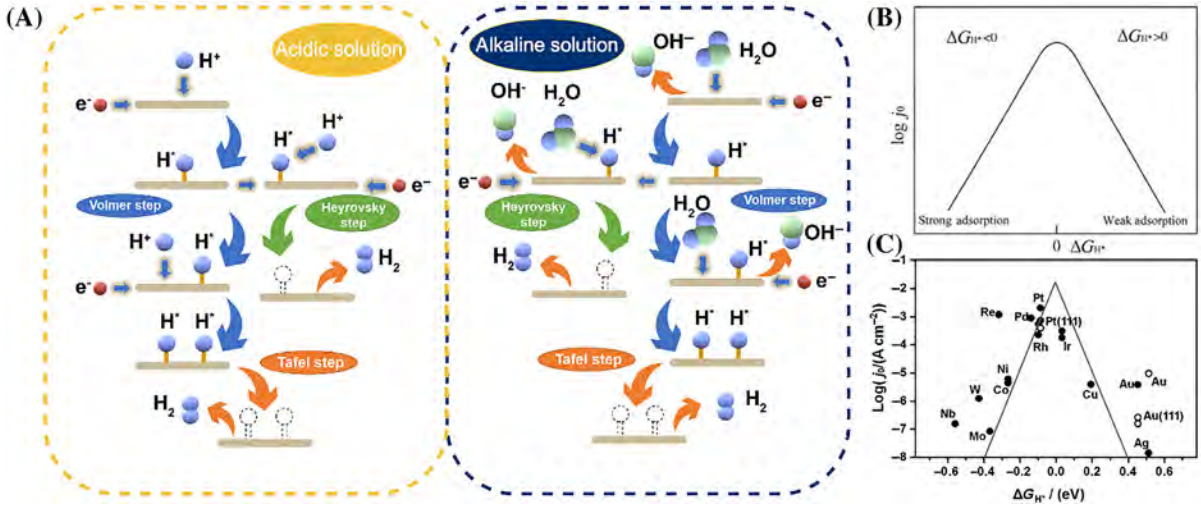

FIGURE 2 (A) Chemical processes in HER under acidic and alkaline conditions. (B) Relationship between the exchange current density (j_0) and hydrogen adsorption free energy under the assumption of the Langmuir adsorption model. Reproduced with permission.[52] Copyright 1958, Royal Society of Chemistry. (C) Volcano plot of the relationship between the exchange current density (j_0) and the free energy of hydrogen adsorption (ΔG_{H^*}) for the surfaces of various metals. Reproduced with permission.[53] Copyright 2005, IOP Publishing

Volmer step:

$$* + H_3O^+ + e^- \rightarrow H^* \quad (1)$$

Heyrovsky step:

$$* + H_3O^+ + e^- + H^* \rightarrow H_2 + 2^* \quad (2)$$

Tafel step:

$$2H^* \rightarrow H_2 + 2^* \quad (3)$$

Butler–Volmer formula:

$$b_V = \frac{2.303RT}{\alpha F} \quad (4)$$

$$b_H = \frac{2.303RT}{(1+\alpha)F} \quad (5)$$

$$b_T = \frac{2.303RT}{2F} \quad (6)$$

In the equations, b represents the Tafel slope, V, H, and T represent the Volmer, Heyrovsky, and Tafel reactions, respectively.[54] And α represents the electron transfer coefficient (0.5), R represents the ideal gas constant (8.314 J mol^{-1} K^{-1}), T stands for absolute temperature, F table Faraday constant (96 487 C mol^{-1}). At 25°C, the Tafel slopes of the three reactions are $b_V \approx 120$ mV dec^{-1}, $b_H \approx 40$ mV dec^{-1}, and $b_T \approx 30$ mV dec^{-1}, respectively.[8]

The HER process in alkaline and neutral media is quite different from acidic media (Figure 2A). In general, the activity in alkaline and neutral systems is 2–3 orders of magnitude lower than that in acidic systems.[14] And the catalytic activity in acidic media is not sensitive to the surface structure of the catalyst, which is in the opposite situation in alkaline and neutral conditions. In the case of alkaline and neutral strips, the activity cannot be judged entirely by the hydrogen adsorption free energy of the volcanic curve.[55] The equations of HER under alkaline and neutral conditions are as follows. The protons in the reaction come from H_2O molecules, and the Volmer step needs to break the H—O—H bond to form OH^- and H* (Equation 7). Therefore, such HER activity depends on the speed of water dissociation. If the water dissociates slowly, the Heyrovsky reaction occurs (Equation 8). But, if the water dissociates quickly, it provides many H*, and the Tafel reaction occurs (Equation 9).[51]

Volmer step:

$$* + H_2O + e^- \rightarrow H^* + OH^- \quad (7)$$

Heyrovsky step:

$$* + H_2O + e^- + H^* \rightarrow H_2 + OH^- + 2^* \quad (8)$$

Tafel step:

$$2H^* \rightarrow H_2 + 2^* \quad (9)$$

According to the Sabatier principle, the adsorption energy of the intermediate adsorbed species at the active site (ΔG_{H^*}) determines the reaction rate. Under proper coverage, the ΔG_{H^*} of various catalysts and the current density maps measured by experiments are calculated by Density Functional Theory (DFT), showing a "volcanic relationship" (Figure 2B,C).[52,53] If the adsorption is too weak ($\Delta G_{H^*} > 0$), the intermediate is not easy to form; the adsorption (Volmer) step will limit the whole reaction rate. If the adsorption is too strong ($\Delta G_{H^*} < 0$), it will lead to the poisoning of the active site, and the desorption (Heyrovsky/Tafel) step will limit the reaction rate. Only the ΔG_{H^*} closer to 0, the better the reaction activity.[56] Since the metal Pt is at the peak of the volcanic curve, it is the best single metal catalyst. For HER in acid solution, ΔG_{H^*} can be directly used as a descriptor of surface catalytic activity. By calculating ΔG_{H^*}, the source of catalytic activity can be explained; simultaneously, the possible catalytic activity of the new catalyst and the activity trend of similar catalysts can be predicted, which guides the design for a better catalyst. Nowadays, the reported actual activity of the catalyst is much lower than the theoretical calculation results. Therefore, preparing the catalyst, which ΔG_H* is close to 0, is essential to improve the reaction activity through reasonable structural design.[57]

Based on the above reaction formula and Sabatier principle, the key to improving the activity and stability of HER is that the catalyst should have excellent water dissociation performance, suitable ΔG_{H^*}, and faster H_2 desorption. Such properties can release the active site as soon as possible without destroying the active site, thereby improving the catalyst's lifetime. Recently, many investigations have combined experiments with DFT theoretical calculations to investigate highly stable HER catalysts with moderate hydrogen adsorption energy and rapid hydrogen desorption.[58–60] However, in alkaline and neutral electrolytes, the HER process requires water electrolysis, making the design of catalysts more complex. By taking into account their ability to adsorb and dissociate from water, the development of the stability of catalysts is hampered.

3 | EVALUATION CRITERIA FOR HER STABILITY AND DEACTIVATION TYPES

Stability or durability, that is, the ability of the catalyst to maintain the initial catalytic activity for a long time, is an important parameter to evaluate whether the catalyst is suitable for industrialized applications. A series of comprehensive factors determine the stability of the HER process, and the apparent stability of the test cannot fully reflect the essential stability of the material. The stability of the electrolytic device performance depends not only on the stability of the catalyst itself. Because the preparation of the water-splitting electrode is to disperse the catalyst on the fluid surface, and the water electrolysis process needs to be carried out in the electrolyte, the adhesion, and dispersion of the catalyst on the collector, the mechanical strength and pore structure of the collector itself, and so on are all critical factors that affect stability. The electrolysis solution's cleanliness, temperature, concentration, and other external factors all determine the stability of the whole electrolysis equipment. Therefore, to effectively eliminate the influence of controllable external factors, such as electrolytes and fluid collectors, the stability of the catalyst is mainly caused by the intrinsic stability, which helps us to analyze the cause of catalyst deactivation fundamentally to improve the stability. The two common stability testing methods are cyclic voltammetry (CV) and chronopotentiometry (CP; current-time curve) or chronoamperometry (CA; potential-time curve). Since the catalysts used commercially need work for long-time stability at the same voltage or current density, the CA and CP curves are mainly referred to in the following details of the HER catalyst stability progress.[1,61,62] Meanwhile, new methodologies are now emerging to assess the stability of catalysts, such as flow cell–inductively coupled plasma–mass spectrometry (FC–ICP–MS)[63] and differential electrochemical mass spectrometry (DEMS).[64] These methods allow for the precise detection of catalyst dissolution during the reaction process, which provides deep insights into the factors influencing stability and provides novel strategies for the design of advanced catalysts with longevity.

Two representative model catalysts have been simulated to demonstrate the importance of stability in practical applications. As shown in Figure 3, Catalyst A starts with higher HER activity (100 mV overpotential) but degrades faster (0.5 mV h^{-1}), while Catalyst B is less active (150 mV) but remains more stable (0.1 mV h^{-1}). When a 500 Wh battery powers Catalyst A and Catalyst B, B can continue to operate for 2000 h, but A can only run for 1228 h. As a result, although Catalyst B presents a much lower initial HER activity than Catalyst A, it saves 44% of the energy cost caused by HER overpotentials after 1228 h continuous operation. It will save even more with a longer operation time. This example indicates that the long-term stability of HER catalysts bears even more weight than consideration of their activity in practical industrial applications. However, in current HER studies, the focus is mostly on activity only, with little mention of the extraordinary importance of stability.

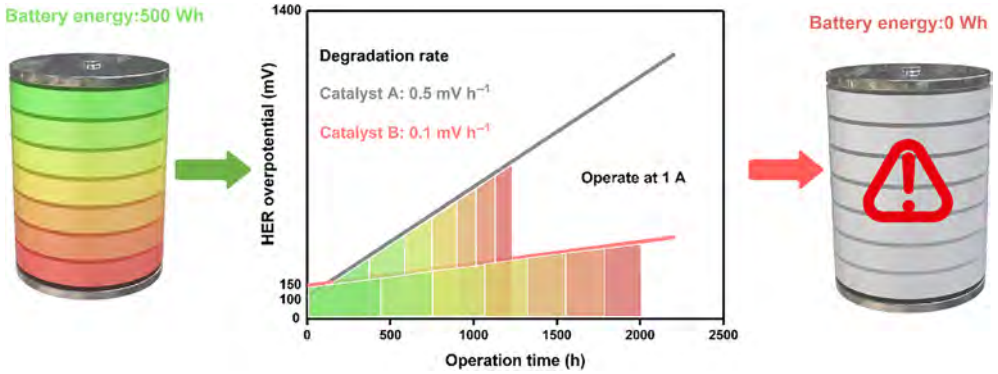

FIGURE 3 Proposed schematic stability test of Catalyst A (overpotential of 100 mV and degradation rate of 0.5 mV h^{-1}) and Catalyst B (overpotential of 150 mV and degradation rate of 0.1 mV h^{-1}) at a current of 1 A. Battery energy of 500 Wh allows Catalyst B to operate continuously for 2000 h but only allows Catalyst A to operate for 1228 h

3.1 | Cyclic voltammetry

CV accelerates the degradation of electrocatalysts at a wide voltage window (the voltage range of LSV) and a higher scanning rate (such as 50 or 100 mV s^{-1}). Generally, the difference of the LSV curve before and after CV is used to evaluate the stability, and the number of CV cycles is typically 1000–10 000 cycles. If the LSV polarization curves almost exactly overlay with the initial one or the overpotential slightly increases by less than 10% compared with the original values, it suggests good endurance.[65]

3.2 | Chronoamperometry or chronopotentiometry

The CA or CP method tests the stability over a long period at a constant current density or voltage. In research, CA is more commonly used than CP. In CA, the current density changes with time, which is carried out at a potential corresponding to a current density of 10 mA cm^{-2}. The more stable the current density is, the better the stability of the catalyst is. To get closer to industrialization, some researchers have also tested the stability of catalysts under the potential corresponding to more significant current density (such as 20, 30, 50, 100, 300 mA cm^{-2}). CP is generally used to measure the change of overpotential by 10 mA cm^{-2} at a constant current density. If the overpotential increases weakly, it means that the catalyst is stable. The stability test should be carried out for the catalysts with high activity and strong redox peaks at higher current densities (50 or 100 mA cm^{-2}).[66]

3.3 | Deactivation types

The stability of a catalyst is intimately linked to its active site. And the inactivation of the active site can reduce the reaction rate, affecting the longevity of the overall catalyst. Therefore, it is crucial to design long-lasting catalysts based on the type of catalyst deactivation.[16] Here, we illustrate the type of catalyst deactivation based on two model catalysts (Figure 4). Model A is typical of metal particles loaded on carbon support with five main types of deactivations: carbon corrosion; dissolution of the metal atoms; Osterwald ripening; agglomeration; and particle detachment. Model B is a typical carrier-free catalyst with three main types of deactivation: demetallation; active site poisoning; and local corrosion. In these cases, improving the corrosion resistance of the catalyst and fixing the metal location are strategies to address the poor stability of the catalyst. Therefore, strategies such as strong metal-support interactions and metal alloying are suitable methods to improve catalyst duration.

4 | RECENT PROGRESS

As shown in the volcano curve in Figure 2C, precious metals are considered commercial catalysts due to their excellent HER performance ($\Delta G_{H^*} \approx 0$).[2] However, improving the stability of precious-metal-based catalysts through different strategies has become a research hotspot owing to their poor stability. Meantime, to reduce the cost, the stability research of transition metal (TM) and metal-free electrocatalysts has also become a hot topic. These researches provide experience for the design of high activity, low cost, and high stability HER catalysts.

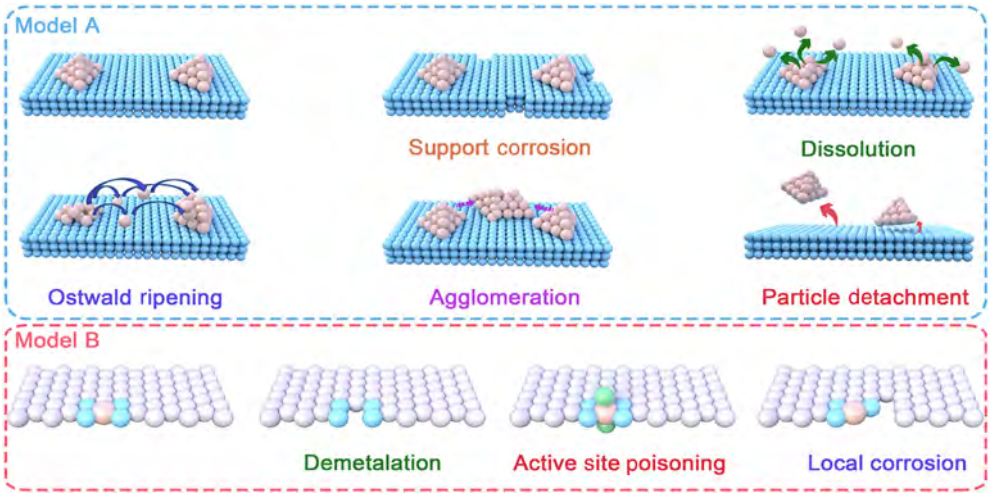

FIGURE 4 Degradation mechanisms of hydrogen evolution reaction (HER) catalysts

4.1 | Precious metal-based hydrogen evolution catalysts

Precious metal catalysts mainly include Pt, Ru, Pd, Rh, and Ir, which generally deliver excellent HER activity but unsatisfied stability for the demands of industrialization. The main reasons for their poor stability are the agglomeration, the leaching of active precious metals, and the corrosion of the supports (such as carbon support) in strongly acidic and basic environments.[67] Moreover, due to the scarcity of precious metal resources and high preparation technology costs, the long-term development goal is to effectively improve the utilization efficiency of precious metal atoms, reduce metal load and stabilize metal sites to ensure high activity and stability. Investigations with the target toward improvements on the catalytic stability of those precious metals for hydrogen evolution have been reported through the alloying with other metals,[68] spacing confinements,[69] metal-support interaction through anchoring, fixing precious metals on functional supports,[70] and the local regulations of coordination environment.[71]

4.1.1 | Platinum-based

Table 1 summarizes recent advances in the durability of Pt-based catalysts for HER. Platinum has an outstanding HER activity because it has the most suitable free energy of hydrogen adsorption, close to zero. But to enhance the stability of Pt-based catalysts for HER is a big challenge. Pt tends to leach, agglomerate, detach, or separate from the support when tested for stability. Thus, searching for suitable supports is one of the strategies to immobilize Pt-based catalysts.[19] Carbon-based supports are primarily used because of their low cost, good conductivity, and chemical stability, including carbon nanotubes, graphene, hollow carbon spheres, or derivatives. Numerous studies have focused on adjusting the coordination environment and electronic structure of platinum by compounding it with nitrogen-doped porous carbon,[84] nitrogen-doped graphene nanosheets,[87] carbon nanotubes containing different nitrogen types,[83] hollow carbon nanospheres,[85] and other carbon-based materials. For example, it is well known that the corners and edges of catalysts tend to be more active; inspired by this, Song et al. dispersed Pt single atoms (SAs) in onion-like carbon (OLC) supports (Pt_1/OLC) with highly curved curvature (Figure 5A,B).[70] Compared to Pt_1/graphene, Pt_1/OLC has better activity in an acidic electrolyte (0.5 M H_2SO_4) and it maintains a constant overpotential of $\eta = 40$ mV for 100 h without degradation. (Figure 5C). The outstanding stability originates from the strong interaction between the Pt SA and the OLC support. Furthermore, simulations and calculations illustrate that the high curvature structure enriches the Pt region with electrons, generating a local electric field, which joins the kinetics of the reaction and the detachment of hydrogen bubbles.

The reduction of Pt cations on chemically inert carbon supports in most Pt/carbon catalysts requires additional reducing agents or complex post-treatment processes.[88] Therefore, identifying suitable non-carbon support is a challenge. Recently, MXenes have emerged as a new family of two-dimensional (2D) materials with high electrical conductivity, hydrophilicity, and reducibility. $Ti_3C_2T_x$ MXene with a low work function has been demonstrated using first-principles calculations and experimental results to consistently reduce precious metal cations into immobilized metal nanoparticles (NPs) without the addition of any reducing agents or

TABLE 1 Summary of hydrogen evolution reaction (HER) durability with Pt-based catalysts under different reaction conditions

Catalyst	Electrolyte	η_{10} (mV) or mA cm^{-2}@mV	Stability			References
			CA/Retention (mV@h@%)	CP/Retention (mA cm^{-2}@h@%)	CV/(cycles) (cycles@%)	
MXene@Pt/SWCNTs	0.5 M H_2SO_4	62	-	10@800@-	-	[72]
Pt_1/OLC	0.5 M H_2SO_4	38	40@100@-	-	6000	[70]
EG-Pt/CoP-1.5.	0.5 M H_2SO_4	21	100@100@-	-	-	[73]
Pt SASs/AG	0.5 M H_2SO_4	12	-	10@24@-	2000	[74]
PtSA-NT-NF	1 M PBS	24	-	100@24@-	-	[75]
Ni_3N/Pt	1 M KOH	50@83	50@24@82.5%	-	-	[76]
Pt_4/Co	0.5 M H_2SO_4	6.9	-	50@24@-	-	[77]
Dr-Pt	1 M KOH	26	-	10@20@-	2000	[78]
PtNi-O/C	1 M KOH	39.8	-	10@10@-	-	[79]
Pt@PCM	0.5 MH_2SO_4/1 M KOH	105/139	150@5@ > 95%/ 150@5@ > 95%	-	-	[80]
SA In-Pt NWs	1 M KOH	46	46@5@-	-	2000	[81]
Pt@CS/CNF	0.5 M H_2SO_4	33	100@10@92.3%	-	10 000	[82]
Pt-HNCNT	0.5 M H_2SO_4	15	-	-	5000@88%	[83]
Pt@NHPCP	0.1 M $HClO_4$	57	-	-	5000@-	[84]
Pt_5/HMCS	0.5 M H_2SO_4/1 M KOH	20.7/46.2	-	-	3000@-/3000@-	[85]
PtCo@PtSn	0.5 M H_2SO_4/1 M KOH/1 M PBS	21/25/18	-	-	100 000@-/ 100 000@-/ 100 000@-	[27]
Pt_1/α-MoC_{1-x}@C-0.75	0.5 M H_2SO_4/1 M KOH/1 M PBS	12/21/36		50@20@-/ 50@20@-/ 50@20@-	-2000@-/2000@-/ 2000@-	[86]

post-treatment. Highly stable electrocatalysts for HER were obtained by using $Ti_3C_2T_x$ MXene (M) as conductive support and reducing agent and single-walled carbon nanotubes (SWCNTs) as conductive binder with a platinum loading of 1% (S–M–1Pt) and 5% (S–M–5Pt) of the mass of M (Figure 5D,E).[72] The S–M–5Pt can operate at a current density of 10 mA cm^{-2} for over 800 h with only a minor decrease (Figure 5F). The hydrophilicity of M and its immobilization of Pt substantially contribute to the stability of S–M–5Pt. Our group loaded Pt NPs onto CoP nanosheets and modified them with ethylene glycol (EG).[73] EG can enrich the local proton concentrations around Pt and subsequent interfacial hydrogen overflow to break the HER catalytic kinetic limitation of CoP. Sample with 1.5 wt% Pt loading (EG-Pt/CoP-1.5) is stable at 100 mV overpotential for 100 h without attenuation (Figure 5G). The permanent stability is attributed to (i) the stronger adsorption at the Pt site facilitates H* enrichment, (ii) the thermally neutral adsorption of H* at the Pt/CoP interface sites (sites b and c) promotes the production and desorption of H_2; (iii) the steadily weakened adsorption of H* from the site a–d supports that the channel through which hydrogen spillover occurs at the Pt → Pt/CoP interface → CoP (Figure 5H).

A prospective approach to go beyond Pt monometallic catalysts is to construct alloyed catalysts of Pt with other metals, as alloying can modulate the d-band center of Pt and affect its ΔG_{H^*}. Yin et al. have constructed Pt-based bimetallic alloys and heterojunction (PtCo@PtSn) by a three-step heat-treatment-hydrothermal-heat treatment process to enhance the stability for pH-universal H_2 evolution.[27] DFT theoretical calculations show that PtCo@PtSn heterojunction presents the lowest ΔG_{H^*} and water dissociation energy (0.03/0.49 eV) compared to PtCo (−0.174/0.61 eV) and PtSn (0.398/0.65 eV), indicating the faster hydrogen adsorption and desorption, as well as timely hydrogen replenishment (Figure 5I). The introduction of Sn and Co elements modulates the

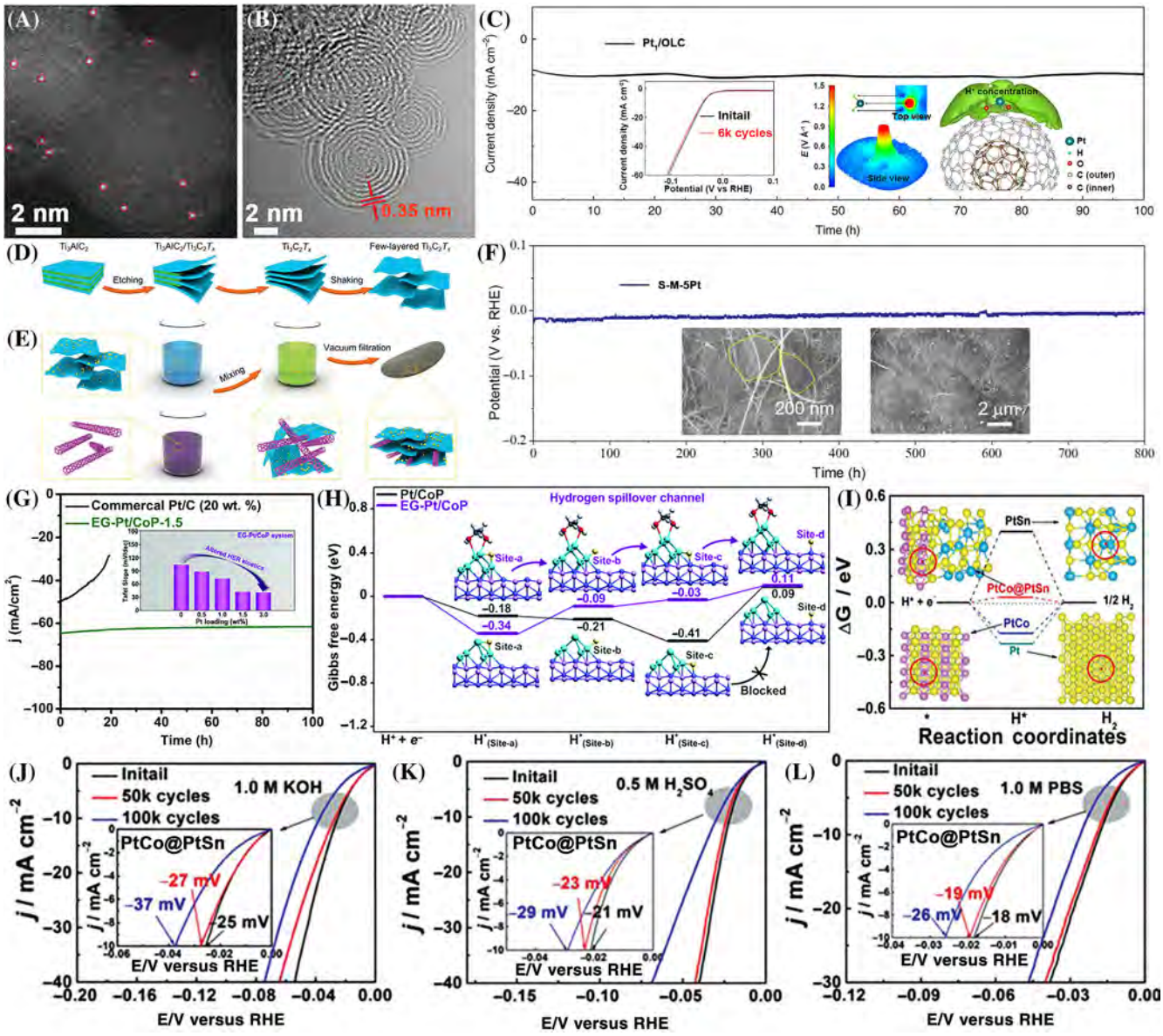

FIGURE 5 The morphological characterization and stability test of Pt_1/OLD. (A) The HAADF-STEM image (the Pt single atoms highlighted by red circles). (B) TEM image shows a multishell fullerene structure. (C) The chronoamperometry test at the overpotential of $\eta = 40$ mV in 0.5 M H_2SO_4. The insets from left to right show the 6000 cycles of the CV acceleration test, the electric field diagram and the Gouy–Chapman–Stern model of Pt_1/OLD. Reproduced with permission.[70] Copyright 2019, Springer Nature. Schematic of (D) fabrication of $Ti_3C_2T_x$ MXene suspension and (E) preparation of MXene@Pt/SWCNTs electrocatalysts. (F) The 800 h of continuous testing of S-M-5Pt at 10 mA cm^{-2}. Insets are the high-resolution and low-resolution SEM images of S-M-5Pt. Reproduced with permission.[72] Copyright 2020, Wiley-VCH. The DFT calculations and electrochemical properties of EG-Pt/CoP. (G) The HER durability test under $\eta = 100$ mV in 0.5 M H_2SO_4. Inset is Tafel slopes of EG-Pt/CoP at each Pt loading. (H) Free energy diagram for hydrogen spillover. Reproduced with permission.[73] Copyright 2019, The Royal Society of Chemistry. (I) ΔG_{H^*} calculated at adsorbing sites for PtCo@PtSn catalyst. CV stability curves of PtCo@PtSn. (J) 1 M KOH. (K) 0.5 M H_2SO_4. (L) 1 M PBS. Reproduced with permission.[27] Copyright 2021, Wiley-VCH

electronic structure of Pt, and the strong electronically interacting heterojunction prevents catalyst aggregation and facilitates charge transfer. With the above advantages, PtCo@PtSn has negligible performance degradation after 100 k cycles of CV-accelerated durability test in 1 M KOH (shift 12 mV), 0.5 M H_2SO_4 (shift 8 mV), and 1 M PBS (shift 8 mV), respectively (Figure 5J–L).

Currently, among platinum-containing catalysts, the catalysts themselves are all highly active due to the presence of Pt, but stability is still a long way from

commercialization. The reports so far still have Pt as the main active site, and aim to reduce the amount of Pt and improve stability by some strategies, such as stabilizing the Pt element by alloying with other elements, space-limited metal atoms, clusters, or strong metal-support interactions. These strategies have been proven effective in improving stability, but to reach the industrial level, more suitable methods need to be found to obtain long-lived Pt-based HER catalysts.

4.1.2 | Ruthenium-based

Ruthenium (Ru) is considered the most promising candidate to replace Pt for the HER, which is only 1/5 the price of Pt.[22] It shows comparable even better activity than Pt and outperforms other metals for water dissociation and OH-chemisorption. Similar to Pt, most of the Ru was loaded on carbon-based supports to study its HER activity and stability.[89] Table 2 summarizes recent advances in the durability of Ru-based catalysts for HER. Ru/C composites in extensive studies have shown superior HER activity, but the studies on stability are still in infancy.[105] The implantation of isolated single-atom Ru on edge-defect-rich carbon matrix (ECM@Ru) exhibits stronger activity and general stability (20 h at 10 mA cm^{-2}).[99] Ru NPs anchored to multi-walled carbon nanotubes (Ru@MWCNT) also exhibit general durability (20 h at 10, 15, and 20 mA cm^{-2}, respectively).[29] Ru SAs and NPs anchored on defective carbon (Ru_{SA+NP}/DC) also have

TABLE 2 Summary of hydrogen evolution reaction (HER) durability with Ru-based catalysts under different reaction conditions

			Stability			
Catalyst	**Electrolyte**	**η_{10} (mV) or mA cm^{-2}@mV**	**CA/Retention (mV@h@%)**	**CP/Retention (mA cm^{-2}@h@%)**	**CV/(cycles) (cycles@%)**	**References**
Cu/Ru@GN	0.5 M H_2SO_4/1 M KOH	10/8	10@ > 600@-/ 8@ > 24@-	-	-	[90]
RuGd-rGO	1 M KOH	12	56@500@100%	-	10 000@100%	[91]
RuCoP	0.5 M H_2SO_4/1 M KOH	11/23	-	10@150@-/ 10@150@-	-	[92]
Ru1/D-NiFe LDH	0.1 M KOH	18	18@50@- + 61@50@-	-	2000@-	[93]
P-Ru-CoNi-LDH	1 M KOH	29	32@100@-	-	-	[94]
CuPor-RuN_3	0.5 M H_2SO_4/1 M KOH/1 M PBS/	73/114/357/	-@60@-/-@60@-/-	-	-	[68]
Ru/np-MoS_2	1 M KOH	30	30@40@-	-	-	[95]
$NiRu_{0.13}$-BDC	1 M KOH/1 M PBS/1 M HCl	34/36/13	-/50@30@-/-	-	-	[96]
RuO_2/KLTO	1 M KOH	20	-	10@25@-	-	[97]
Ru SAs@PN	0.5 M H_2SO_4	24	-	160@24@-	5000@-	[98]
Ru/RuS_2-2	0.5 M H_2SO_4	45	45@24@-	-	3000@-	[30]
ECM@Ru	0.5 M H_2SO_4/1 M KOH/	63/83	-	10@20@-	-	[99]
Ru@MWCNT	0.5 M H_2SO_4/1 M KOH/	13/17	-	20 mA@20	10 000@-/ 10 000@-	[29]
Ru_{SA+NP}/DC	0.5 M H_2SO_4/1 M KOH/	16.6/18.8	-@20@-/-@20@-	-	2000@-/2000@-	[100]
RuP_2@PC	0.5 M H_2SO_4/1 M KOH/1 M PBS/	77.2/78.8/179.6	-/-@10@82%/-	-	1000@-/1000@-/ 1000@-	[101]
RuCr@C	0.5 M H_2SO_4/1 M KOH/1 M PBS/	18/19/32.6	-/19@10@-/-	-	-	[69]
RuMn NSBs-250	0.5 M H_2SO_4/1 M KOH	18/20	-	-	-	[102]
Ru@CDs	1 M KOH	30	-	-	10 000@-	[103]
R-NiRu	1 M KOH	16	30@12@-	-	5000@-	[104]

the stability of 20 h at 10 mA cm^{-2}.[100] Various Ru/C composites exhibit less durable stability, so alloying Ru with TMs is a strategy to improve their stability on carbon supports. Kim and coworkers synthesized two different types of isolated metal from Ru and Cu dispersed on N-doped graphitic-matrix (G_N) by immiscibility-driving ($Cu/Ru@G_N$).[90] Figure 6A–D shows the HRTEM images of $Cu/Ru@G_N$ and $Ru@G_N$ under continuous beam illumination, respectively, from which it can be seen that the NPs in $Cu/Ru@G_N$ do not aggregate. At the same time, the pure Ru-NPs in $Ru@G_N$ form larger Ru crystals after illumination. The Ru NPs and Cu SAs synergistically enhance conductivity and charge transfer on the G_N matrix for fast kinetics. In addition, due to the immiscibility of Cu and Ru, Cu SAs coordinated to N atoms bridged to the Ru surface, which introduces new active sites and provides long-term stability (over 600 h in 0.5 M H_2SO_4, over 2 days in 1 M KOH) by preventing the aggregation of Ru-NPs (Figure 6E,F). More importantly, to be in line with the industry, the authors kept the $Cu/Ru@G_N$ stable for 3 days (72 h) in proton exchange membrane (PEM) water-electrolysis by the CA method (Figure 6G). In addition to Ru forming immiscible alloys with Cu, Zhao et al. formed alloys of Ru with rare earth elements (Gd, Er, Yb, and La) of about 5 nm by solvent-free microwave reduction.[91] Because RuGd-rGO NPs have large exothermic energy (−1.34 eV), which facilitates the dissociation of H_2O, they can be

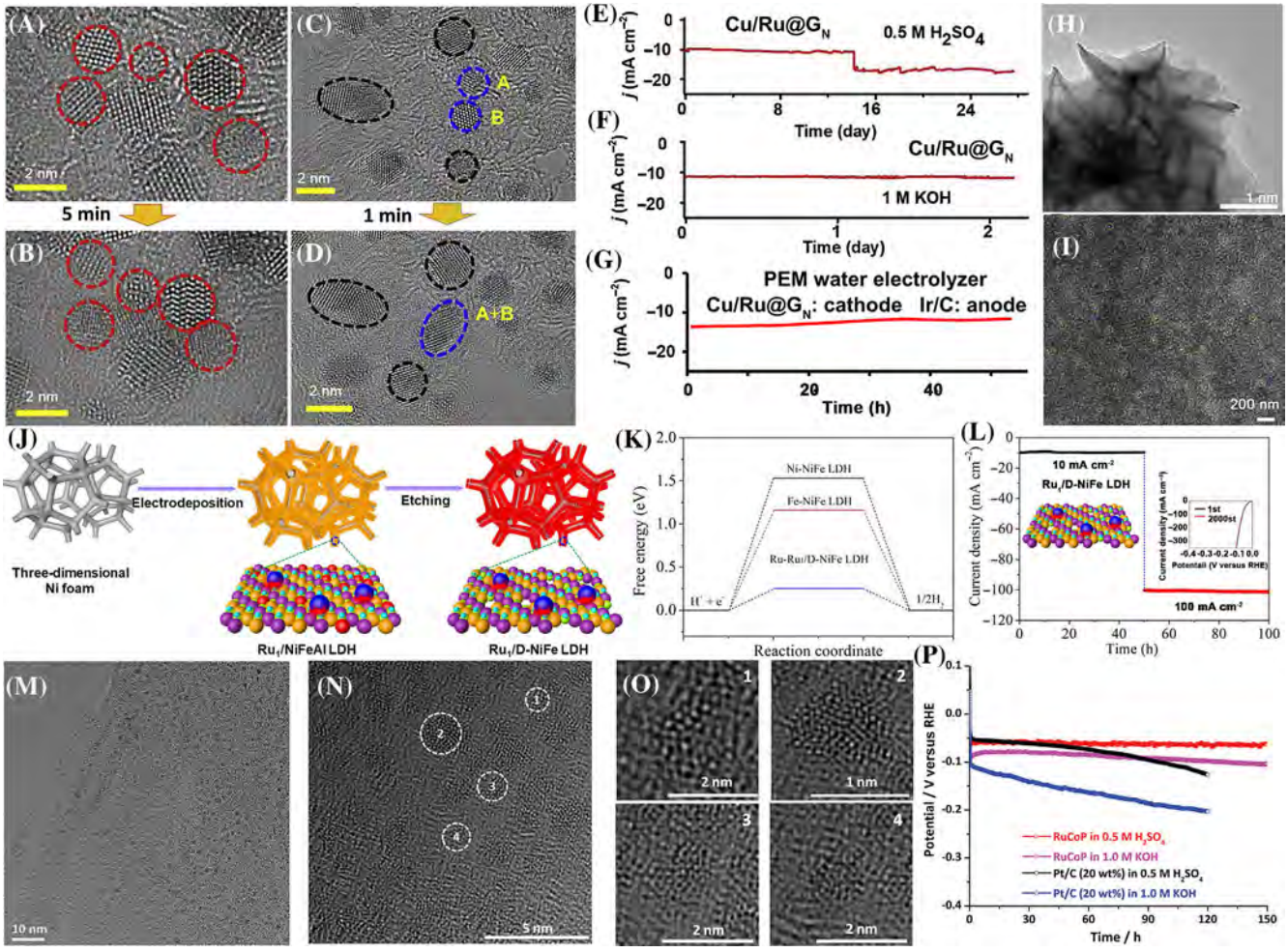

FIGURE 6 Continuous HRTEM analysis. (A-B) for $Cu/Ru@G_N$, (C-D) for $Ru@G_N$. Long-term stability test of $Cu/Ru@G_N$. (E) 0.5 M H_2SO_4. (F) 1 M KOH. (G) PEM water electrolyzer. Reproduced with permission.[90] Copyright 2020, Elsevier. Synthetic schematic and morphological characterization of Ru_1/D-NiFe LDH. (H) TEM image. (I) Aberration-corrected TEM image. (J) Synthesis illustration. (K) Free energy diagram of HER process on different active sites. (L) Time-dependent current density curves at −0.018 and −0.061 V versus RHE. Inset is LSV curves before and after 2000 cycles. Reproduced with permission.[93] Copyright 2021, Springer Nature. Structural morphology and stability analysis of RuCoP. (M) TEM. (N) HRTEM. (O) HRTEM images of individual clusters denoted in (N). (P) At 10 mA cm^{-2} in 0.5 M H_2SO_4 and 1 M KOH, respectively. Reproduced with permission.[92] Copyright 2018, The Royal Society of Chemistry

stable for 500 h without decay at high current densities under 1 M KOH.

In addition to carbon-based support materials, many efforts are trying to find other new support materials, such as MoS_2,[95] CoP,[92] perovskite oxide,[97] amorphous phosphorus nitride imide nanotubes,[98] nickel-iron layered double hydroxide (NiFe LDH),[93] and so on. As shown in Figure 6H–J, Hou et al. obtained Ru SAs stabilized NiFeAl LDH by electrodeposition on nickel foam (NF) and then removed Al by etching in alkaline solution to form the Ru SAs loaded defective NiFe LDH (Ru_1/D-NiFe LDH).[93] The defective NiFe LDH can immobilize many Ru SAs and prevent aggregation during the reaction. Based on the precise modulation of the local coordination environment of the active site and the presence of defects, Ru_1/D-NiFe LDH optimizes the favorable regulation of H adsorption energies for HER (Figure 6K). Ru_1/D-NiFe LDH is stable for 100 h under alkaline electrolyte and 50 h each at −0.018 (10 mA cm^{-2}) and −0.061 V (20 mA cm^{-2}) versus RHE, respectively (Figure 6L). After HER stability testing, the morphology and composition of Ru_1/D-NiFe LDH have little changed by SEM and element mappings characteristics. Amorphous phosphorus nitride imide nanotubes (HPN) have also been reported to be supports to anchor Ru SAs by strong coordination of the d orbitals of Ru with the lone pair of electrons of N located in the HPN.[98] However, it was only stable for 24 h at overpotentials of 70, 120, and 160 mV, respectively. Therefore, it is still essential to find suitable and durable supports for Ru metal.

Because the unique electron distribution of phosphorus (P) makes it a proton acceptor for HER initiation, the combination of Ru and P changes the electronic and physicochemical properties and has received much attention in recent years.[106] Several recent studies on Ru phosphide have shown only comparable HER activity to Pt, but with less than satisfactory stability.[107] Han et al. encapsulated Ru diphosphide NPs in P-doped porous carbon (RuP_2@PC), a structure with ultrasmall RuP_2 NPs, hierarchically porous and abundant active sites.[101] They maintain 10 h without significant degradation tested at the overpotential of 78.9 mV. Mu et al. used nitrogen N, P dual-doped carbon to encapsulate Ru diphosphide NPs (RuP_2@NPC) for application in HER in pH-universal electrolytes.[108] Stability in various solutions is around 10 h, and all slightly deteriorate. Liu and co-workers obtained hybrid ruthenium-cobalt phosphide (RuCoP) clusters by phosphorizing chemically reduced RuCo alloy.[92] Ru clusters are uniformly dispersed on the CoP surface and are poorly crystalline, with apparent defects and strained lattice (Figure 6M–O). RuCoP catalyst is continuously maintained for 150 h at 10 mA cm^{-2} with only a minor decline under constant galvanostatic electrolysis in both acidic and alkaline solutions, suggesting excellent catalytic stability (Figure 6P). The outstanding stability of the RuCoP hybrid comes from its hydrogen adsorption energy very close to that of Pt and the difference between the adsorption of water and OH^- with pristine Ru.

Ru is presented as the strongest candidate to replace Pt for price considerations. Similar to Pt-based catalysts, Ru acts as the main active site in Ru-based catalysts, so the stability of Ru elements is crucial.[22] In addition to the stability-enhancing strategies used for Pt-based catalysts described above, the formation of insoluble alloys of Ru with certain metallic elements (Cu, Gd, Er, Yb, La, etc.) offers the promise of long-lived catalysts.[91] More unlike Pt, Ru can form compounds with P elements that have a unique electron distribution and act as a proton acceptor to excite HER, improving the activity of the material and the stability of the Ru element.[109,110]

4.1.3 | Palladium-based

Palladium (Pd) is also a candidate to replace platinum because it has a similar lattice structure and lattice constant to Pt and has a lower cost. However, the Pd-based electrocatalysts are not easy to desorb the adsorbed hydrogen because of the strong Pd—H bond, which decreases the reaction rate and stability.[2] Therefore, rational regulation of the hydrogen adsorption energy of Pd-based catalysts is a significant factor in improving their stability. Table 3 summarizes recent advances in the durability of Pd-based catalysts for HER. Zero-valent palladium complexes are the active products of many organocatalytic transformations, but their application in HER is relatively rare. Li et al. studied the HER activity and stability on zero-valent palladium (Pd^0) anchored on ultrathin nanosheet graphdiyne (Pd^0/GDY) (Figure 7A–D).[71] The high-resolution XPS spectrum of Pd 3d orbitals demonstrates the presence of metallic Pd (Figure 7E). GDY with both sp-hybridization and sp^2-hybridization facilitates the chelation of single metal atoms and strong charge transfer between metal atoms and GDY. By these advantages, Pd^0/GDY can be continuously worked for 1000 cycles from −0.6 to +0.2 V (vs. RHE) under an acidic solution. More impressively, the chronoamperometric experiment conducted at constant overpotential revealed almost no degradation in current density within 72 h, confirming the robust stability of Pd^0/GDY. After Pd^0/GDY stability testing, SEM and XPS data further demonstrate its superb structural stability (Figure 7F).

In addition to loading Pd onto carbon supporters, recently, the combination of precious metals with TM materials has been considered the most promising

TABLE 3 Summary of hydrogen evolution reaction (HER) durability with Pd-based catalysts under different reaction conditions

Catalyst	Electrolyte	η_{10} (mV) or mA cm^{-2}@mV	Stability			References
			CA/Retention (mV@h@%)	CP/Retention (mA cm^{-2}@h@%)	CV/(cycles) (cycles@%)	
Pd^0/GDY	0.5 M H_2SO_4	55	58@72@-	-	1000@-	[71]
Pd/$NiFeO_x$	0.5 M H_2SO_4/ 1 M KOH/ 1 M PBS/	169/180/310	-/80@50@-/-	-	-	[111]
N-Pd/A-Co (II)	1 M KOH	58	-	10@30@-	-	[112]
1%Pd-MoS_2/CP	0.5 M H_2SO_4	89	-	10@100@-	5000@-	[31]
Pd_2/BP 3%	0.5 M H_2SO_4	-	-	5@1@-	-	[113]
$PdCu_{0.2}H_{0.43}$/C	0.5 M H_2SO_4	28	-	-	5000@-	[32]
GDY-Pd1	0.5 M H_2SO_4	500@201	-@45@-	-	-	[114]
$Pd_4S/Pd_3P_{0.95}$	0.5 M H_2SO_4/ 1 M KOH	28/42	284@20@-/ 387@20@-	-	2000@-/2000@-	[115]
sub-MoS_x/ CNTs/Pd	0.5 M H_2SO_4	23	200@24@-	-	-	[116]
Pd-e-NiCo-PBA-C	0.5 M H_2SO_4/ 1 M KOH	48/147	-	-	5000@-/5000@-	[117]

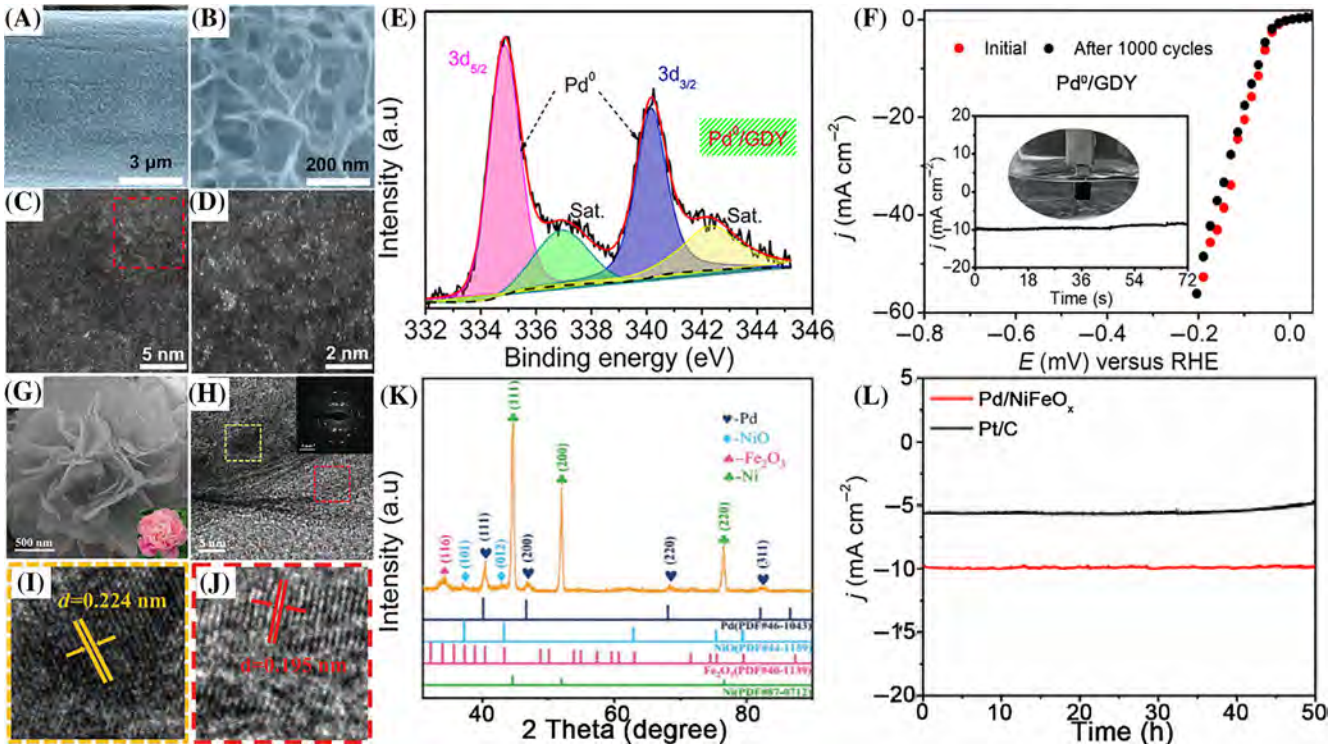

FIGURE 7 Morphology and structure Characterizations and HER stability of Pd^0/GDY. (A,B) SEM. (C,D) HADDF image and enlarged image of the selected region. (E) XPS Pd 3d spectrum. (F) CV Acceleration Test of 1000 cycles. Inset: time-dependent current density curve at an overpotential of 58 mV. Reproduced with permission.[71] Copyright 2019, Elsevier. Morphology and structure characterizations of Pd/$NiFeO_x$ nanosheets. (G) SEM. Inset is a digital photograph of peony. (H) HRTEM. Inset is the SAED pattern of Pd/NiFeOx nanosheets. (I,J) The enlarged images of the selected regions in Figure 7H. (K) XRD pattern. (L) Pd/$NiFeO_x$ and Pt/C at a constant current density of 10 mA cm^{-2} in alkaline media. Reproduced with permission.[111] Copyright 2021, Wiley-VCH

strategy to improve the materials' physicochemical properties and enhance the catalytic activity and stability further. Wang group grew peony-like Pd/$NiFeO_x$ on NF with tightly arranged petals and uniform mesoporous structure (Figure 7G–J).[111] Pd NPs are mainly distributed at the edges of pores and lamellae in 2D structures to provide active sites, and the presence of Pd NPs was determined using x-ray diffraction (Figure 7K). This 2D structure has a large specific surface area to expose more active sites and a high electrical conductivity, facilitating the diffusion of electrolytes and the generation and release of H_2 bubbles. As shown in Figure 7L, the stability of Pd/$NiFeO_x$ has negligible attenuation over 50 h (the overpotential is 80 mV) testing by the CA method. After the long-term reaction, the morphological structure of Pd still maintains the porous 2D nanostructure, providing outstanding structural stability. Furthermore, metals' electronic structure and physicochemical properties could be modulated by binding with S and P. Chen et al. constructed $Pd_4S/Pd_3P_{0.95}$ heterostructures by interface engineering.[115] It continued to operate without decay for 20 h during high current density HER under acidic and alkaline conditions. DFT calculations showed that $Pd_4S/Pd_3P_{0.95}$ heterostructures as the most considerable oxygen atom conductivity and adsorption energy and a low kinetic energy barrier for the dissociation of water molecules.

Therefore, strong hydrogen adsorption significantly hampered Pd catalysts' HER activity and stability. But making ΔG_{H^*} closer to 0 by compounding Pd with materials with weaker hydrogen adsorption is a vital strategy to improve material activity and further enhance stability, such as Pd compounded with MoS_2, which has $\Delta G_{H^*} > 0$.[31,116]

4.1.4 | Other precious metals or precious metal complexes

Table 4 summarizes recent advances in the durability of other precious metals or precious metal complexes catalysts for HER, such as Rh, Ir, Au, and Ag, which are also selected as candidates for HER electrocatalysts compared to Pt-group metals. In terms of Rh, many Ru-based catalysts, including Rh NPs loaded on silicon nanowires,[119] Rh alloyed with TMs,[120] Rh-based phosphides with phosphorus defects,[123] and so on, showed improved HER activity but unsatisfied stability. Ir-based catalysts, such as Ir nanoclusters loaded on nitrogen and sulfur dual-doped graphene[121] and heterostructures of crystalline mesoporous Ir with amorphous nickel-boron oxides[125] have also made less progress in terms of electrocatalyst stability. Because Au is an inert noble metal that weakly adsorbs hydrogen, it is often alloyed with stronger hydrogen adsorbers to produce unique geometric and electronic structures. Similarly, Ag has been little studied because of its weak hydrogen adsorption. Still, in 2019, Du et al. prepared L-catalysts with platinum-like activity by laser irradiation of Ag targets that maintained 98.5% activity after 160 h of continuous operation.[135]

Because Pt group metals have more suitable hydrogen adsorption energy, to further obtain electrocatalysts with more excellent activity and stability, two or more metals are usually alloyed to improve the electronic structure and physicochemical properties of materials.[136] Lee and co-workers synthesized $Cu_{2-x}S@IrS_y@IrRu$ nanoparticles (CIS@IrRu NPs) with hollow structures and cactus-like dendrites, which showed promising stability in 0.1 M $HClO_4$ (Figure 8A–C).[127] By regulating the composition of IrRh NPs, $CIS@Ir_{48}Ru_{52}$ displayed the best stability and HER performance. $CIS@Ir_{48}Ru_{52}$ has a small amount of decay after the 100 h continuous stability test. Such ability is mainly attributed to the protection of IrRu NPs by the IrS_y shell, which prevents the aggregation and dislodgement of the particles (Figure 8D). Our group has also made significant progress in Pt-based noble metal alloys with high longevity. Inspired by the phenomenon of hydrogen spillover through strong metal-support interactions during thermal hydrogenation, alloyed NPs of Pt with various other precious metals (Ir, Rh, Pd, Ag, and Au) are anchored to CoP.[126] It found that the extremely small NPs exhibited high activity and extreme stability (Figure 8E). Theoretical analysis revealed that the difference in the work function ($\Delta\Phi$) between the metal and the support would affect the interfacial charge accumulation and proton adsorption, which in turn influence the catalytic activity, and the activity would be higher when $\Delta\Phi$ is smaller. As displayed in Figure 8F, Pt_2Ir_1/CoP (0.02 eV) has smaller $\Delta\Phi$ than Pt_2Pd_1/CoP (0.15 eV), Pt/CoP (0.19 eV), Pt_2Au_1/CoP (0.22 eV), Pt_2Rh_1/CoP (0.13 eV), and Pt_2Ag_1/CoP (0.38 eV). The TEM image shows that PtIr alloyed NPs of ~1.6 nm are uniformly dispersed on the CoP nanosheets (Figure 8G). Pt_2Ir_1/CoP can keep 50 000 cycles in CV acceleration test and 500 h without significant degradation under the CA test (Figure 8H). The ICP-MS, XPS, and HRTEM characterization after stability testing also illustrate insignificant changes in structure and composition. Moreover, Jia et al. fabricated a 3D self-supporting high-entropy alloy metallic glass (HEMG) ribbon (PtPdCuNiP) for further industrialization of water electrolysis (Figure 8I).[34] Metallic glasses have the advantages of multi-component, chemical homogeneity, high atomic diffusivity, sub-stable properties, and excellent mechanical strength, while high-entropy alloys have unique mechanical and physicochemical properties. The SEM and AFM images verified the 3D nanosponge-like

TABLE 4 Summary of hydrogen evolution reaction (HER) durability with other precious metals and complexes catalysts

Catalyst	Electrolyte	η_{10} (mV) or mA cm^{-2}@mV	Stability			References
			CA/Retention (mV@h@%)	CP/Retention (mA cm^{-2}@h@%)	CV/(cycles) (cycles@%)	
Pt-IrO_2/CC	0.5 M H_2SO_4/ 1 M KOH/ 1 M PBS	5/22/26	-	-@20@-/-@20@-/-@20@-	10 000@-/10 000@-/ 10 000@-	[118]
Rh/SiNW	0.5 M H_2SO_4	100@180	300@138.9@-	-	-	[119]
RhCo-ANAs	1 M PBS	31	50@5@-	-	-	[120]
Ir-NSG	0.1 M $HClO_4$/ 1 M KOH/ 1 M PBS/	17/18.5/22	-	-@11.1@-/-@18@-/-@18@-	-	[121]
Rh-MoS_2	0.5 M H_2SO_4	67	67@20@92.5%	-	5000@-	[122]
P-defect Rh_2P	0.5 M H_2SO_4/ 1 M KOH	14.3/4.3	5@16.7@-/ 5@16.7@-		2000@-/2000@-	[123]
Rh_2Sb NBs/C	0.1 M KOH	40	100@5.6@93.5%	-	-	[124]
Ni-Bi/meso-Ir	1 M KOH	26.8	-	10@18@-	1000@-	[125]
Pt_2Ir_1/CoP	0.5 M H_2SO_4	20@7	-	40@500@-	50 000@-	[126]
CIS@$Ir_{48}Ru_{52}$	0.1 M $HClO_4$	7.6	-	5@100@-	-	[127]
PdPtCuNiP	0.5 M H_2SO_4/ 0.05 M H_2SO_4/1 M KOH/0.1 M KOH	62/73/32/93	-	20@ ≈ 100@-/20@ ≈ 100@-/ 20@ ≈ 100@-/20@ ≈ 100@-	-	[34]
us-HEA/C	0.5 M H_2SO_4	27	-@100@100%	-	10 000@-	[128]
PtPd NSs	0.5 M H_2SO_4	22	22@12@79%	-	1000@-	[129]
PtRhCo PAANFs	0.5 M KOH	36	70@12@92.4%	-	1000@-	[130]
RhPd-H/CP	1 M KOH	40	-@10@-	-	10 000@-	[131]
RuAu-0.2	1 M KOH	24	-@10@-	-	1000@92%	[132]
$RuRh_2$	0.5 M H_2SO_4/1 M KOH/1 M PBS	34/24/12	-	-	30 000@-/20 000@-/-	[133]
PtRu/mCNTs	0.5 M H_2SO_4/1 M KOH/1 M PBS	28/15/17		10@48@-/10@48@-/10@48@-	3000@-/3000@-/ 3000@-	[134]

surface morphology (Figure 8J,K), conducive to electron transfer, electrolyte transport, and the generation and release of bubbles. And in the HADDF-STEM image (Figure 8L), HEMG has many nanopores with amorphous structures. Thus, PtPdCuNiP exhibits ultra-reliable stability under acidic and alkaline solutions, with a duration of about 100 h, without elemental leaching and structural deterioration (Figure 8M). The presence of P in the PtPd sublattice causes lattice distortion and optimizes the electronic structure, stabilizing the adsorption, and desorption of hydrogen (Figure 8N).

Compared to Au and Ag, the ΔG_{H^*} of Rh and Ir is closer to zero, and their performance can be further enhanced by using more suitable supports, alloying with non-precious metals, or forming compounds. However, they still have a long way to extend to market

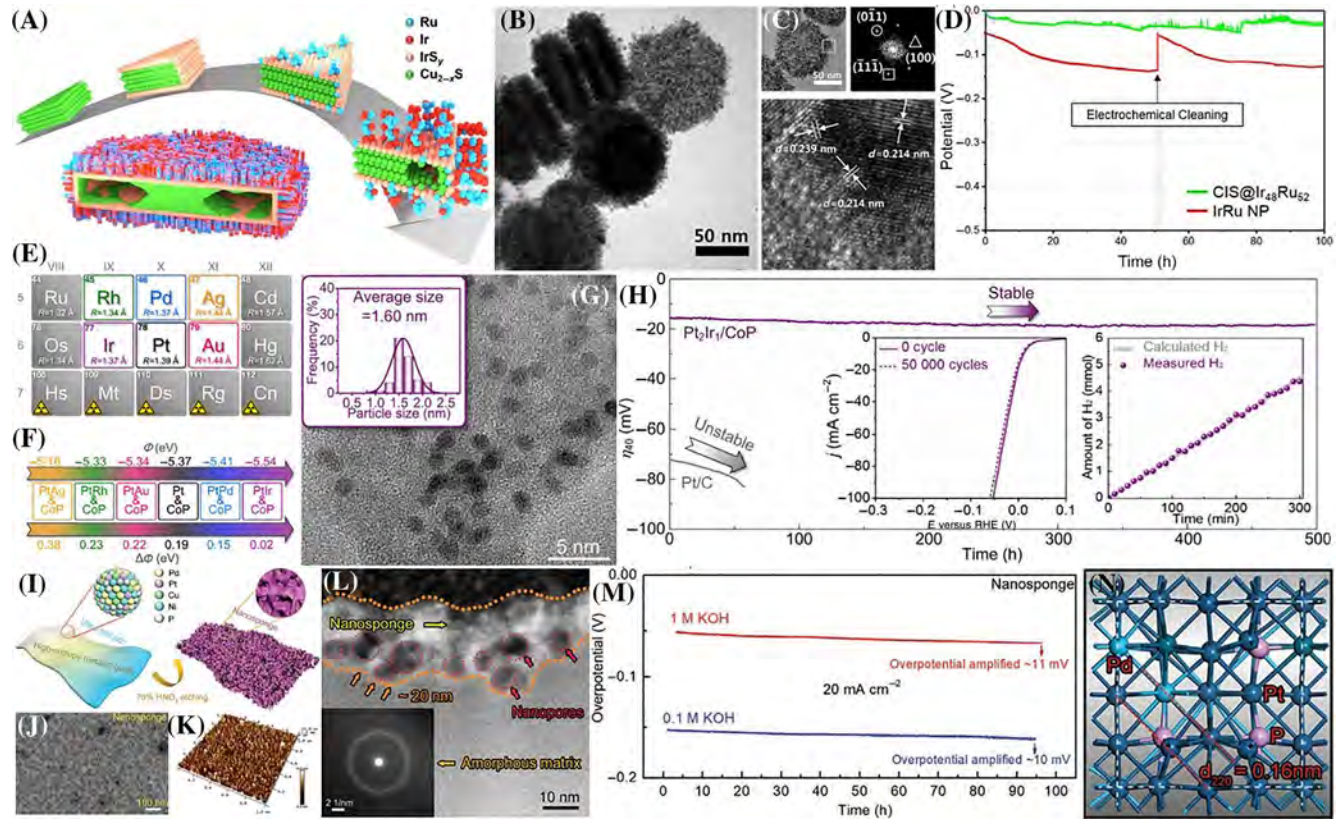

FIGURE 8 Synthetic route of CIS@$Ir_{48}Ru_{52}$ and morphological characterization and stability test. (A) Schematic illustration. (B) TEM image. (C) HRTEM and magnified HRTEM image, corresponding to its FFT pattern with the zone axis of [011]. (D) HER stability in 0.1 M $HClO_4$. Reproduced with permission.[127] Copyright 2018, The Royal Society of Chemistry. (E,F) The PtM/CoP catalysts with the controllable $\Delta\Phi$. (G) TEM images for the Pt_2Ir_1/CoP. Inset is the size of the PtIr nanoparticle of ~1.60 nm on CoP nanosheets. (H) Long-term stability of Pt_2Ir_1/CoP through a time-overpotential profile at 40 mA cm^{-2}. Insets are cycle performance of LSV curves and Faradic efficiency. Reproduced with permission.[126] Copyright 2021, Springer Nature. Conceptional design and surface characterization of the nanoporous PdPtCuNiP HEMG. (I) Schematic illustration. (J) SEM image. (K) 3D AFM image. (L) Aberration-corrected HAADF-STEM image. Inset is the corresponding SAED pattern of the predominantly amorphous matrix. (M) The time-dependent HER stability at a current density of 20 mA cm^{-2} in 1 and 0.1 M KOH solutions. (N) DFT atomic modeling of the $Pt_5Pd_3P_2$ nanocrystals showing the lattice distortion caused by interstitial alloying of P. Reproduced with permission.[34] Copyright 2021, Wiley-VCH

applications. Therefore, most studies have alloyed two or more noble metals to stabilize the active phase and obtain ultra-stable catalysts for HER through the synergistic effect of various noble metals. Multiple noble metal compounds can also be designed to form heterogeneous structures by interface engineering, which could accelerate electron transfer and improve interfacial coordination to obtain high longevity catalysts.

4.2 | TM-based hydrogen evolution catalyst

A series of metal elements in the d and ds regions of the periodic table are called TMs. The d zone elements include elements in the period series III B–VII B, VII group except for lanthanides and actinides. The ds region includes group I B–II B elements of the periodic table.[137] TMs have unfilled valence layer d orbitals, many of which have a single electron. This helps them be easily combined with other metal or nonmetal elements to reach a stable state. As we know, Pt and other precious-metal-based materials are limited by their scarce resources and high price. To reduce the cost and maintain high catalytic activity and stability, researchers are working on synthesizing catalyst materials with low noble metal content by combining them with non-precious metals to improve the utilization efficiency of noble metal atoms (see Section 4.1). Accordingly, to further reduce the cost of non-noble metals, kinds of TM-based electrocatalysts have been extensively developed and studied, mainly for several TMs shown

in Figure 1. By preparing TM particles, SAs, alloy or TM-based phosphates, sulfides, selenides, carbides, nitrides, oxides, and hydroxides formed by combing multiple TMs with nonmetallic elements, efficient and stable electrocatalysts can be obtained.

4.2.1 | Nickel-based

Nickel (Ni) resources are abundant globally and have good mechanical strength and ductility. Because nickel atoms have unpaired 3d electrons, they are easily coupled with H 1s to form Ni—H bonds in the process of hydrogen evolution.[138] But the highly efficient and stable catalysts need good adsorption capability and desorption ability, and nickel dissolves easily in acid conditions, thereby hindering the stability. Therefore, researchers prepare nickel-based catalysts with reasonable modulation of the coordination environment to obtain catalysts with long-term stability. Table 5 summarizes recent advances in the durability of Ni-based catalysts for HER.

In recent years, many reports focused on the in-depth study of the HER stability of nickel monomers and nickel-based complexes.[12,137,138] Single-atom catalysts have attracted much attention due to their high atomic efficiency, and the related work of Ni single-atom supported on carbon supports also shows strong stability.[152] Ni single-atoms anchored to nanoporous graphene (Ni-doped np-G), which still maintained 90% of the initial activity after 120 h of continuous operation at 150 mV overpotential in 0.5 M H_2SO_4, showing outstanding stability (Figure 9A).[142] The experiment and theoretical calculation results agree that the structure and morphology of Ni-doped np-G catalysts are stable (Figure 9B). From DFT calculations, it was found that Ni atom with three adjacent carbon atoms forms the bonds with energy of −7.54 V, and that the sp-d orbital charge transfer between the Ni atom and the adjacent carbon atom results in an empty C-Ni hybrid orbital close to E_f, transforming the local structural unit composed of Ni atoms and surrounding carbon atoms into an active catalytic site (Figure 9C). In addition, chemical bonds formed by charge transfer between nickel atoms and surrounding carbon atoms significantly stabilize Ni under acidic conditions.

Combining with other nonmetals (C, N, O, P, S, Se, etc.) can introduce heteroatoms in the lattice of Ni, increasing valence electrons and adjusting the electronic structure to obtain higher activity and stability Ni-based catalysts.[150,153] Among them, Ni-based sulfide and selenides are a kind of promising electrocatalysts for

TABLE 5 Summary of hydrogen evolution reaction (HER) durability with Ni-based catalysts under different reaction conditions

			Stability			
Catalyst	**Electrolyte**	**η_{10} (mV) or mA cm^{-2}@mV**	**CA/Retention (mV@h@%)**	**CP/Retention (mA cm^{-2}@h@%)**	**CV/(cycles) (cycles@%)**	**References**
v-$Ni_{12}P_5$	1 M KOH	27.7	-	-@504@-	10 000@-	[139]
$NiS_{0.5}Se_{0.5}$	1 M KOH	70	-	10, 100@300@-	10 000@-	[140]
$Ni(OH)_2/Ni_3S_2$	1 M KOH	200@142	-	20@240@-	-	[141]
NF-Ni_3Se_2/Ni	1 M KOH	203	200@200@-	-	2000@-	[49]
Ni-doped np-G	0.5 M H_2SO_4	~180	150@120@-	-	1000@-	[142]
$Ni_{11}(HPO_3)_8(OH)_6$/NF	1 M KOH	121	130@25@-	-	-	[143]
Co-NiS_2 NSs	1 M KOH	80	-	-@90@-	-	[144]
$NiSe_2$-450	0.5 M H_2SO_4	117	-	12.5@67@-	3000@-	[145]
Ni_3N/Ni/FTO	1 M KOH	89	89@ > 72@-	-	-	[146]
NC/Ni/TiO_2 NPAs	1 M KOH	88	226@15@94% + 326@15@94%	-	-	[147]
SANi-I	1 M KOH	100@60	-	20@24@-	10 000@-	[148]
Ni NPs/Ni SAs/SGNCs	1 M KOH	27	27@22@-	-	5000@-	[149]
Co-Ni/Ni_3N	1 M KOH	60	-@20@-	-	1000@-	[150]
Ni-SA/NC	1 M KOH/1 M KOH + Seawater	102/139	200@14@-	-	5000@-	[151]

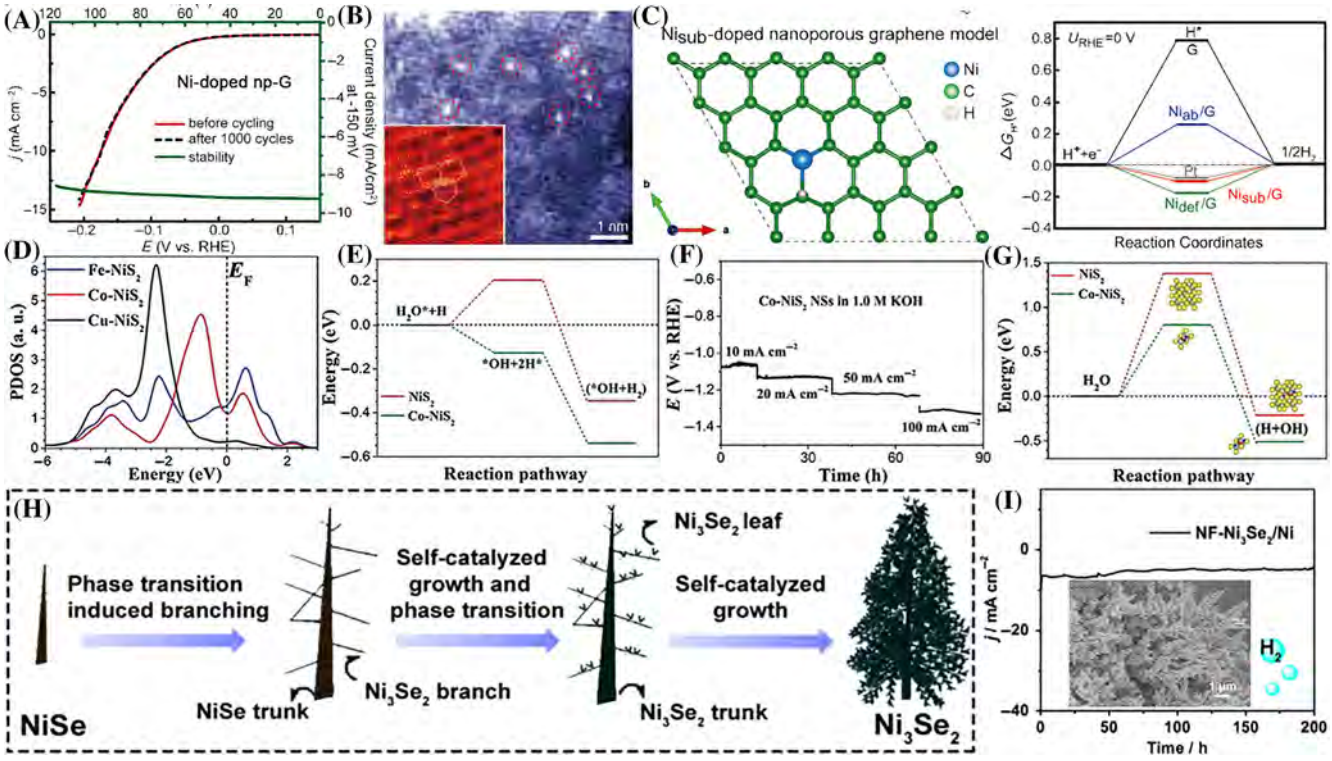

FIGURE 9 (A) Stability of Ni-doped np-G at the overpotential of 150 mV in 0.5 M H_2SO_4. Inset is LSV curves before and after 1000 cycles. (B) HAADF-STEM image of Ni-doped np-G. (C) Hydrogen adsorption sites and configuration of the Ni_{sub}/G model with $\Delta G_{H^*} = -0.10$ eV (left) and calculated Gibbs free energy diagram (right). Reproduced with permission.[142] Copyright 2015, Wiley-VCH. (D) Partial density of states (PDOSs) of 3d-bands of Co, Fe, and Cu dopants. (E) Energetic pathway of HER. (F) Chronoamperometric response of the Co-NiS_2 NSs at different current densities. (G) Transition state barrier for H_2O-splitting; Insets are models for $*H_2O$ and $*H^+$ absorbed on NiS_2 and Co-NiS_2 NSs. Reproduced with permission.[144] Copyright 2019, Wiley-VCH. (H) Schematic diagram of the preparation of Ni_3Se_2 nanoforest on Ni foam. (I) Durability of NF-Ni_3Se_2/Ni at −0.200 V versus RHE in 1 M KOH. Inset is the SEM image after the HER stability test. Reproduced with permission.[49] Copyright 2016, Elsevier

hydrogen evolution because of their high electrical conductivity, good mechanical properties, and thermal stability. However, simple Ni-based sulfide has poor stability and can only remain stable for 10 h at a current density of 10 mA cm^{-2}.[154] In this case, metal doping is an excellent strategy to improve the adsorption energy of hydrogen and catalyst stability. V-doped Ni_xS_y exhibits stability at 12 h (at the overpotential of 130 mV) through the synergistic effect between Ni and V.[155] Furthermore, improving the d-band electron configuration is a design strategy for improving the activity and stability of TM materials. The TMs Cu, Fe, and Co are introduced into NiS_2 nanosheets (Cu-NiS_2 NSs, Fe-NiS_2 NSs, and Co-NiS_2 NSs) to adjust the electron configuration and atomic arrangement flexibly.[144] The Co-NiS_2 NSs require a smaller e_g-t_{2g} splitting gap, improving the electron transfer efficiency on E_f (the Fermi level). Moreover, it has the ideal e_g^1 electron configuration and the increase of Ni^{3+} content, which significantly improves HER under alkaline condition (Figure 9D,E). The catalyst shows excellent stability at various current densities for 90 h, with good morphology and no change in electronic structure after the test (Figure 9F). It also has high selectivity to activate H_2O molecules, and the adsorbed OH species has metallic properties so as to easily adsorb and remove electrons from the surface (Figure 9G). Adjusting the surface properties of the catalysts is also a way to affect the stability and speed of the catalytic reaction. Xu et al. synthesized nanoforest-like Ni_3Se_2 on the surface of Ni foam (Ni_3Se_2/NF) through self-catalyzed growth and phase transition (Figure 9H).[49] After an extended stability test of 200 h, the attenuation was negligible, and the crystal shape of the original morphology was still maintained (Figure 9I). This improved stability is entirely benefited by the metal characteristics of Ni_3Se_2, and the hydrophilic surface and gas-phobic structure, so that the reaction can continue without damaging the catalyst. It is also an effective strategy to develop effective electrocatalysts by introducing lattice strains into Ni-based chalcogenides. For example, $NiS_{0.5}Se_{0.5}$ nanosheets@nanorods hybrids (Figure 10A) with a lattice strain ≈2.7% can not only work steadily for 300 h without attenuation under low current density

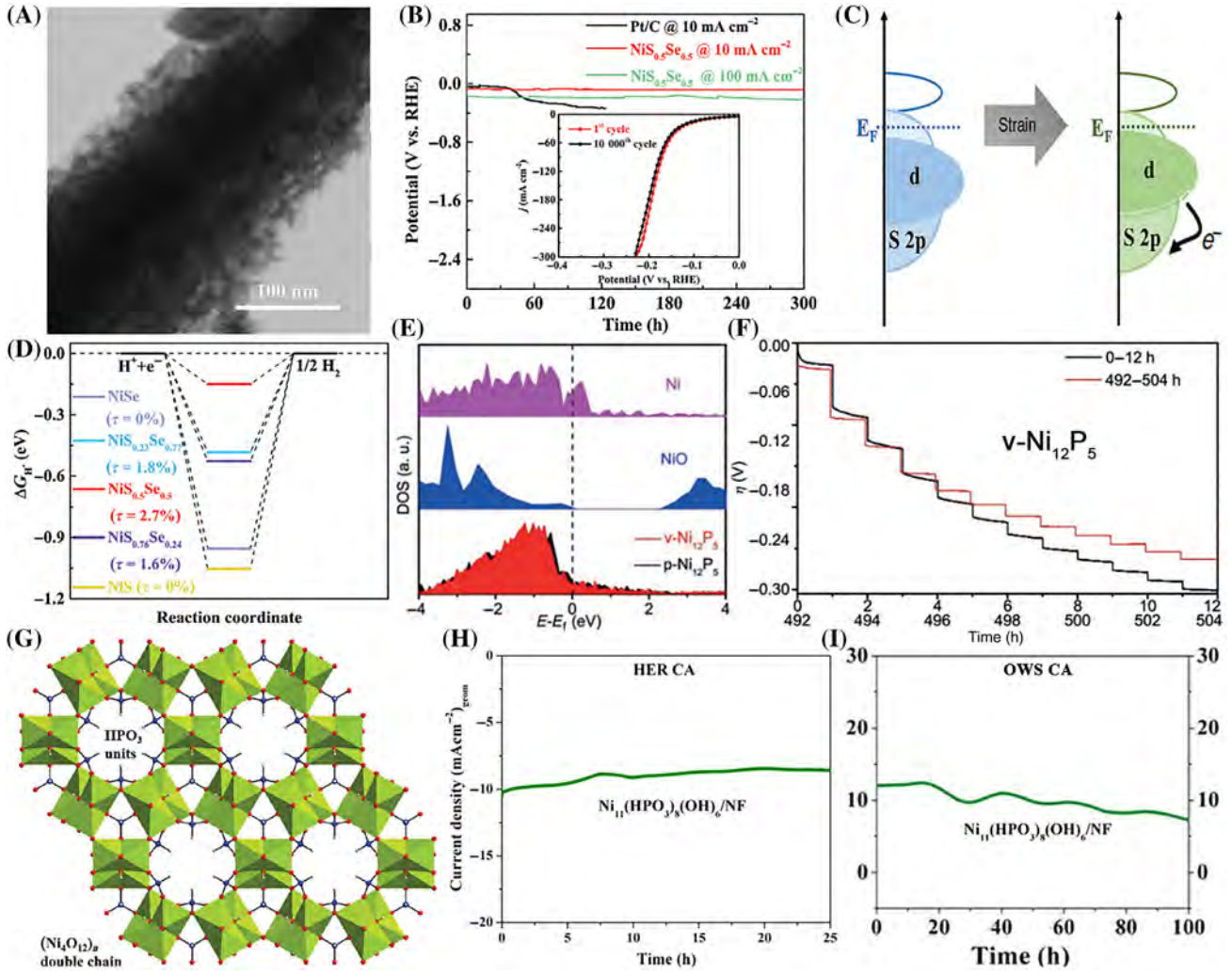

FIGURE 10 (A) TEM image of $NiS_{0.5}Se_{0.5}$. (B) Durability test of $NiS_{0.5}Se_{0.5}$ at a current density of 10 and 100 mA cm^{-2} in 1 M KOH. Inset is LSV curves before and after 10 000 cycles. (C) Schematic of the electron exchange for the lattice-strained surface of $NiS_{0.5}Se_{0.5}$. (D) Gibbs free-energy diagram. Reproduced with permission.[140] Copyright 2020, Wiley-VCH. (E) The v-$Ni_{12}P_5$ and p-$Ni_{12}P_5$ catalysts of Ni 3d for density of states (DOS). (F) Chronoamperometry test of v-$Ni_{12}P_5$ in 1 M KOH at various current densities (5, 10, 20, 30, 40, 50, 60, 70, 80, 90, 100 mA cm^{-2}). Reproduced with permission.[139] Copyright 2020, Wiley-VCH. (G) Crystal structure of $Ni_{11}(HPO_3)_8(OH)_6$. The long-term stability test of $Ni_{11}(HPO_3)_8(OH)_6$/NF. (H) HER stability at an overpotential of 130 mV in 1 M KOH. (I) The overall water splitting stability at 1.65 V versus RHE. Reproduced with permission.[143] Copyright 2018, The Royal Society of Chemistry

(10 mA cm^{-2}), but also for 300 h under high current density (100 mA cm^{-2}), which makes Ni-based chalcogenides closer to the industrial level (Figure 10B).[140] This $NiS_{0.5}Se_{0.5}$ with lattice strain reduces the overlap of the metal d-orbital, resulting in a narrower bandwidth and closer to the d-band center of the Fermi level (Figure 10C). Therefore, $NiS_{0.5}Se_{0.5}$ has ideal H adsorption and desorption kinetics and exhibits unprecedented stability for HER (Figure 10D).

Modified metal phosphating is the boulevard to push the catalysts to industrialization. For metal phosphide, because the electronegativity of the P atom is greater than that of the metal atom, the electron cloud of the metal atom will be biased toward the P atom, making the partially negatively charged P atom into a proton acceptor. P will also change the adsorption–desorption behavior of H on the surface of metal phosphide, which makes the metal phosphide have good HER electrocatalytic performance. Qiao et al. manipulated the electronic structure by creating phosphorus vacancies (Pv) in $Ni_{12}P_5$ using the vacancy engineering strategy (v-$Ni_{12}P_5$).[139] Pv attenuates the hybridization of Ni 3d and P 2p orbitals, increases the electron density of Ni and P atoms nearby Pv, and facilitates H* desorption, thus reducing the damage of the intermediate to the catalyst itself (Figure 10E). The v-$Ni_{12}P_5$ has shown

convincing stability. The CA test could continuously be operated for up to 504 h at current densities of 2, 5, 10, 20, 30, 40, 50, 60, 70, 80, 90, 100 mA cm^{-2} in 1 M KOH; more importantly, there is no decay of activity. Besides, nickel phosphite also shows signs of stability (Figure 10F). Driess et al. rearranged two nickel phosphides (Ni_2P and Ni_2P_5) through the surface structure to form nickel phosphite ($Ni_{11}(HPO_3)_8(OH)_6$) as a catalyst for overall water splitting.[143] $Ni_{11}(HPO_3)_8(OH)_6$ is a unique phosphorus-based inorganic material with a layered double-hydroxide structure (Figure 10G). Although $Ni_{11}(HPO_3)_8(OH)_6$ can only be stabilized for 25 h in HER semi-reaction (Figure 10H), but it only attenuates a little after 100 h in overall water splitting (Figure 10I). The combination of phosphite $(HPO_3)^{2-}$ anion and Ni^{2+} cation can act as the active catalytic site to enhance HER and display excellent stability. TM doping is another effective way to improve the activity of nickel-based phosphides, such as Fe-doped Ni_2P nanosheet array,[156] Co-doped Ni_2P,[157] Mo doped Ni_2P nanowire arrays,[158] V-doped Ni_2P nanosheet arrays,[159] Cu-doped Ni_2P nanosheets,[160] and a series of electrocatalysts that exert synergistic effect through doping modification. However, the stability of these catalysts is less than 30 h, so they are not described detailed here.

In addition to the nickel-based phosphides described above, nickel-based nitrides, hydroxides, and nickel-based alloys also show different stability properties of HER. Pt decorated Ni_3N nanosheet with high metallic conductivity and abundant active sites exhibit excellent stability of 82.5% current retention after 24 h of operation.[76] $Ni(OH)_2$ is generally used as an OER catalyst, but Yuan et al. prepared Fe-doped $Ni(OH)_2$, showing excellent activity and stability (20 h at 10 mA cm^{-2}).[161] The partial charge transfer in the Ni center induced by Fe doping dramatically improves the mechanical stability of the material. However, nickel-based nitrides, oxides, and hydroxides are much less stable than nickel-based sulfides, selenides, and phosphides, so new strategies need to be explored to improve the stability of the materials for future commercial applications.

In a word, nickel has garnered much attention for its excellent activity and low price. Nickel-based sulfides, phosphides, and selenides have excellent HER activity, and their stability is ensured by methods such as defect engineering, stress engineering, and doping effects. NF is generally used as a substrate for the preparation of nickel-based catalysts because of its 3D structure. The porous structure facilitates the rapid transport of reactants and products, resulting in ultra-long-lived catalysts. Therefore, the rational design based on NF may lead to the creation of commercially available alkaline electrolytic water catalysts.

4.2.2 | Cobalt-based

Table 6 summarizes recent advances in the durability of Co-based catalysts for HER. Many cobalt-based materials have recently been used in electrocatalytic HERs, mainly including metallic Co, cobalt-based compounds (sulfides, phosphides, selenides, fluoride, nitrides, oxides, hydroxides, alloys, etc.).[177] The loading of single-atom Co or Co NPs on carbon supports shows excellent HER activity and unremarkable advantages in terms of stability. For instance, single-atom cobalt dispersion in phosphorized carbon nitride (Co_1/PCN) is only stable for 24 h in 1 M KOH.[178] Single-atom Co sites embedded in hierarchically ordered porous N-doped carbon (Co-SAS/HOPNC) can maintain durability for 20 h.[47] Co NP-encapsulated 3D conductive films (Co/CNFs) show the stability of the 1000 cycles of the CV acceleration test.[179] By calculating the free energies of 27 possible HER active sites in graphene-based Co SAs, Lee and his colleagues found that the edge sites (zigzag and armchair) are more responsible for HER activity and stability.[164] Based on the calculation results, they synthesized edge-rich (E) graphene-based cobalt single-atom catalysts (E-Co SAs) with 65.49% of Co-4N-plane (Co-4N-P), 13.64% in Co-2N-armchair (Co-2 N-A), and 20.86% in Co-2N-zigzag (Co-2N-Z). Co-2N-A and Co-2N-Z have a lower HER energy barrier, higher tip effect, higher conductivity, and lower d-band center than Co-4N-P. The low d-band center in graphene-based materials facilitates water dissociation and enhances the binding energy of hydrogen (Figure 11A). As shown in Figure 11B, many isolated but widely distributed cobalt SAs are at the edges. Then, long-term tests were conducted to evaluate the stability of E-Co SAs at constant current densities of 10 and 500 mA cm^{-2}, respectively, demonstrating the fantastic stability that could be maintained for 480 h at 10 mA cm^{-2} and at least 200 h at 500 mA cm^{-2} without loss of activity (Figure 11C,D).

Cobalt-based compounds have awakened the interest of researchers because of their advantages of abundant reserves, good electrical conductivity, high corrosion resistance, redistributed d-band electronic structure, chemical stability, and so on. CoS_2, as a type of pyrite, has poor stability in HER because of easy surface oxidation, catalyst leaching, and unstable chemical structure, so long-term CoS_2 catalysts need to be prepared by rational design and modulation. In 2019, our group doped different amounts of rare earth metal (Cerium, Ce) into CoS_2 (Ce-CoS_2), which weakened the oxygen adsorption at the interface and also consolidated the lattice structure of CoS_2 (Figure 11E), improving the electrochemical stability and chemical stability of pyrite electrocatalysts.[165] To further approach the industrial level, we grew CoS_2

TABLE 6 Summary of hydrogen evolution reaction (HER) durability with Co-based catalysts under different reaction conditions

Catalyst	Electrolyte	η_{10} (mV) or mA cm^{-2}@mV	Stability			References
			CA/Retention (mV@h@%)	CP/Retention (mA cm^{-2}@h@%)	CV/(cycles) (cycles@%)	
Porous Co-P	0.5 MH_2SO_4/ 1 M KOH	-/100@141	-	1000@ > 30@-/ 1000@3000@-	-	[162]
CeO_2/CoS_2/Ti	1 M KOH	35	-@1000@ > 90%	-	-	[163]
E-Co SAs	1 M KOH	59	-	10@480@- + 500@200@-	-	[164]
Ce-CoS_2(2)/Ti	1 M KOH	82	-	20@250-	-	[165]
R-CoF_2	1 M KOH	54	-@110@-	-	3000@-	[166]
CoFePO	1 M KOH	87.5	-@100@90%	-	-	[167]
Ga-CoP NSs/CFP	1 M KOH	44	-@100@81%	-	-	[168]
SSM/CoOP	1 M KOH	21	-	100@100@ ~ 100%	-	[169]
AB&CTGU-5(1:4)	0.5 M H_2SO_4	100	255@96@-	-	-	[170]
C-Co_2P	1 M KOH	30	-	10 + 100, +1000@60@-	-	[171]
N − Co_2P/CC	0.5 M H_2SO_4/ 1 M KOH/ 1 M PBS	27/34/42	-	10@33.3@-/10@33.3@-/ 10@33.3@-	3000@-/3000@-/ 3000@-	[172]
Co-NC-AF	0.5 M H_2SO_4	100@174	-	1000@32@-	-	[173]
PANI/CoP HNWs-CFs	0.5 M H_2SO_4	57	120@30@-	-	-	[174]
Se-Co_4N-150	1 M KOH	95	95@24@-	-	4000@-	[175]
S-CoP	1 M KOH	100@114	-	100@20@-	1000@-	[176]

doped with 1.47 atom% Ce on a Ti plate (Ce-CoS_2(2)/Ti) as the self-supporting electrode, which can maintain negligible attenuation for 250 h in alkaline electrolytes at 20 mA cm^{-2} (Figure 11F). The O_2 temperature-programmed desorption (O_2-TPD) and corrosion polarization curves illustrate that the doping of Ce weakens the adsorption ability of oxygen and the corrosion of CoS_2. The morphological and structural characterization after stability measurement also demonstrates that Ce doping strengthened the structural stability and electrochemical stability of CoS_2. Based on the above work, we coupled CeO_2 with easy water dissociation and CoS_2 nanowire arrays with antioxidant ability on the Ti plate (CeO_2/CoS_2/Ti).[163] HRTEM images demonstrate the formation of CeO_2/CoS_2 hybrid catalysts (Figure 11G). The Lewis acid–base Ce · · · S pairs constructed at the interface of CeO_2 and CoS_2, which are neither strongly nor weakly acidity-basicity, were experimentally and theoretically proven to be active sites. The interfacial Ce · · · S pairs provide ideal catalytic sites for the adsorption and dissociation of water and induce surface charge migration to form an antioxidant surface (Figure 11H). Also, CeO_2/CoS_2/Ti exhibited distinguished viability in 1 M KOH for more than 1000 h and still maintains more than 90% of catalytic activity (Figure 11I). More impressively, the CeO_2/CoS_2/Ti catalyst can keep over 500 h of operation in an approximate industrial alkaline electrolyzer at 60°C (Figure 11J).

Cobalt phosphide-based catalysts have good electrochemical activity, so they have extracted extensive research interests. Various strategies such as metal doping, anion doping, and small molecule modification have been used further to enhance intrinsic activity and structural and electrochemical stability. Zhang et al. developed a simple two-step method (electrodeposition and phosphorization) to prepare doped gallium (Ga) into ultrafine CoP nanosheets (Ga-CoP NSs), where the performance was maintained at a low current density for 50 h and an 81% activity retention at high current density for 100 h (Figure 12A–D).[168] DFT calculations revealed that the introduction of Ga atoms could enhance the adsorption of H_2O, weaken the adsorption of OH, and optimize the adsorption and desorption of H (Figure 12E). In addition, the unique 3D structural advantages of the material would also get good electrochemical stability. Anion (O) and cation (Fe) co-doping modulate Co_2P growth on NF (CoFePO) with porous

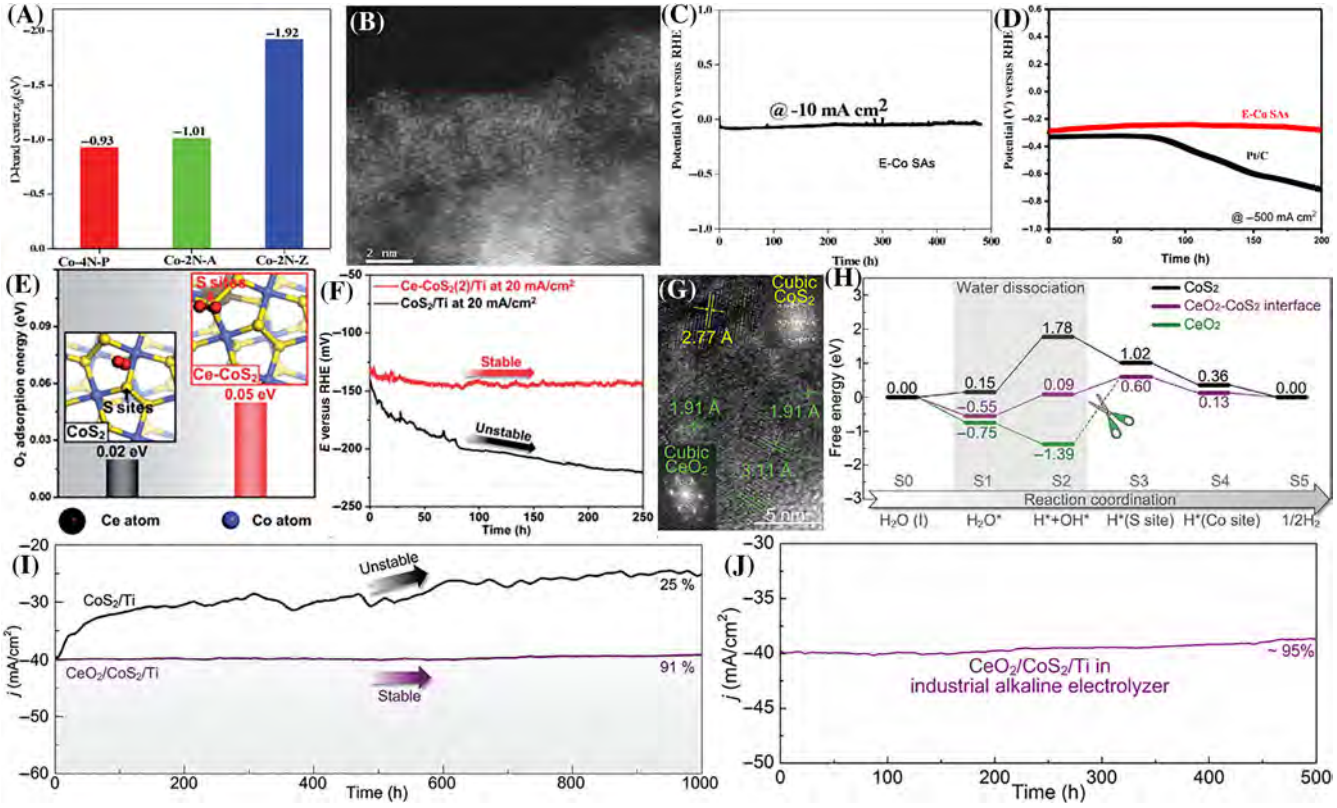

FIGURE 11 (A) The d-band center of Co-4N-P, Co-2N-A, and Co-2N-Z systems. (B) HAADF-STEM image of the E-Co SAs. (C) Time-dependent overpotential curve of E-Co SAs obtained at 10 mA cm^{-2} in 1 M KOH. (D) Stability test at 500 mA cm^{-2} for 200 h. Reproduced with permission.[164] Copyright 2021, Wiley-VCH. (E) O_2 adsorption energy on the S sites adjacent to Ce for Ce-CoS_2. (F) Time–overpotential profiles at 20 mA cm^{-2} in 1 M KOH. Reproduced with permission.[165] Copyright 2019, The Royal Society of Chemistry. Physical characterization and electrochemical test of CeO_2/CoS_2/Ti. (G) High-resolution TEM image. (H) Calculated free energy diagram for HER. (I) Catalytic durability at 40 mA cm^{-2} in 1 M KOH. (J) Catalytic durability through a time-overpotential profile in 1 M KOH at 60 °C. Reproduced with permission.[163] Copyright 2021, Wiley-VCH

structure, which facilitates charge transfer (Figure 12F–H).[167] CoFePO kept more than 90% of the initial current density after 100 h of stability testing under 1 M KOH (Figure 12I). Besides Ga, Fe cations, O anion doping, Cu, V, Ni, Mn, Zn, and Ce cations and carbon (C), sulfur (S), and nitrogen (N) anions are all efficient dopants to cobalt-based phosphides for modulating electronic structure, improving activity and stability, which have been summarized in the following table. To achieve industrialization, self-supporting electrodes with larger active areas are needed. The porous cobalt phosphide foam based on cobalt foam (Porous Co-P) prepared by Li et al. by a three-step method (Figure 12J) can operate continuously at high currents of 1000 mA cm^{-2} for 3000 h with only a little attenuation (Figure 12K).[162] In terms of cobalt-based nitrides, oxides, and selenides, their stability is less studied because the inherent defects lead to shorter lifetimes, so they are only summarized in the table.

For cobalt-based electrocatalysts in HER, the self-supporting electrodes prepared with cobalt foam show extraordinary stability (3000 h) and long-lasting activity in acidic and alkaline solutions. Therefore, to better market them, the cobalt foam is a promising substrate and valuable to be continually studied, on which the stability of the loadings can be adjusted using novel strategies. In addition, the cationic and anionic doping of cobalt-based catalysts can change the material's electronic structure and coordination environment, which allows for an in-depth analysis of strategies to improve stability.

4.2.3 | Molybdenum-based

Molybdenum (Mo) is an element of the VI B group with atomic number 42. From the volcano diagram in Figure 2C, it is clear that Mo adsorbs H strongly, which is not conducive to H desorption and thus limits the catalytic activity and stability. Table 7 summarizes recent advances in the durability of Mo-based catalysts for HER. Most of the works have improved the electronic structure

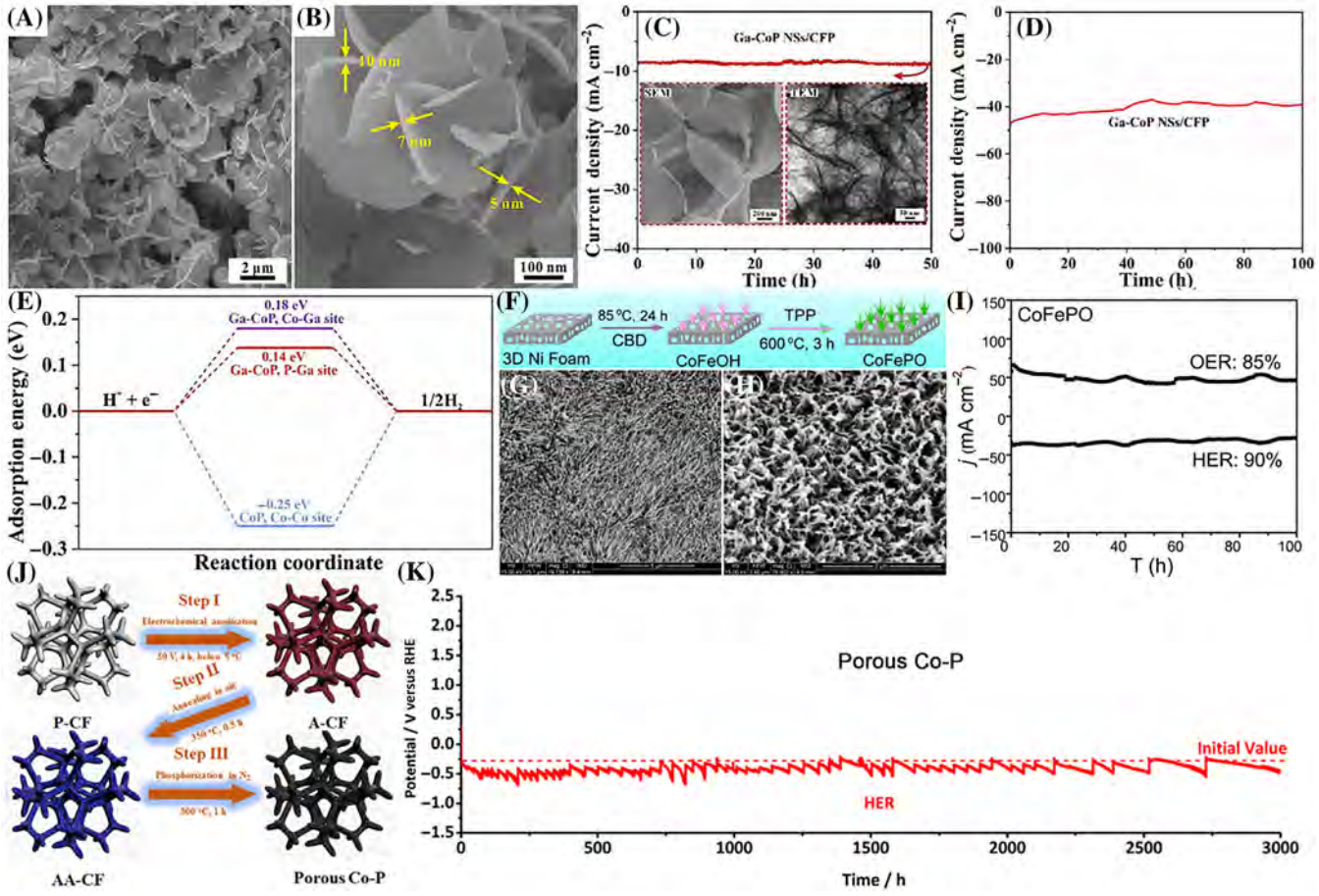

FIGURE 12 Morphological characterization and electrochemical stability testing of Ga-CoP NSs. (A) Low-magnification SEM. (B) High-magnification SEM. (C) *I–t* curve at 10 mA cm^{-2} in 1 M KOH. (D) *I–t* curve at 50 mA cm^{-2}. (E) Adsorption energy diagram for H adsorption on the surface of pure CoP and Ga-CoP. Reproduced with permission.[168] Copyright 2022, Elsevier. Synthetic path and morphological characterization of CoFePO. (F) The synthesis procedure. (G-H) Field Emission-SEM. (I) Chronoamperometric response of CoFePO tested for 100 h in 1 M KOH. Reproduced with permission.[167] Copyright 2016, American Chemical Society. (J) Synthesis Procedure for Porous Co-P Foam Electrode. (K) Chronopotentiometric curve of porous Co-P recorded at a constant current density of 1000 mA cm^{-2} in 1 M KOH. Reproduced with permission.[162] Copyright 2020, American Chemical Society

by introducing nonmetallic atoms to form Mo-based sulfides, selenides, phosphides, borides, nitrides, carbides, and so on, to make Mo-based compounds with neither solid nor weak hydrogen adsorption free energies.[187] Molybdenum disulfide (MoS_2), a typical 2D layered material, is considered a strong candidate for replacing precious metal Pt-based catalysts due to its excellent HER activity. However, the stability of MoS_2 without further modification only lasts about 5–20 h. The active sites of MoS_2 in HER activity usually come from its edges, and Zhu et al. activated the monolayer MoS_2 basal plane by introducing structural domain boundaries (including 2H–2H structural domain boundaries and 2H–1T phase boundaries [PB]).[182] The 2H–2H structural domain boundaries can be obtained by Ar plasma treatment under different times with different densities of 2H–1T. The sample treated for 40 s can be continuously stabilized for 200 h without significant decay at an overpotential of 150 mV (Figure 13A). DFT calculations revealed the Gibbs free energies of the adsorbed H on 2H–1T PB and various other models; it showed that PB exhibited $\Delta G_{H^*} = -0.13$ eV, very close to zero, indicating the most active HER (Figure 13B). More appealingly, catalysts with composite boundaries can be easily scaled up, as shown in Figure 13C, where a 4-in. wafer-scale catalyst. So far, strategies such as defect engineering, functional group modification, and the presence of heterostructures of different phases (1T and 2H phase) have been used to improve the activity and stability of MoS_2. Still, none of them can substantially enhance the stability of the material.

Mo-based carbides (MoC, Mo_2C) have emerged as a promising HER catalyst due to their similar d-band

TABLE 7 Summary of hydrogen evolution reaction (HER) durability with Mo-based catalysts under different reaction conditions

Catalyst	Electrolyte	η_{10} (mV) or mA cm^{-2}@mV	Stability			References
			CA/Retention (mV@h@%)	CP/Retention (mA cm^{-2}@h@%)	CV/(cycles) (cycles@%)	
LSC/K-$MoSe_2$	1 M KOH	68	-	100@2500@-(Overall Water Splitting)	-	[180]
MoC-Mo_2C-790	0.5 M H_2SO_4/ 1 M KOH	114/98.2	150@1000@-/ 150@1000@-	-	-	[181]
Multi-hierarchy MoS_2	0.5 M H_2SO_4/ 1 M KOH	136/176	150@200@-	-	-	[182]
MoC@NC	0.5 M H_2SO_4	300@270	-@70@-	-	-	[183]
α-MoB_2	0.5 M H_2SO_4	149	500@60@-	-	15 000@-	[45]
A-MoP@PC	0.5 M H_2SO_4/ 1 M KOH	68/67	-@40@-/-@40@-	-	3000@-/-	[184]
MoN-NC	0.5 M H_2SO_4	62	66@16.7@97%	-	3000	[185]
MoP/NPG	0.5 M H_2SO_4/ 1 M KOH/ 1 M PBS	219/126/150	180@60@-/ -@12@-/-@30@-	-	3000@-/3000@-/ 3000@-	[186]

electronic structure to Pt. Liu et al. electrodeposited MoC-Mo_2C heterojunction layer on a Mo sheet and formed a self-supporting electrode (MoC-Mo_2C-790) with 3D hierarchical honeycomb-like nanostructure by using molten salt electrolysis (Figure 13D).[181] The MoC-Mo_2C-790 heterojunction exhibits the smallest value of $|\Delta G_{H^*}|$, indicating its better HER activity (Figure 13E). As shown in Figure 13F, MoC-Mo_2C-790 can maintain strong vitality for 1000 h at small current densities in acidic (36 mA cm^{-2}) and alkaline solutions (30 mA cm^{-2}). Even better, the stability of the MoC-Mo_2C-790 tested at high current densities of 100, 200, and 500 mA cm^{-2} in 0.5 M H_2SO_4 and 1 M KOH kept 400 h, respectively. Also, it can be stabilized for 50 h (500 mA cm^{-2}) at 70°C under alkaline conditions. The above 2400 h were tested with the same electrode, after which a comparison of the LSV curves before and after stability was performed and found no degradation, demonstrating superb stability (Figure 13G). Cheng et al. combined molybdenum carbide-based nanoribbons with nitrogen-doped crystalline carbon nanolayers (MoC@NC nanoribbon) that could be stabilized in acidic electrolytes for 70 h with negligible attenuation.[183]

Mo-based sulfides and carbides with excellent activity have harvested much attention.[181,188] The interface inertness of MoS_2, where the main active site is the marginal S-site, is enhanced by functional group modification, defect engineering, and increasing the content of 1T MoS_2, thereby enhancing the activity and stability.[18] Similarly, the synthesis of Mo-based catalysts on Mo sheets can exhibit long-lasting stability in self-supporting structures such as NF and cobalt foam. Therefore, it is feasible to explore Mo sheets as self-supporting support possibilities.

4.2.4 | Others and TM mixed-based

Table 8 summarizes recent advances in the durability of others and TM mixed-based catalysts for HER. Other TMs such as iron (Fe), tungsten (W), copper (Cu), vanadium (V), manganese (Mn), and tantalum (Ta) have also been used to investigate their potential in HER stable catalysts. HER catalysts for these TMs have been studied mainly based on their monomers, phosphides, sulfides, selenides, and carbides, or further modified by doping with nonmetallic or TM elements. The HER stability of Fe-based, W-based, Cu-based, V-based, and Mn-based composites has not improved significantly, mostly remaining around 20 h. Therefore, much research is still needed to modulate the electronic structure and ΔG_{H^*} of the materials to obtain highly stable electrocatalysts. Liu and coworkers reported a monolithic catalyst (Ta-TaS_2 MC) by preparing a type of disulfide metal (e.g., tantalum sulfide) bound vertically to the same conductive substrate of tantalum metal (Ta foil) through strong covalent bonds (Figure 14A).[44] The presence of covalent bonds eliminates catalyst peel-off problems at high current density operation and provides strong mechanical stability. And ΔG_{H^*} of Ta-TaS_2 MC is close to Pt. It has a near-zero resistance interface, resulting in excellent HER durability and an overpotential of

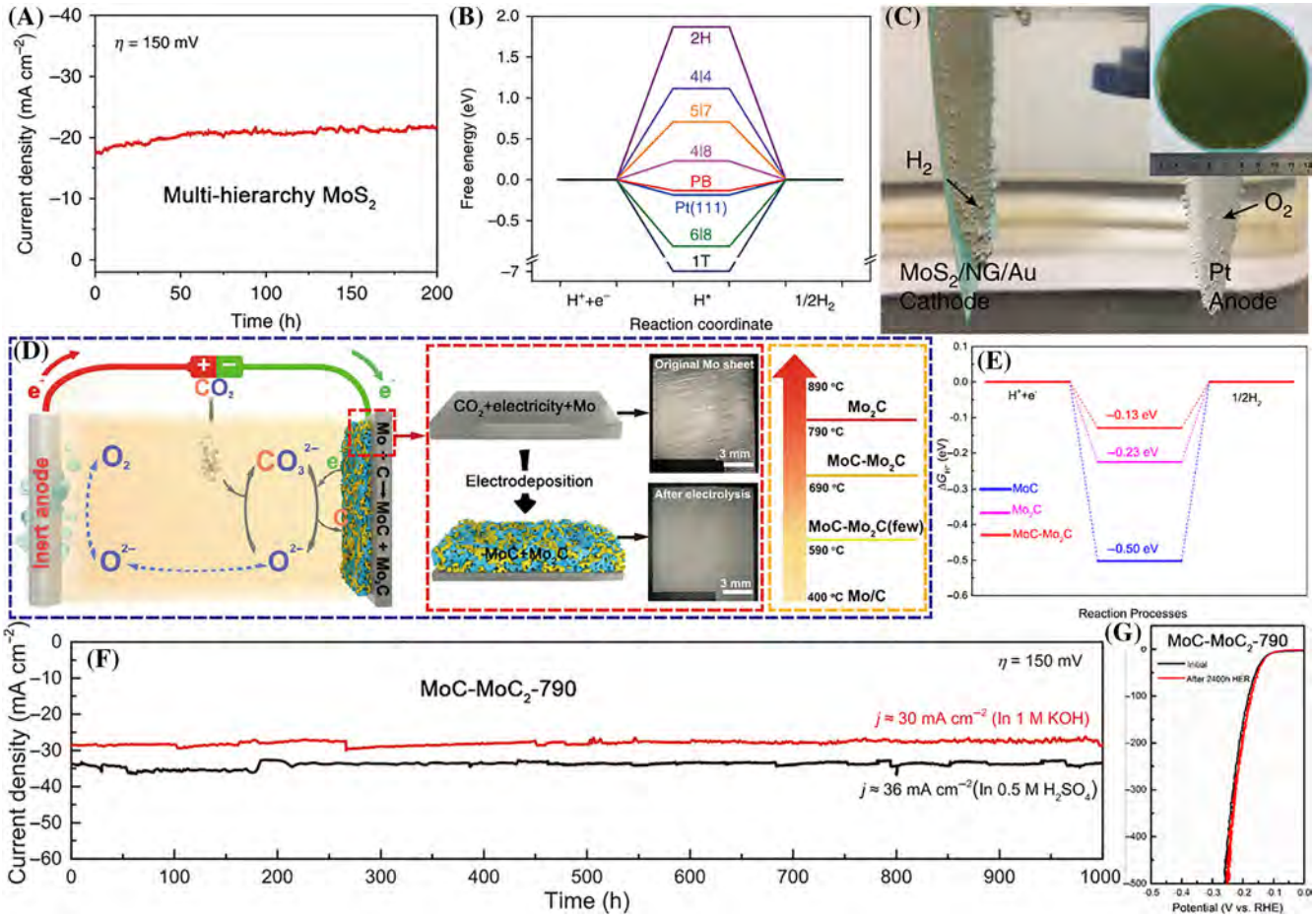

FIGURE 13 (A) *I–t* curve of a multi-hierarchy MoS_2 catalyst under the overpotential of 150 mV in 0.5 M H_2SO_4. (B) A comparison of the Gibbs free energies of the adsorbed H on 2H–1T-phase boundaries (PBs) and other samples. (C) Digital photograph of HER of multi-hierarchy MoS_2 catalyst under acidic electrolyte. Inset: Picture of multi-hierarchy MoS_2 catalyst with a diameter of 4 inches. Reproduced with permission.[182] Copyright 2019, Springer Nature. (D) Schematic diagram of MoC-Mo_2C-790 prepared by molten carbonate and digital photos of Mo electrodes before and after electrolysis. (E) Calculated ΔG_{H^*} diagram of the HER in acid electrolyte. (F) The long-term electrolysis stability test of MoC-Mo_2C-790 at $\eta = 150$ mV in 0.5 M H_2SO_4 and 1 M KOH. (G) LSV polarization curves before and after 2400 h stability test. Reproduced with permission.[181] Copyright 2021, Springer Nature

398 mV, reaching the industry-required current density of 2000 mA cm^{-2}. More importantly, it can continue to work for 200 h at a high current density under 0.5 M H_2SO_4 with negligible decay (Figure 14B). Such MC can also be produced on a large scale, which shows a 35 cm^2 Ta-TaS_2 MC catalyst with similar morphology of various parts after SEM observation (inset of Figure 14B).

The construction of binary TM-based compound materials (e.g., alloys, sulfides, borides, phosphides, selenides, oxides, hydroxides, and nitrides) is another strategy to improve electrocatalytic performance and longevity. Bimetallic alloys are promising candidates to replace Pt catalysts due to their high electrical conductivity, low price, and good structural stability, such as FeCo alloys,[222] NiMo alloys,[201] NiCu alloys,[223] and so on. NiMo alloys are of great interest due to their inherent excellent HER activity. However, in work by McKone et al., after 100 h of continuous operation at 2 M KOH, HER activity decayed more severely, mainly because of the easy leaching of Mo elements, which leads to material activity loss.[224] Our group adsorbed various amines (ethylamine-EA, ethylenediamine-EDA, dodecylamine-DDA, hexanediamine-HDA, and 1,12-dodecanediamine-DDDA) on the surface of NiMo alloys to investigate the surface characteristics of the material.[201] When modified on the NiMo alloy surface, EDA not only reduced the charge transfer resistance, but also modulated the electronic structure of the active interfacial sites, which significantly increased the HER activity (Figure 14C). It could operate stably for 100 h at a high current density of ~70 mA cm^{-2} upon overpotential of 300 mV (Figure 14D). The bimetallic oxide-spinel structure is used for electrocatalytic HER because of the bimetallic atoms' synergistic effect and structural stability. However, since the oxides

TABLE 8 Summary of hydrogen evolution reaction (HER) durability with others and transition metal mixed-based catalysts under different reaction conditions

Catalyst	Electrolyte	η_{10} (mV) or mA cm^{-2}@mV	Stability			References
			CA/Retention (mV@h@%)	CP/Retention (mA cm^{-2}@h@%)	CV/(cycles) (cycles@%)	
Ta-TaS_2 MC	0.5 M H_2SO_4	2000@398	-@200@-	-	20 000@-	[44]
N-WC nanoarray	0.5 M H_2SO_4	193	144@10@97.1% + 156@10@98.1%	-	-	[189]
WS_2 MSLs	0.5 M H_2SO_4	60	200@20@-	-	-	[190]
$Cu_2O_xS_{1-x}$/Cu	1 M KOH	40	113@12@-	-	1000@-	[191]
FeP_x/Fe-N-C/NPC	0.5 M H_2SO_4/ 1 M KOH	75/182	-	-	2000@-/-	[192]
FeP/Ti	0.5 M H_2SO_4/1 M KOH	79/95	-@10@-/-@10@-	-	-	[193]
N-$NiCo_2S_4$	1 M KOH	41	50@1000@68.2%	-	-	[194]
Ni-Mo-B HF	1 M KOH	68@50	1.8 V@300@- (OWS)	-	500@-	[195]
MoO_x/Ni_3S_2/NF	1 M KOH	106	110@200@-	-	10 000@-	[196]
P-NiMoHZ	1 M KOH	23	-	1000@200@-	-	[197]
$NiCo_2O_4$/Cu_xO/Cu	1 M KOH	92	-@150@-	-	500@-	[198]
$CN_{Ni2P/CoP-150}$	0.5 M H_2SO_4	160	-	10@120@-	5000@-	[199]
WO_3/C@CoO/NF	1 M KOH	55	-	10@110@-	2000@-	[200]
NiMo-EDA	1 M KOH	72	350@100@-	-	-	[201]
NiFe LDH@NiCoP/ NF	1 M KOH	120	-	10@100@-	-	[202]
FeS_2/CoS_2 NSs	1 M KOH	78.2	-	10@80@93.5%	20 000@-	[203]
FeCoNi–HNTAs	1 M KOH	58	326@80@-	-	-	[204]
VN/Co-NC	0.5 M H_2SO_4/1 M KOH/1 M PBS	22/44/163	-@75@-/- @75@-/-@70@-	-	1000@-/1000@-/ 1000@-	[205]
$Zn_{0.30}Co_{2.70}S_4$	0.5 M H_2SO_4/1 M KOH/1 M PBS	89/85/90	100@60@-/-/-	-	1000@-/-/-	[206]
MoS_2–Ni_3S_2 HNRs/ NF	1 M KOH	98	150@50@-	-	10 000@-	[207]
a-$CoMoP_x$/CF	1 M KOH	59	-	100@50@-	-	[208]
$CoNiSe_2$@CoNi-LDHs/NF	1 M KOH	106	200@50@-	-	10 000	[209]
Ni-CoP/Co_2P@NC	1 M KOH	117	-@50@-	-	-	[210]
$(Fe,Ni)_3P$/NiCoP	0.5 M H_2SO_4/1 M KOH/1 M PBS	50.9/52.3/70.5	-	50@50@-/50@50@-/ @20@50@-	-	[211]
$CePO_4$/MoP/CC	1 M KOH	48	55@35@-	-	5000@-	[212]
W_2C-$Ni(OH)_2$	1 M KOH	60	-	10@20 + 100@10@-	-	[213]
$CoNiMoO_4$-21/ CuO_x/CF	1 M KOH	46	-	10@28@-	1000@-	[214]
CC/MOF-$CoSe_2$@$MoSe_2$	1 M KOH	109.87	111@24@-	-	-	[215]
$MnCo_2O_4$@Ni_2P	1 M KOH	57	-	10@20@-	-	[216]

TABLE 8 (Continued)

Catalyst	Electrolyte	η_{10} (mV) or mA cm^{-2}@mV	Stability			References
			CA/Retention (mV@h@%)	CP/Retention (mA cm^{-2}@h@%)	CV/(cycles) (cycles@%)	
CoV/CF-CWs	1 M KOH	118	-	20@20@-	-	[217]
FeNiP/MoO_x/$NiMoO_4$/NF	1 M KOH	100@97	100@20@-	-	-	[218]
$1T_{0.81}$-MoS_2@Ni_2P	0.5 M H_2SO_4/1 M KOH	38.9/95	-@16@-	-	-	[219]

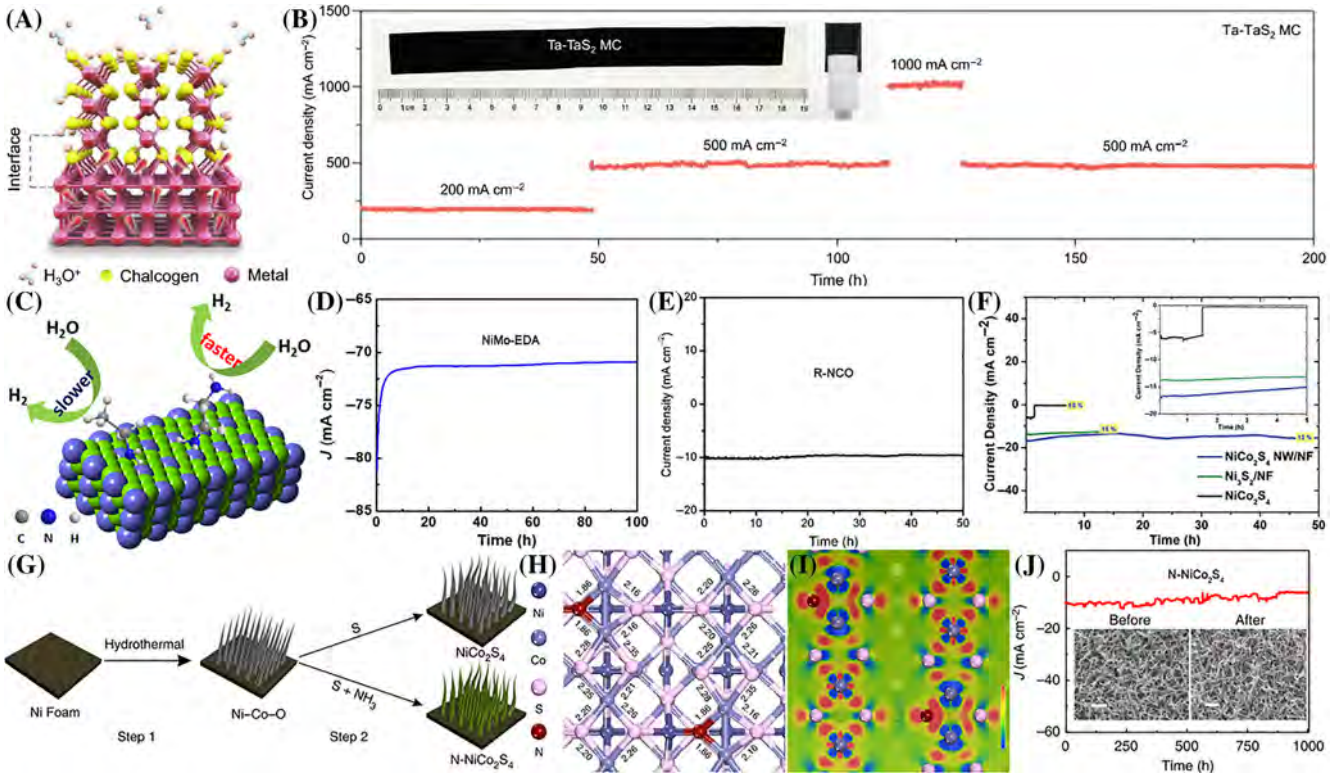

FIGURE 14 (A) Atomic structure of the Ta-TaS_2 MC. (B) *I–t* curves of the Ta-TaS_2 MC at 200, 500, and 1000 mA cm^{-2} in a 0.5 M H_2SO_4 electrolyte. Inset is a photograph of self-supporting electrode Ta-TaS_2, about 35 cm^{-2}. Reproduced with permission.[44] Copyright 2021, Springer Nature. (C) Surface modification scheme of NiMo nanoparticles with EDA. (D) The durability test of NiMo-EDA under the overpotential of 300 mV in 1 M KOH. Reproduced with permission.[201] Copyright 2017, American Chemical Society. (E) The stability test of R-NCO with a constant voltage of 0.135 V in 1 M KOH. Reproduced with permission.[220] Copyright 2018, American Chemical Society. (F) Time-dependent current density curves of $NiCo_2S_4$ NW/NF at a static potential of −0.323 V versus RHE for 50 h, in 1 M KOH. Reproduced with permission.[221] Copyright 2016, Wiley-VCH. (G) Schematic diagram of the preparation of N-$NiCo_2S_4$. (H) The top-view structures of N-$NiCo_2S_4$ (100). (I) The top-view electron density difference of N-$NiCo_2S_4$ (100), ranging from −0.1 to 0.1. (J) *I–t* curves of N-$NiCo_2S_4$ recorded for 1000 h at 50 mV versus RHE in 1 M KOH. Inset is the SEM images for N-$NiCo_2S_4$ before and after the stability test, and the scale bar is 1 μm. Reproduced with permission.[194] Copyright 2018, Springer Nature

themselves are sluggish for H_2 production, the catalyst surface state and electronic structure are usually improved by modulating the morphology and composition to achieve catalyst modification and give strong HER stability. Replacement or adding cations or forming oxygen vacancies to improve charge transport, to adjust ΔG_{H^*} and hydrolysis ability are all the main strategies to achieve excellent HER in spinel structures. Huang et al. found that zirconium (Zr) doping into $CoFe_2O_4$ could modulate the nanosheet morphology

and electronic structure around the Co and Fe sites, thus optimizing the adsorption energy and effectively improving the intrinsic activity of the active sites.[225] Peng et al. prepared oxygen-defect-rich $NiCo_2O_4$ (R-NCO) by reduction treatment, which can be continuously stabilized at an overpotential level of 135 mV for 50 h in 1 M KOH, demonstrating good stability (Figure 14E).[220] To further prolong its stable operating time, replacing oxygen with a less electronegative element (S, P, Se, B, N, etc.) is an appealing strategy. $NiCo_2S_4$ has the advantages of excellent electrical conductivity and hybridized d orbitals. The one-dimensional (1D) Ni nanowire arrangement grown on NF ($NiCo_2S_4$ NW/NF) can be continuously stabilized for 50 h in 1 M KOH solution (Figure 14F).[221] However, the catalytic activity and stability remain unsatisfactory, mainly owing to the strong interaction between the adsorbed H (H*) and the highly electronegative sulfur sites, which significantly hinders the desorption of H* to produce free H_2. Wu et al. used N as a modulator to change the surface electron density and d-band centers of $NiCo_2S_4$ (N-$NiCo_2S_4$), and this increased its activity to the level of Pt catalysts (Figure 14G).[194] As shown in Figure 14H,I, DFT theoretical calculations reveal that the electrons of the metal atom tend to flow more toward the N atom due to the presence of the N dopant, forming a robust Co—N bond, resulting in a more negative charge for the N and a lower electron density for the metal. Although the increase in electron density around the N site makes H* less susceptible to desorption and acts as a sacrificial site, the opposite electron density nearby the S atom favors the desorption of H*. Coupled with the presence of N dopant, which also facilitates the HO–H cleavage in water molecules, N-$NiCo_2S_4$ can maintain 68.2% activity after 1000 h of continuous operation at an overpotential of 50 mV under 1 M KOH (Figure 14J). Besides, the substitution by B elements also exhibits excellent structural and electrochemical stability. For example, Liu et al. prepared monolithic Ni-Mo-B HF catalysts that can sustain the water electrolysis at high current densities of 450 mA cm^{-2} for 300 h (Figure 15A) and even at ultra-high current densities of 1, 2, and 5 A cm^{-2} for 170, 54, and 20 h each in alkaline electrolytes (insets of Figure 15A).[195] The optical photo of H_2 bubbles attached to Ni-Mo-B HF revealed that their H_2 bubble diameters were much smaller than those on pure NF. The small stretching force generated by the small bubbles will minimize the damage to the electrode and thus prolong the life of the electrode (Figure 15B,C).

Hybridization of two or more TM-based composites to form heterostructures is also an attractive strategy to obtain long-term HER electrocatalysts resulting from the enhanced charge transfer and modulated the electronic structure in the interface of heterostructures. Most hybrid catalysts are grown on self-supporting electrodes, like NF and copper foam (CF). These porous metal foam structures facilitate the desorption of hydrogen gas bubbles, resulting in HER catalysts that can operate at high current densities for long operational lifetimes. Wu et al. used hydrothermal vulcanization to grow hollow MoO_x/Ni_3S_2 composite microspheres on NF (MoO_x/Ni_3S_2/NF) with a high catalytically active exposure sites density.[196] The Tafel slope value of MoO_x/Ni_3S_2/NF indicates that its HER proceeds through the Volmer–Heyrovsky mechanism (Figure 15D), while Ni_3S_2/NF follows the Volmer step, indicating that the presence of MoO_x changes the reaction mechanism and facilitates the electrochemical adsorption of hydrogen atoms. MoO_x/Ni_3S_2/NF can continue to operate at a constant current density of 15 mA cm^{-2} for 200 h (Figure 15E). The structural stability is also proved by the SEM, TEM, XPS, and other physical characterizations. Zhang et al. prepared ultrathin NiFe LDH with NiCoP nanowires on NF (NiFe LDH@NiCoP/NF) through a three-step hydrothermal-phosphorylation-hydrothermal process (Figure 15F), and this 3D hierarchical heterogeneous structure is beneficial for H_2 release and fast charge transfer.[202] It can operate continuously for 100 h at 10 mA cm^{-2} in 1 M KOH (Figure 15G). Morphology modulation can also increase its specific surface area and the number of active sites, improve hydrophilicity, and enhance stability. Octopus tentacle-like tungsten oxide and carbon-coated cobalt oxide (Ar/H_2-treated WO_3/C@CoO) catalysts on NF (Figure 15H) benefit from their special morphological effect to accelerate the HER and the release of H_2.[200] In the long-term test at 10 mA cm^{-2}, CoO only lasted 40 h with severe decay, while Ar/H_2-treated WO_3/C@CoO still had high catalytic activity after 100 h of operation (Figure 15I,J). The SEM image after the stability test shows that the structure remains intact and has good structural stability (Figure 15K). Ouyang et al. obtained NiCo precursors by low-temperature hydrothermal growth on chemically etched CF ($Cu(OH)_2$/Cu), followed by calcination in the air to obtain $NiCo_2O_4$/Cu_xO/Cu with a large specific surface area and abundant reaction channels (Figure 16A,B).[198] $NiCo_2O_4$/Cu_xO/Cu can operate continuously in an alkaline solution for 150 h, and the activity retention rate is much better than that of precious metal catalysts (Figure 16C). The robust stability comes from the strong chemical bond between Cu_2O and $NiCo_2O_4$ (the binding energy is −40.6108 eV) and the inherent metallic properties of this heterojunction as shown in DOS calculations (Figure 16D,E). In addition to catalysts grown on self-supporting electrodes, preparing powder catalysts for HER is common. Jiao and colleagues combined self-assembled Ni/Co phosphide complexes

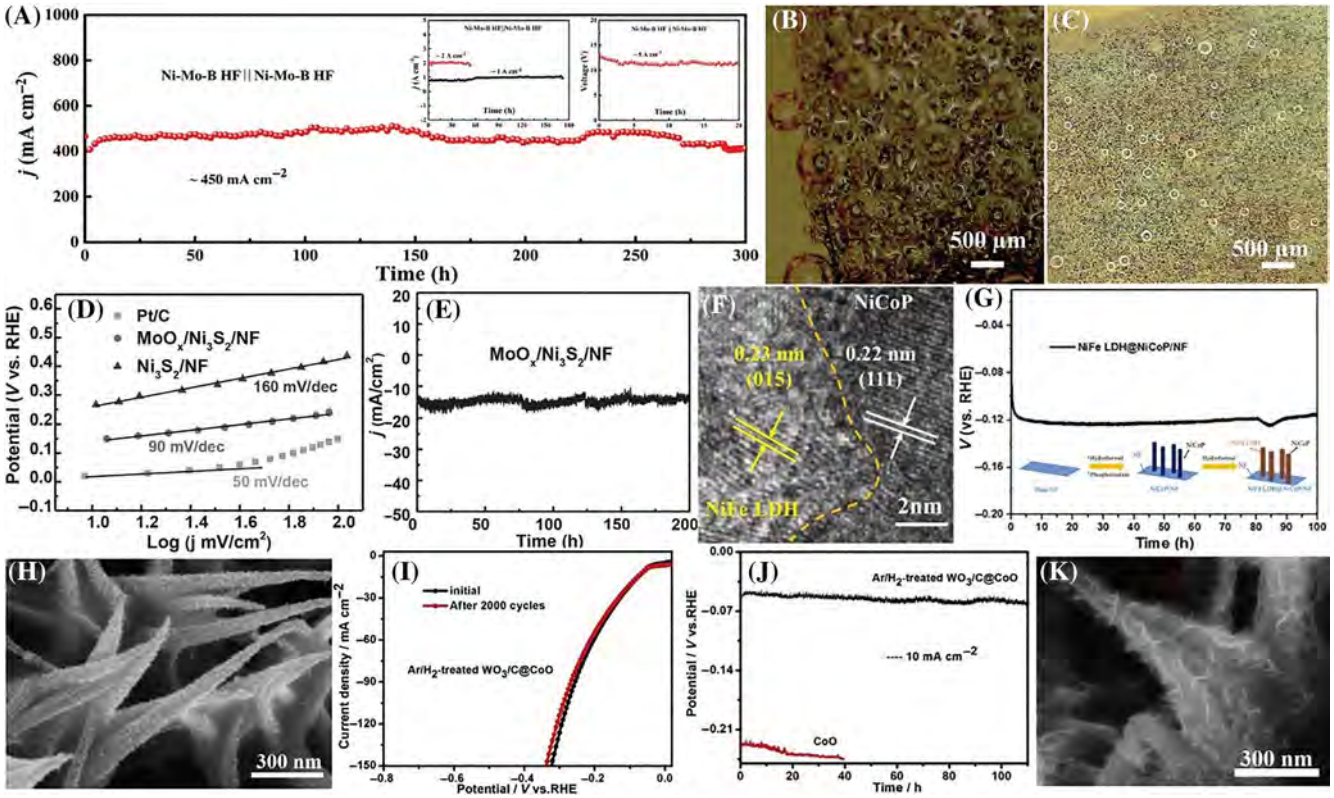

FIGURE 15 (A) The overall water splitting stability test of Ni-Mo-B HF at 450 mA cm^{-2} in 1 M KOH. Insets are the stability test at 1, 2, and 5 A cm^{-2}. Optical photos of H_2 bubbles attached to catalysts at low current density (20 mA cm^{-2}). (B) Pure nickel foam. (C) Ni-Mo-B HF. Reproduced with permission.[195] Copyright 2021, Wiley-VCH. Electrochemical testing of MoO_x/Ni_3S_2/NF. (D) Tafel plots. (E) *I–t* curve at an overpotential of 110 mV in 1 M KOH. Reproduced with permission.[196] Copyright 2016, Wiley-VCH. (F) HRTEM image of the NiFe LDH@NiCoP nanowire highlighting the interface between nanowire and nanosheets. (G) Long-term stability of the NiFe LDH@NiCoP/NF at 10 mA cm^{-2}. Inset is the synthesis route of electrodes. Reproduced with permission.[202] Copyright 2018, Wiley-VCH. Physical characterization and electrochemical testing of Ar/H_2-treated WO_3/C@CoO. (H) SEM image. (I) The LSV curves before and after 2000 cycles. (J) The chronopotentiometry curve at 10 mA cm^{-2}. (K) SEM image after the HER stability test. Reproduced with permission.[200] Copyright 2018, Elsevier

with nitrogen-doped carbon spheres ($CN_{Ni2P/CoP-150}$) by hydrothermal method (Figure 16F), exposing more HER active sites and suitable hydrogen adsorption and desorption energies.[199] Micron-sized carbon spheres encapsulated by Ni/Co phosphide complexes with uniform distribution of each element (Figure 16G–K). Given the morphological and compositional modulation, $CN_{Ni2P/CoP-150}$ showed no significant decline in activity after 120 h of long-term testing, demonstrating excellent stability (Figure 16L).

Other TM materials have been less investigated due to their unsuitable ΔG_{H^*}. However, ΔG_{H^*} is not the only standard to determine the activity of HER catalysts, especially the stability property. There are still catalysts with long-lasting stability even if they do not have a ΔG_{H^*} close to zero. So finding the factors influencing stability is a necessary step to take in future research. TM composite-based catalysts are among the strongest candidates to replace expensive Pt catalysts. Many transitions metal-based catalysts have excellent activity and stability. When two or more TM-based catalysts form heterojunction structures, the components interact with each other, dramatically accelerating the mass charge transfer and consolidating stability.

4.3 | Metal-free hydrogen evolution catalyst

In the past several years, to reduce the cost of catalysts, and decrease the environmental pollution caused by the release of metal ions, metal-free catalysts, especially metal-free carbon-based catalysts, have attracted much attention from researchers.[226] Until now, the activity and stability of most reported metal-free catalysts are relatively poor, so most of the main works aim to improve the HER activity of CNT, graphitic carbon nitride ($g\text{-}C_3N_4$), and graphene by doping nonmetallic elements,

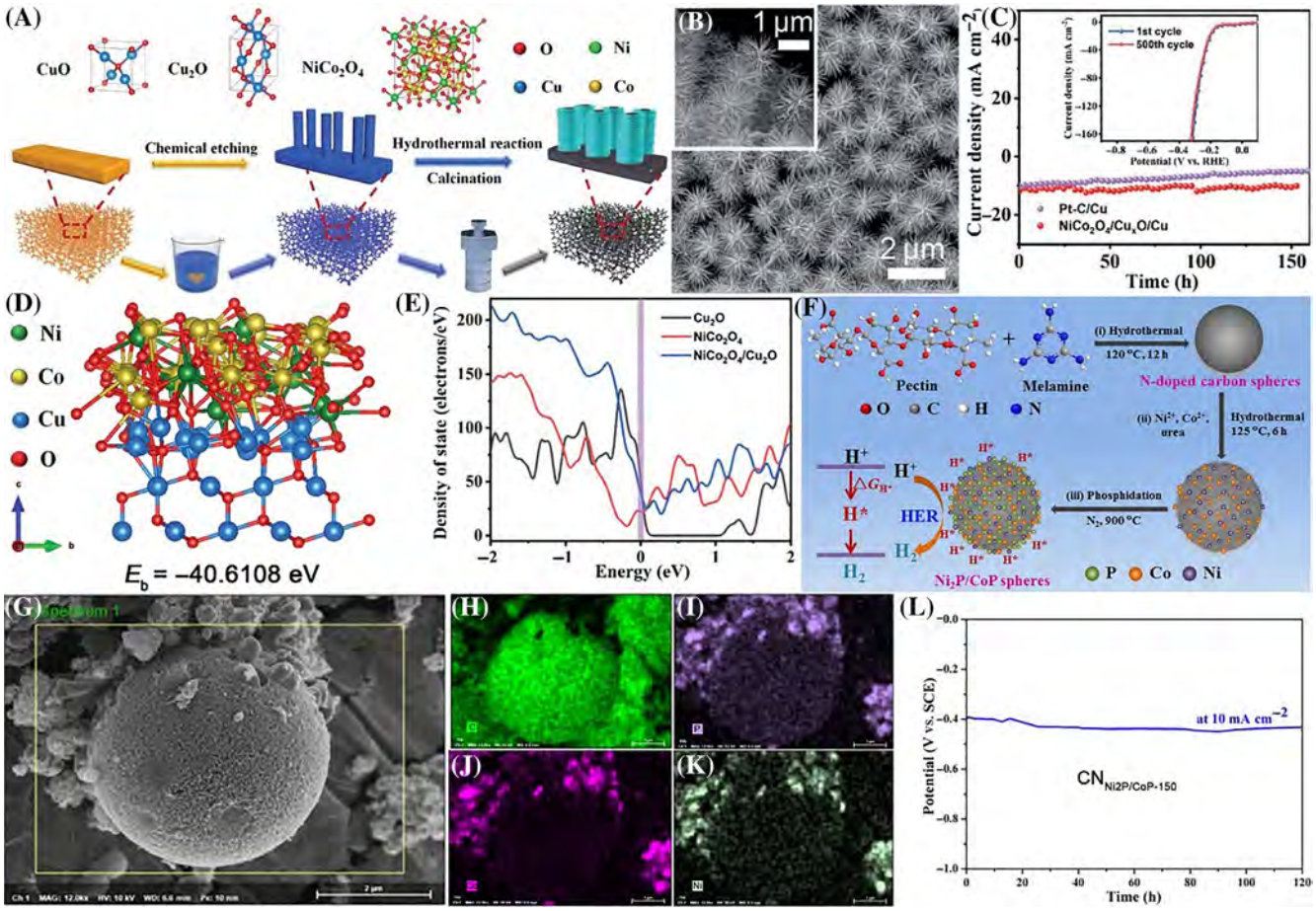

FIGURE 16 Preparation, characterization and electrochemical test of $NiCo_2O_4/Cu_xO/Cu$. (A) Schematic illustration. (B) SEM image. Inset is a SEM image in the side view. (C) Chronoamperometry curves at 10 mA cm^{-2} in 1 M KOH. Inset is LSV curves before and after 500 CV cycles. (D) DFT-optimized structure of $NiCo_2O_4/Cu_2O$ in the main view. (E) Calculated density of states. Reproduced with permission.[198] Copyright 2021, The Royal Society of Chemistry. (F) Schematic diagram of the preparation process of $CN_{Ni2P/CoP-150}$. (G–K) EDX images. (L) Voltage-time curve. Reproduced with permission.[199] Copyright 2020, Elsevier

combining various carbon materials to adjust the electronic structure.[227] However, very few articles emphasize the improvement of their stability. Some researchers have obtained high activity metal-free catalysts while maintaining good stability through ingenious design. Table 9 summarizes recent advances in the durability of metal-free catalysts for HER.

The preparation of metal-free carbon-based catalysts with large specific surface area and multiple electron transport channels has excellent potential for obtaining high stability catalysts. The g-C_3N_4 has low electron conductivity and low surface area, whereas graphene has a larger specific surface area and excellent electrical properties. Qu et al. prepared the three-dimensional (3D) interconnections by coupling 1D g-C_3N_4 with 2D graphene sheets (g-C_3N_4 nanoribbon-G).[242] This hierarchical architecture (Figure 17A) can promote the charge transfer from graphene to g-C_3N_4 and provide better transfer channels for reactants and products. As shown in Figure 17B, g-C_3N_4 nanoribbon-G showed only slight attenuation after a long-term cycle test of 54 000 s, which provided a promising future for preparing metal-free carbon-based catalysts with high stability. Such methods by combining two kinds of carbon materials are promising to create a more durable and stable metal-free carbon-based catalyst. For example, nitrogen-doped graphene is integrated with porous C_3N_4 to form a 3D flexible film,[243] sulfur and selenium co-doped graphene is coupled with g-C_3N_4,[244] carbon nanotubes and graphene hybrid,[245] and many other metal-free carbons are combined. However, these studies only improved the catalytic activity and did not significantly improve the stability. In 2019, A N-doped carbon framework derived from MOFs (MHCF) as electron acceptors, higher-Fermi-level pure CNTs as electron donors, and carboxyl-group-rich polymers as the surface modification was designed to form self-supporting nanoporous hybrid MHCF-CNTs@PEMAc membranes (Figure 17C,D).[230] As

TABLE 9 Summary of hydrogen evolution reaction (HER) durability with metal-free catalysts under different reaction conditions

Catalyst	Electrolyte	η_{10} (mV) or mA cm^{-2}@mV	Stability			References
			CA/Retention (mV@h@%)	CP/Retention (mA cm^{-2}@h@%)	CV/(cycles) (cycles@%)	
NS-500	0.5 M H_2SO_4	276	200@168@90%	-	1000@90%	[228]
O-SiBCN/rGO	0.5 M H_2SO_4	590	-	2.5 + 5 + 7.5@150@-	-	[229]
MHCFCNTs@PEMAc/CuF	0.5 M H_2SO_4/1 M KOH/1 M PBS	317/289/278	325@100@ ~ 95%/ 300@100@ ~ 95%/ 295@100@ ~ 95%	-	-	[230]
CNT@NPC-900	0.5 M H_2SO_4/1 M KOH/1 M PBS	167/304/440	167@100@-/ 304@100@-/ 440@100@-	10@100@-/ 10@100@-/ 10@100@-	3000@-/3000@-/ 3000@-	[231]
C_{60}-SWCNT$_{15}$	0.5 M H_2SO_4/0.1 M KOH/1 M PBS	320/380/329	350@80@-/-/ 350@80@91.2%	-	-	[232]
P-RPNPs	0.5 M H_2SO_4	218	500@50@-	-	6000@-	[39]
3DSG-Ar	0.5 M H_2SO_4	-	310@30@-	-	2000@-	[233]
SiO_2/PPy NTs-CFs	1 M PBS	-	300@30@-	-	-	[40]
NPCF	0.5 M H_2SO_4	248	103@20	-	2000	[234]
P-NSG	0.5 M H_2SO_4/1 M KOH	149/197	200@20@-/ 200@20@-	-	3000@-/3000@-	[235]
NPG900	0.5 M H_2SO_4	213	213@20@-	-	1000@-	[37]
NOPHC$_{10}$-900	1 M KOH	290	-@20@-	-	-	[236]
BCN-1	0.5 M H_2SO_4	70	-	20@24@83%	-	[237]
3DNG-P	0.5 M H_2SO_4/1 M KOH/1 M PBS	128/169/217	100@20@-/ 200@20@-/ 150@20@-	-	2000@-/2000@-/ 2000@-	[238]
EBP@NG	1 M KOH	191	-@16@ > 90%	-	-	[36]
NCN-1000-5	0.5 M H_2SO_4	90	150@3.3@-	-	500@-	[239]
30P-rGO-g-C_3N_4	0.5 M H_2SO_4	575	670@2	-	500@-	[240]
PNPC-900	0.5 M H_2SO_4	150	-@10@-	-	5000@-	[241]

illustrated in Figure 17E,F, the experimental data (XPS, Raman, and Kelvin probe force microscopy.) and calculated data (charge density) prove the electron transfer relationship between MHCF and CNT. And the PEMAc can locally enrich H^+ in acidic media and enhance water dissociation and activation in neutral and alkaline media. Through a combination of surface and dual electronic modulation strategies, the MHCF-CNTs@PEMAc maintains a retention rate of more than 95% after 100 h of stability testing in acidic, neutral, and alkaline solutions (Figure 17G). In addition to the combination of two different carbon materials, 2D/2D heterostructure (EBP@NG) was obtained by coupling the black phosphorus nanosheets (EBP) and nitrogen-doped graphene (NG) (Figure 18A).[36] And after 2 weeks, there was no significant aggregation, as evidenced by the Tyndall effect (Figure 18B). The activity remained more than 90% after 16 h of continuous test on overpotential at 10 mA cm^{-2} (Figure 18C). The superior stability is due to the difference in Fermi energy levels between EBP and NG. The electron interaction between them induces directional interfacial electron transfer and optimizes hydrogen adsorption and desorption (Figure 18D).

Besides coupling metal-free materials to improve their stability, anionic doping (single doping, co-doping, multi-doping, etc.) is also an efficient way to change the electronic structure of materials and obtain high stability catalysts. Anions include N, S, P, F, Se, and so on. Chen et al. prepared graphene by chemical vapor deposition (CVD) at different temperatures and synthesized nitrogen

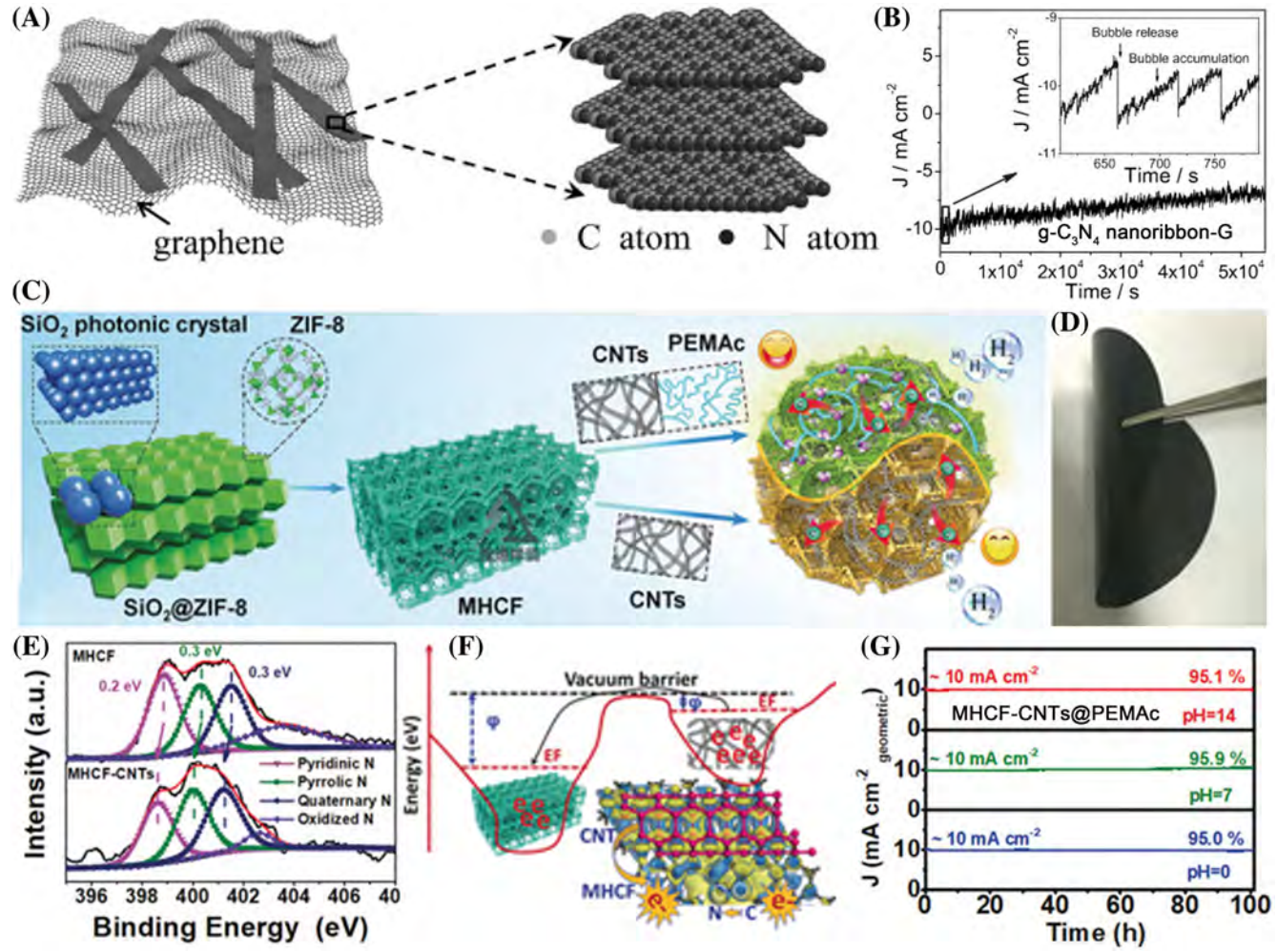

FIGURE 17 The g-C_3N_4 nanoribbon-G: (A) A possible structural model. (B) Time dependence of the current density at 200 mV versus RHE. Reproduced with permission.[242] Copyright 2014, Wiley-VCH. MHCF-CNTs@PEMAc: (C) The preparation process. (D) A photograph of the MHCF-CNTs@PEMAc membrane. (E) High-resolution N1s XPS spectra of MHCF and MHCFCNTs. (F) The interfacial charge separation and the charge density difference($\Delta\rho$) of the MHCF@CNTs model, where the yellow and blue regions represent net electron depletion and accumulation, respectively (top views of the adsorption sites). (G) Time-dependent current density curve of MHCF-CNTs@PEMAc under astatic overpotential of 325 mV (0.5 M H_2SO_4) 300 mV (1 M KOH) and 295 mV (1 M PBS) over 100 h. Reproduced with permission.[230] Copyright 2019, Wiley-VCH

and sulfur co-doped nanoporous graphene (NS-500 and NS-800) using pyridine and thiophene as N and S sources, respectively.[228] S and N co-doped not only introduce structural defects into the graphene lattice, but also provide a fast electron transfer path for HER due to the combination of the positively charged N dopants and the negatively charged S dopants at a lattice defect. Lower CVD temperatures increase N and S content in graphene, resulting in more defects with relatively weak hydrogen evolution stability. At a constant voltage of −0.2 V (vs. RHE), the NS-800 maintained 90% durability after 7 days, but the NS-500 had less than 70% (Figure 18E). The Raman spectra of NS-500 and NS-800 before and after the stability test indicated that graphene still had high crystallinity (Figure 18F), but NS-500 was not stable enough due to the excessive structural defects in the graphene lattice. There are also many studies worked on the effect of anion doping on the stability of HER in metal-free carbon-based materials, including N-doped ultrathin carbon nanosheets,[239] N and P dual-doped graphene,[246] N-doped porous carbon fibers,[234] P and N co-doped porous carbon,[241] S-doped graphene,[233] N and F dual-doped porous graphene-nanosheets[35] and N, S co-doped porous carbon.[247] However, the stability was not satisfied, indicating that although anionic doping can increase the stability of the material to some extent, it is not an optimal scheme, and there is a big gap compared with the stability of metal-containing catalysts. Therefore, the improvement of the stability of metal-free catalysts by anionic doping alone is limited, and a variety of

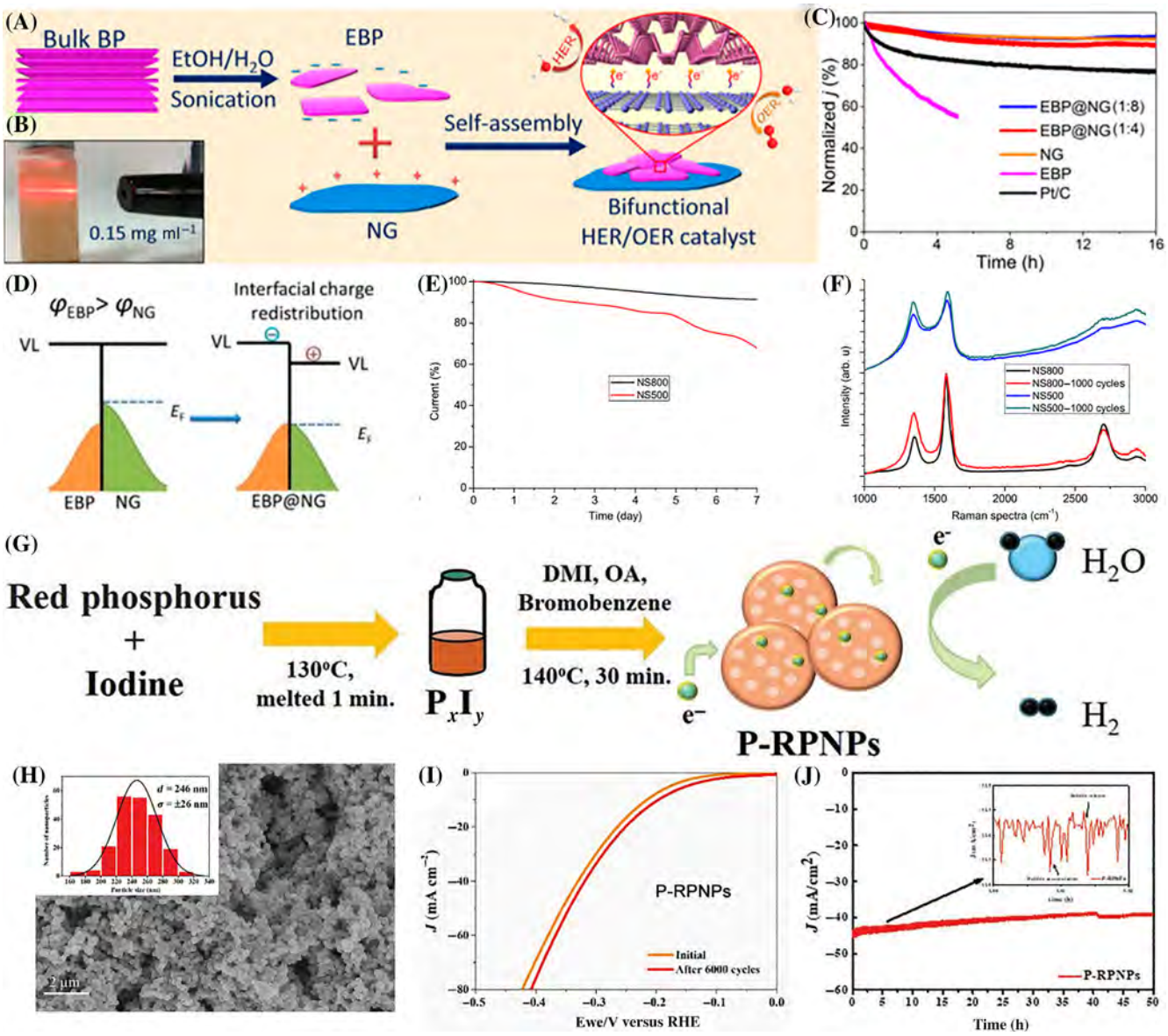

FIGURE 18 The EBP@NG catalyst: (A) Diagram of preparation process. (B) Photograph of an EBP dispersion with the concentration up to 0.15 mg ml^{-1}, showing a Tyndall effect. (C) Chronoamperometric curves of EBP@NG. (D) Illustration of interfacial charge redistribution between NG and EBP. Reproduced with permission.[36] Copyright 2019, American Chemical Society. NS-500 and NS-800: (E) HER activity. (F) Durability at −0.2 V. Reproduced with permission.[228] Copyright 2015, Wiley-VCH. P-RPNPs: (G) Diagram of preparation process. (H) SEM image, the inset shows the histograms of size distribution. (I) HER durability test at the voltage from 0.2 to −0.6 V for 6000 cycles in 0.5 M H_2SO_4. (J) Stability test at the current density of −0.5 V (vs. RHE) for 50 h. Reproduced with permission.[39] Copyright 2020, The Royal Society of Chemistry

promotion strategies should be combined to improve its stability and reduce the gap with the stability of metal-based catalysts.

In addition to the above carbon-based metal-free HER catalysts, Tuan et al. developed a one-pot thermal injection method to obtain porous red phosphorus nanoparticles (P-RPNPs) to act as HER electrocatalysts (Figure 18G).[39] P-RPNPs with an average diameter of 246 ± 26 nm (Figure 18H) exhibited excellent endurance and stability at 0.5 M H_2SO_4. The LSV curve of P-RPNPs after 6000 cycles CV (−0.6–0.2 V vs. RHE) is similar to the initial curve (Figure 18I), showing outstanding cyclic stability. At −0.5 V (vs. RHE), the performance of P-RPNPs only decayed a little after a long period of 50 h, showing superior durability, which is even better than the stability of metal-based catalysts described in some articles (Figure 18J). Therefore, metal-free catalysts have great prospects for development, but it is necessary to find appropriate strategies to obtain catalysts with high stability.

Therefore, metal-free catalysts have a promising future because of their high economic efficiency. Although less research has been carried out so far, it is still possible that metal-free catalysts can be intelligently designed to achieve long-lasting stability. The activity of metal-free catalysts is still distant from that of the precious metal and TM-based catalysts described previously. Still, it can be seen from Figure 3 that in the case of smaller attenuation, the longer the stability, the better the economy. So exploring new strategies to enhance metal-free carbon-based catalysts and expanding metal-free non-carbon-based catalysts will open up new avenues for HER catalysts.

5 | CHALLENGES AND PERSPECTIVES

Obtaining high-purity hydrogen by water electrolysis is currently the safest and most important way to meet the requirements of sustainable development. Therefore, developing high longevity HER catalysts is a compulsory way to pursue industrialization. This review systematically summarizes the different HER catalysts with various stability properties published in recent years, which are mainly classified into noble metal-based, TM-based, and metal-free catalysts. Noble metal-based catalysts have attracted much attention because of their moderate Gibbs hydrogen adsorption free energy, but their stability is inferior. To further improve the stability, a lot of research has been conducted to stabilize precious metals through alloying, strong metal support interactions, and spacing confinement, which has obtained improved catalysts that were initially stable for only a few hours to several hundred hours. Due to the low price and excellent HER activity, TM-based catalysts have been presented as a promising alternative candidate to noble metal-based catalysts. Numerous studies have shown that the activity of TM-based catalysts is comparable to that of noble metal catalysts. Still, the stability of these catalysts is also a big challenge. The cobalt-based self-supporting electrode exhibited a long-term continuous operation for 3000 h, further bringing TM-based HER catalysts closer to industrialization.[162] The activity and stability of metal-free catalysts are relatively poor. Still, since they are economical and efficient, many works have been devoted to improving their commercial possibilities through different strategies, such as doping metal-free carbon-based materials with nonmetallic elements, coupling with multiple carbon materials to increase active sites, and so on. In addition, other non-carbon-based metal-free catalysts have also been developed, and some progress has been made, such as the porous red phosphorus NPs with the maintained catalytic stability for 50 h.[39] The progress of metal-free catalysts brings hopes for their replacement of noble metals. From the above brief summary of noble metal based, TM based and metal free electrocatalysts, it is notable that TM based catalysts are a formidable competitor with the noble metal catalysts developed to date, but their activity still needs to be improved and therefore loading small amounts of noble metal onto long-life TM catalysts is a major strategy for their commercial application.

Whether precious-metal-based, TM-based, or metal-free HER catalysts, their stability has been significantly improved in recent years, but they are still far from industrial applications. In order to obtain more stable HER electrocatalysts, we propose the following perspectives.

1. Understanding the deactivation mechanism, dynamic interface, and catalytic mechanism of HER electrocatalysts under operating conditions at the atomic scale. So far, the majority of the state-of-the-art investigations focus on the design and synthesis of electrocatalysts with very high catalytic HER activity. The catalytic durability of those electrocatalysts is generally tested for a short period, far from the demands of practical applications. The deactivation mechanism of HER electrocatalysts under various electrolytes is seldomly explored in literature, limiting the further developments of HER electrocatalysts with high stability. Exploring the structure–composition–stability relationship at the atomic level requires the use of various advanced in-situ characterization techniques, such as TEM, XAS, XRD, ICP-MS, Raman, and other characterizations, to probe the actual active center and monitor the structural evolution of the catalysts during operation and to further reveal the intrinsic causes of degradation of catalytic stability. Also, since the dynamic tracking of the surface physicochemical properties of electrocatalysts under reaction conditions is still incomplete and insufficient to provide detailed information on the evolution of the catalyst surface, the sensitivity, response time, and data acquisition speed of the in situ operational characterization methods need to be improved. Understanding the dynamic changes of the electrocatalysts during the reaction process offers the opportunity to design new electrocatalysts with both high activity and stability.
2. Developing the latest theoretical calculation methodologies with experimentation to provide insights into the mechanism of HER electrocatalysts for activity and stability. Based on the experimental results, the stability mechanisms are explored in-depth with the help of theoretical calculations, such as DFT calculations that allow observing how different surfaces affect HER catalysis and what relationships exist

between the adsorption/desorption energies of water, protons, and hydroxyl ions and how they affect the final reaction rate. Thus, considering theoretical calculations and experimental results, advanced electrocatalysts can be adapted to overcome their stability challenges and extend their applications. However, in computational engineering, the theoretical model building must be strictly based on the structure of the real active center rather than the crystal structure of the original catalyst. In addition, pioneering computational methods such as big data analysis and computer-guided machine learning should be developed to analyze all possible models or structures and transformations.

3. Developing novel synthesis approaches for catalytically active electrodes with high mechanical strength and facile gas desorption. Mechanical fatigue after long periods of operation and stresses caused by the formation of large numbers of H_2 bubbles can significantly deteriorate the stability of the catalyst and make it irrecoverable. H_2 bubbles that are not quickly released from the catalyst surface can cover and drag the active sites, thus creating undesirable factors such as stress, reducing the number of active sites. The design of fatigue-resistant, hydrophilic, gas-hydrophobic materials that can rapidly desorb hydrogen is essential for improving stability.
4. Designing electrocatalysts capable of maintaining long-term stability at high current density. Industrial electrocatalysts require continuous and stable operation at high current densities, which can be achieved by designing the self-supporting electrodes. Nowadays, the main types of self-supported electrodes are NF, cobalt foam, Ti flakes, and carbon paper. In situ growth of active species on these highly conductive 3D substrates increases their conductivity and active surface area. It creates intimate contact with the collector to decrease charge transfer resistance, and the 3D morphology exposes more active sites. There is a growing trend to prepare self-supporting electrocatalysts as they can be used directly as working electrodes without any polymer binders, thus greatly improving conductivity and stability.
5. Long-term stability under "dirty" environments. So far, most of the current research for electrocatalytic hydrogen evolution is performed in water with high purity. The study of seawater or other "dirty" water resources in various impurities, including dust, microorganism, and corrosive ions (e.g., halogen, SO_4^{2-}), is also a critical step toward the large-scale and long-term operation. Some electrocatalysts currently show high stability in buffered electrolytes but are far from durable and corrosion-resistant in unbuffered electrolytes or seawater. The poor hydrogen production in "dirty" water is mainly attributed to microbial growth in the water that covers the active sites, corrosion by Cl^- ions, and other problems. Therefore, suitable membranes need to be prepared to address contamination and blockage by interfering ions and microorganisms and modifications to the catalyst surface to resist contamination and blockage to mitigate corrosion and improve hydrolysis stability.
6. Scale-up and the cost of large-area electrodes at an industrial scale are anticipated for their translation to plants. Developing cost-effective and scalable synthetic strategies is a prerequisite for moving toward industrialization. However, most synthetic processes are currently limited to the laboratory level. The electrocatalytic electrode with high surface areas is highly desired in practical applications. However, there are few fundamental and stability studies on the design and fabrication of electrodes with large size surfaces. Therefore, a deeper understanding of catalyst fundamentals and stability issues from the micro to macro scale should be gained.
7. The origins of the enhanced stability of electrocatalysts. Many factors influence catalyst stability and most of the published articles are based on different strategies to enhance specific factors. These factors include the inherent physical and chemical stability of the catalyst, hydrophilicity, aerophobicity, electrical conductivity, and the adhesion and dispersion of the catalyst when dispersed on the glassy carbon electrode. Combining multiple strategies to address multiple factors can make catalysts more commercially desirable.

ACKNOWLEDGMENTS

This work was financially supported by the National Natural Science Foundation of China (21872109). Authors also acknowledge the support from Fundamental Research Funds for the Central Universities (D5000210829 and D5000210601). This work was also financially supported by the Environment and Conservation Fund of Hong Kong SAR, China (No. ECF 2020-13).

CONFLICT OF INTEREST

The authors declare no conflict of interest.

ORCID

Johnny C. Ho https://orcid.org/0000-0003-3000-8794
Zhengfei Dai https://orcid.org/0000-0002-3709-8895
Yongquan Qu https://orcid.org/0000-0002-6202-1929

REFERENCES

1. Tang Z, Zhao S, Yang Y. Insight into structural evolution, active site and stability of heterogeneous electrocatalysts. *Angew Chem Int Ed*. 2021;61(11):202110186.

2. Zhu J, Hu L, Zhao P, Lee LYS, Wong KY. Recent advances in electrocatalytic hydrogen evolution using nanoparticles. *Chem Rev*. 2020;120(2):851-918.
3. McCrum IT, Koper MTM. The role of adsorbed hydroxide in hydrogen evolution reaction kinetics on modified platinum. *Nat Energy*. 2020;5(11):891-899.
4. Dresselhaus MS, Thomas IL. Alternative energy technologies. *Nature*. 2001;414(6861):332-337.
5. Chu S, Majumdar A. Opportunities and challenges for a sustainable energy future. *Nature*. 2012;488(7411):294-303.
6. Chu S, Cui Y, Liu N. The path towards sustainable energy. *Nat Mater*. 2017;16(1):16-22.
7. Subbaraman R, Tripkovic D, Strmcnik D, et al. Enhancing hydrogen evolution activity in water splitting by tailoring Li^+-$Ni(OH)_2$-Pt interfaces. *Science*. 2011;334(6060):1256-1260.
8. Zhu Y, Lin Q, Zhong Y, Tahini HA, Shao Z, Wang H. Metal oxide-based materials as an emerging family of hydrogen evolution electrocatalysts. *Energ Environ Sci*. 2020;13(10):3361-3392.
9. Yang H, Feng Z, Teng X, Guan L, Hu H, Wu M. Three-dimensional printing of high-mass loading electrodes for energy storage applications. *InfoMat*. 2021;3(6):631-647.
10. Xue K, Mo Y, Long B, et al. Single-atom catalysts supported on ordered porous materials: synthetic strategies and applications. *InfoMat*. 2022;4:12296.
11. Zahra R, Pervaiz E, Yang M, et al. A review on nickel cobalt sulphide and their hybrids: earth abundant, pH stable electrocatalyst for hydrogen evolution reaction. *Int J Hydrogen Energy*. 2020;45(46):24518-24543.
12. Zhou Z, Pei Z, Wei L, Zhao S, Jian X, Chen Y. Electrocatalytic hydrogen evolution under neutral pH conditions: current understandings, recent advances, and future prospects. *Energ Environ Sci*. 2020;13(10):3185-3206.
13. Sun H, Yan Z, Liu F, Xu W, Cheng F, Chen J. Self-supported transition-metal-based electrocatalysts for hydrogen and oxygen evolution. *Adv Mater*. 2020;32(3):1806326.
14. Wang X, Zheng Y, Sheng W, Xu ZJ, Jaroniec M, Qiao SZ. Strategies for design of electrocatalysts for hydrogen evolution under alkaline conditions. *Mater Today*. 2020;36:125-138.
15. Zhu J, Mu S. Defect engineering in carbon-based electrocatalysts: insight into intrinsic carbon defects. *Adv Funct Mater*. 2020;30(25):2001097.
16. Zhao L, Zhu J, Zheng Y, et al. Materials engineering toward durable electrocatalysts for proton exchange membrane fuel cells. *Adv Energy Mater*. 2021;12(2):2102665.
17. Jin H, Ruqia B, Park Y, et al. Nanocatalyst design for long-term operation of proton/anion exchange membrane water electrolysis. *Adv Energy Mater*. 2020;11(4):2003188.
18. Hu X, Zhang W, Liu X, Mei Y, Huang Y. Nanostructured Mo-based electrode materials for electrochemical energy storage. *Chem Soc Rev*. 2015;44(8):2376-2404.
19. Hu C, Zhang L, Gong J. Recent progress made in the mechanism comprehension and design of electrocatalysts for alkaline water splitting. *Energ Environ Sci*. 2019;12(9):2620-2645.
20. Hu C, Dai L. Carbon-based metal-free catalysts for electrocatalysis beyond the ORR. *Angew Chem Int Ed*. 2016;55(39):11736-11758.
21. Fei H, Dong J, Chen D, et al. Single atom electrocatalysts supported on graphene or graphene-like carbons. *Chem Soc Rev*. 2019;48(20):5207-5241.
22. Bae S-Y, Mahmood J, Jeon I-Y, Baek J-B. Recent advances in ruthenium-based electrocatalysts for the hydrogen evolution reaction. *Nanoscale Horiz*. 2020;5(1):43-56.
23. Shi F, Gao W, Shan H, et al. Strain-induced corrosion kinetics at nanoscale are revealed in liquid: enabling control of corrosion dynamics of electrocatalysis. *Chem*. 2020;6(9):2257-2271.
24. Masa J, Andronescu C, Schuhmann W. Electrocatalysis as the nexus for sustainable renewable energy: the gordian knot of activity, stability, and selectivity. *Angew Chem Int Ed*. 2020;59(36):15298-15312.
25. Karmodak N, Andreussi O. Catalytic activity and stability of two-dimensional materials for the hydrogen evolution reaction. *ACS Energy Lett*. 2020;5(3):885-891.
26. Jiao Y, Zheng Y, Davey K, Qiao S-Z. Activity origin and catalyst design principles for electrocatalytic hydrogen evolution on heteroatom-doped graphene. *Nat Energy*. 2016;1(10):16130.
27. Chen J, Qian G, Zhang H, et al. PtCo@PtSn heterojunction with high stability/activity for pH-universal H_2 evolution. *Adv Funct Mater*. 2021;32(5):2107597.
28. Baek DS, Jung GY, Seo B, et al. Ordered mesoporous metastable α-MoC_{1-x} with enhanced water dissociation capability for boosting alkaline hydrogen evolution activity. *Adv Funct Mater*. 2019;29(28):1901217.
29. Kweon DH, Okyay MS, Kim SJ, et al. Ruthenium anchored on carbon nanotube electrocatalyst for hydrogen production with enhanced faradaic efficiency. *Nat Commun*. 2020;11(1):1278.
30. Zhu J, YaoGuo LF, et al. Regulative electronic states around ruthenium/ruthenium disulphide heterointerfaces for efficient water splitting in acidic media. *Angew Chem Int Ed*. 2021;60(22):12382-12334.
31. Luo Z, Ouyang Y, Zhang H, et al. Chemically activating MoS_2 via spontaneous atomic palladium interfacial doping towards efficient hydrogen evolution. *Nat Commun*. 2018;9:2120.
32. Jia Y, Huang TH, Lin S, et al. Stable Pd-Cu hydride catalyst for efficient hydrogen evolution. *Nano Lett*. 2022;22(3):1391-1397.
33. Wan R, Luo M, Wen J, Liu S, Kang X, Tian Y. Pt-Co single atom alloy catalysts: accelerated water dissociation and hydrogen evolution by strain regulation. *J Energy Chem*. 2022;69:44-53.
34. Jia Z, Nomoto K, Wang Q, et al. A self-supported high-entropy metallic glass with a nanosponge architecture for efficient hydrogen evolution under alkaline and acidic conditions. *Adv Funct Mater*. 2021;31(38):2101586.
35. Yue X, Huang S, Jin Y, Shen PK. Nitrogen and fluorine dual-doped porous graphene-nanosheets as efficient metal-free electrocatalysts for hydrogen-evolution in acidic media. *Cat Sci Technol*. 2017;7(11):2228-2235.
36. Yuan Z, Li J, Yang M, et al. Ultrathin black phosphorus-on-nitrogen doped graphene for efficient overall water splitting: dual modulation roles of directional interfacial charge transfer. *J Am Chem Soc*. 2019;141(12):4972-4979.
37. Jiang H, Zhu Y, Su Y, et al. Highly dual-doped multilayer nanoporous graphene: efficient metal-free electrocatalysts for the hydrogen evolution reaction. *J Mater Chem A*. 2015;3(24):12642-12645.
38. Li Y, Huang H, Chen S, Wang C, Liu A, Ma T. Killing two birds with one stone: a highly active tubular carbon catalyst

with effective N doping for oxygen reduction and hydrogen evolution reactions. *Catal Lett*. 2018;149(2):486-495.

39. Chan CY, Chang CH, Tuan HY. Colloidal synthesis of porous red phosphorus nanoparticles as a metal-free electrocatalyst for the hydrogen evolution reaction. *Chem Commun*. 2020; 56(19):2937-2940.
40. Feng JX, Xu H, Ye SH, Ouyang G, Tong YX, Li GR. Silica-polypyrrole hybrids as high-performance metal-free electrocatalysts for the hydrogen evolution reaction in neutral media. *Angew Chem Int Ed*. 2017;56(28):8120-8124.
41. Hu Q, Li G, Liu X, et al. Superhydrophilic phytic-acid-doped conductive hydrogels as metal-free and binder-free electrocatalysts for efficient water oxidation. *Angew Chem Int Ed*. 2019;58(13):4318-4322.
42. Zhu X, Zhang T, Sun Z, et al. Black phosphorus revisited: a missing metal-free elemental photocatalyst for visible light hydrogen evolution. *Adv Mater*. 2017;29(17):1605776.
43. Zhu Z, Yin H, He CT, et al. Ultrathin transition metal dichalcogenide/3d metal hydroxide hybridized nanosheets to enhance hydrogen evolution activity. *Adv Mater*. 2018;30(28): 1801171.
44. Yu Q, Zhang Z, Qiu S, et al. A Ta-TaS_2 monolith catalyst with robust and metallic interface for superior hydrogen evolution. *Nat Commun*. 2021;12(1):6051.
45. Chen Y, Yu G, Chen W, et al. Highly active, nonprecious electrocatalyst comprising borophene subunits for the hydrogen evolution reaction. *J Am Chem Soc*. 2017;139(36):12370-12373.
46. Tang Y-J, Wang Y, Wang X-L, et al. Molybdenum disulfide/-nitrogen-doped reduced graphene oxide nanocomposite with enlarged interlayer spacing for electrocatalytic hydrogen evolution. *Adv Energy Mater*. 2016;6(12):1600116.
47. Sun T, Zhao S, Chen W, et al. Single-atomic cobalt sites embedded in hierarchically ordered porous nitrogen-doped carbon as a superior bifunctional electrocatalyst. *PNAS*. 2018; 115(50):12692-12697.
48. Pan Y, Sun K, Lin Y, et al. Electronic structure and d-band center control engineering over M-doped CoP (M = Ni, Mn, Fe) hollow polyhedron frames for boosting hydrogen production. *Nano Energy*. 2019;56:411-419.
49. Xu R, Wu R, Shi Y, Zhang J, Zhang B. Ni_3Se_2 nanoforest/Ni foam as a hydrophilic, metallic, and self-supported bifunctional electrocatalyst for both H_2 and O_2 generations. *Nano Energy*. 2016;24:103-110.
50. Zeng L, Sun K, Wang X, et al. Three-dimensional-networked Ni_2P/Ni_3S_2 heteronanoflake arrays for highly enhanced electrochemical overall-water-splitting activity. *Nano Energy*. 2018;51:26-36.
51. Zheng Y, Jiao Y, Vasileff A, Qiao SZ. The hydrogen evolution reaction in alkaline solution: from theory, single crystal models, to practical electrocatalysts. *Angew Chem Int Ed*. 2018;57(26):7568-7579.
52. Parsons R. The rate of electrolytic hydrogen evolution and the heat of adsorption of hydrogen. *Trans Fraday Soc*. 1958;54: 1053-1063.
53. Nørskov JK, Bligaard T, Logadottir A, et al. Trends in the exchange current for hydrogen evolution. *J Electrochem Soc*. 2005;152(3):J23.
54. Wang J, Xu F, Jin H, Chen Y, Wang Y. Non-noble metal-based carbon composites in hydrogen evolution reaction: fundamentals to applications. *Adv Mater*. 2017; 29(14):1605838.
55. Mahmood N, Yao Y, Zhang JW, Pan L, Zhang X, Zou JJ. Electrocatalysts for hydrogen evolution in alkaline electrolytes: mechanisms, challenges, and prospective solutions. *Adv Sci*. 2018;5(2):1700464.
56. Zhang L, Jia Y, Yan X, Yao X. Activity origins in nanocarbons for the electrocatalytic hydrogen evolution reaction. *Small*. 2018;14(26):1800235.
57. Zhai W, Sakthivel T, Chen F, du C, Yu H, Dai Z. Amorphous materials for elementary-gas-involved electrocatalysis: an overview. *Nanoscale*. 2021;13(47):19783-19811.
58. Kou Z, Zhang L, Ma Y, et al. 2D carbide nanomeshes and their assembling into 3D microflowers for efficient water splitting. *Appl Catal B: Environ*. 2019;243:678-685.
59. Chen G, Wang T, Zhang J, et al. Accelerated hydrogen evolution kinetics on NiFe-layered double hydroxide electrocatalysts by tailoring water dissociation active sites. *Adv Mater*. 2018;30(10):1706279.
60. Park H, Lee E, Lei M, Joo H, Coh S, Fokwa BPT. Canonic-like HER activity of $Cr_{1-x}Mo_xB_2$ solid solution: overpowering Pt/C at high current density. *Adv Mater*. 2020;32(28):2000855.
61. Hu S, Li W-X. Sabatier principle of metal-support interaction for design of ultrastable metal nanocatalysts. *Science*. 2021; 374:1360-1365.
62. Cherevko S. Stability and dissolution of electrocatalysts: building the bridge between model and "real world" systems. *Curr Opin Electrochem*. 2018;8:118-125.
63. Cherevko S, Geiger S, Kasian O, et al. Oxygen and hydrogen evolution reactions on Ru, RuO_2, Ir, and IrO_2 thin film electrodes in acidic and alkaline electrolytes: a comparative study on activity and stability. *Catal Today*. 2016; 262:170-180.
64. Abd-El-Latif AA, Bondue CJ, Ernst S, et al. Insights into electrochemical reactions by differential electrochemical mass spectrometry. *TrAC Trends Anal Chem*. 2015;70:4-13.
65. Wang S, Teng Z, Wang C, Wang G. Stable and efficient nitrogen-containing carbon-based electrocatalysts for reactions in energy-conversion systems. *ChemSusChem*. 2018; 11(14):2267-2295.
66. Chen F-Y, Wu Z-Y, Adler Z, Wang H. Stability challenges of electrocatalytic oxygen evolution reaction: from mechanistic understanding to reactor design. *Joule*. 2021;5(7):1704-1731.
67. Jiao Y, Zheng Y, Jaroniec M, Qiao SZ. Design of electrocatalysts for oxygen- and hydrogen-involving energy conversion reactions. *Chem Soc Rev*. 2015;44(8):2060-2086.
68. Wang T, Guo L, Jiang Z, et al. Ru-pincer complex-bridged Cu-porphyrin polymer for robust (photo)electrocatalytic H_2 evolution via single-atom active sites. *Adv Funct Mater*. 2021; 31(50):2107290.
69. Bao F, Yang Z, Yuan Y, et al. Synergistic cascade hydrogen evolution boosting via integrating surface oxophilicity modification with carbon layer confinement. *Adv Funct Mater*. 2021; 32(6):2108991.
70. Liu D, Li X, Chen S, et al. Atomically dispersed platinum supported on curved carbon supports for efficient

electrocatalytic hydrogen evolution. *Nat Energy*. 2019;4(6): 512-518.
71. Yu H, Xue Y, Huang B, et al. Ultrathin nanosheet of graphdiyne-supported palladium atom catalyst for efficient hydrogen production. *iScience*. 2019;11:31-41.
72. Cui C, Cheng R, Zhang H, et al. Ultrastable MXene@Pt/SWCNTs' nanocatalysts for hydrogen evolution reaction. *Adv Funct Mater*. 2020;30(47):2000693.
73. Li J, Liu H-X, Gou W, et al. Ethylene-glycol ligand environment facilitates highly efficient hydrogen evolution of Pt/CoP through proton concentration and hydrogen spillover. *Energ Environ Sci*. 2019;12(7):2298-2304.
74. Ye S, Luo F, Zhang Q, et al. Highly stable single Pt atomic sites anchored on aniline-stacked graphene for hydrogen evolution reaction. *Energ Environ Sci*. 2019;12(3):1000-1007.
75. Zhang L, Han L, Liu H, Liu X, Luo J. Potential-cycling synthesis of single platinum atoms for efficient hydrogen evolution in neutral media. *Angew Chem Int Ed*. 2017;56(44):13694-13698.
76. Wang Y, Chen L, Yu X, Wang Y, Zheng G. Superb alkaline hydrogen evolution and simultaneous electricity generation by Pt-decorated Ni_3N nanosheets. *Adv Energy Mater*. 2017; 7(2):1601390.
77. Sun L, Li Q, Zhang S, et al. Heterojunction-based electron donators to stabilize and activate ultrafine Pt nanoparticles for efficient hydrogen atom dissociation and gas evolution. *Angew Chem Int Ed*. 2021;60(49):25766-25770.
78. Liu S, Shen Y, Zhang Y, et al. Extreme environmental thermal shock induced dislocation-rich Pt nanoparticles boosting hydrogen evolution reaction. *Adv Mater*. 2021;34(2):2106973.
79. Zhao Z, Liu H, Gao W, et al. Surface-engineered PtNi-O nanostructure with record-high performance for electrocatalytic hydrogen evolution reaction. *J Am Chem Soc*. 2018;140(29): 9046-9050.
80. Zhang H, An P, Zhou W, et al. Dynamic traction of lattice-confined platinum atoms into mesoporous carbon matrix for hydrogen evolution reaction. *Sci Adv*. 2018;4(1):aao6657.
81. Zhu Y, Zhu X, Bu L, et al. Single-atom in-doped subnanometer Pt nanowires for simultaneous hydrogen generation and biomass upgrading. *Adv Funct Mater*. 2020;30(49): 2004310.
82. Yoo S, Kim Y, Yoon Y, Karuppannan M, Kwon OJ, Lim T. Encapsulation of Pt nanocatalyst with N-containing carbon layer for improving catalytic activity and stability in the hydrogen evolution reaction. *Int J Hydrogen Energy*. 2021; 46(41):21454-21461.
83. Zhang L, Wang Q, Si R, et al. New insight of pyrrole-like nitrogen for boosting hydrogen evolution activity and stability of Pt single atoms. *Small*. 2021;17(16):2004453.
84. Ying J, Jiang G, Cano ZP, et al. Nitrogen-doped hollow porous carbon polyhedrons embedded with highly dispersed Pt nanoparticles as a highly efficient and stable hydrogen evolution electrocatalyst. *Nano Energy*. 2017;40:88-94.
85. Wan XK, Wu HB, Guan BY, Luan D, Lou XW. Confining subnanometer Pt clusters in hollow mesoporous carbon spheres for boosting hydrogen evolution activity. *Adv Mater*. 2020; 32(7):1901349.
86. Wang W, Wu Y, Lin Y, et al. Confining zero-valent platinum single atoms in α-MoC_{1-x} for pH-universal hydrogen evolution reaction. *Adv Funct Mater*. 2022;32(12):2108464.
87. Cheng N, Stambula S, Wang D, et al. Platinum single-atom and cluster catalysis of the hydrogen evolution reaction. *Nat Commun*. 2016;7:13638.
88. Seh ZW, Kibsgaard J, Dickens CF, Chorkendorff I, Nørskov JK, Jaramillo TF. Combining theory and experiment in electrocatalysis: insights into materials design. *Science*. 2017;355(6321):eaad4998.
89. Yu J, He Q, Yang G, Zhou W, Shao Z, Ni M. Recent advances and prospective in ruthenium-based materials for electrochemical water splitting. *ACS Catal*. 2019;9(11): 9973-10011.
90. Harzandi AM, Shadman S, Ha M, et al. Immiscible bi-metal single-atoms driven synthesis of electrocatalysts having superb mass-activity and durability. *Appl Catal B: Environ*. 2020;270:118896.
91. Zhao H, Zhang D, Yuan Y, et al. Rapid and large-scale synthesis of ultra-small immiscible alloy supported catalysts. *Appl Catal B: Environ*. 2021;304:120916.
92. Xu J, Liu T, Li J, et al. Boosting the hydrogen evolution performance of ruthenium clusters through synergistic coupling with cobalt phosphide. *Energ Environ Sci*. 2018;11(7):1819-1827.
93. Zhai P, Xia M, Wu Y, et al. Engineering single-atomic ruthenium catalytic sites on defective nickel-iron layered double hydroxide for overall water splitting. *Nat Commun*. 2021;12(1):4587.
94. Li Q, Huang F, Li S, Zhang H, Yu XY. Oxygen vacancy engineering synergistic with surface hydrophilicity modification of hollow Ru doped CoNi-LDH nanotube arrays for boosting hydrogen evolution. *Small*. 2021;18(2):2104323.
95. Jiang K, Luo M, Liu Z, et al. Rational strain engineering of single-atom ruthenium on nanoporous MoS_2 for highly efficient hydrogen evolution. *Nat Commun*. 2021;12(1):1687.
96. Sun Y, Xue Z, Liu Q, et al. Modulating electronic structure of metal-organic frameworks by introducing atomically dispersed Ru for efficient hydrogen evolution. *Nat Commun*. 2021;12(1):1369.
97. Hu C, Hong J, Huang J, et al. Surface decoration accelerates the hydrogen evolution kinetics of a perovskite oxide in alkaline solution. *Energ Environ Sci*. 2020;13(11):4249-4257.
98. Yang J, Chen B, Liu X, et al. Efficient and robust hydrogen evolution: phosphorus nitride imide nanotubes as supports for anchoring single ruthenium sites. *Angew Chem Int Ed*. 2018;57(30):9495-9500.
99. Zhang H, Zhou W, Lu XF, Chen T, Lou XW. Implanting isolated Ru atoms into edge-rich carbon matrix for efficient electrocatalytic hydrogen evolution. *Adv Energy Mater*. 2020; 10(23):2000882.
100. Zhang L, Jang H, Wang Y, et al. Exploring the dominant role of atomic- and nano-ruthenium as active sites for hydrogen evolution reaction in both acidic and alkaline media. *Adv Sci*. 2021;8(15):2004516.
101. Li J-S, Huang M-J, Zhou Y-W, et al. RuP_2-based hybrids derived from MOFs: highly efficient pH-universal electrocatalysts for hydrogen evolution reaction. *J Mater Chem A*. 2021;9(20):12276-12282.
102. Li L, Bu L, Huang B, et al. Compensating electronic effect enables fast site-to-site electron transfer over ultrathin RuMn nanosheet branches toward highly electroactive and stable water splitting. *Adv Mater*. 2021;33(51):2105308.
103. Liu Z, Li B, Feng Y, et al. Strong electron coupling of Ru and vacancy-rich carbon dots for synergistically

enhanced hydrogen evolution reaction. *Small*. 2021; 17(41):2102496.
104. Chen X, Wan J, Wang J, et al. Atomically dispersed ruthenium on nickel hydroxide ultrathin nanoribbons for highly efficient hydrogen evolution reaction in alkaline media. *Adv Mater*. 2021;33(44):2104764.
105. Li W, Liu Y, Wu M, et al. Carbon-quantum-dots-loaded ruthenium nanoparticles as an efficient electrocatalyst for hydrogen production in alkaline media. *Adv Mater*. 2018; 30(31):1800676.
106. Yu J, Guo Y, She S, et al. Bigger is surprisingly better: agglomerates of larger RuP nanoparticles outperform benchmark Pt nanocatalysts for the hydrogen evolution reaction. *Adv Mater*. 2018;30(39):1800047.
107. Chen D, Yu R, Lu R, et al. Tunable Ru-Ru_2P heterostructures with charge redistribution for efficient pH-universal hydrogen evolution. *InfoMat*. 2022;4(5):e12287.
108. Pu Z, Amiinu IS, Kou Z, Li W, Mu S. RuP_2-based catalysts with platinum-like activity and higher durability for the hydrogen evolution reaction at all pH values. *Angew Chem Int Ed*. 2017;56(38):11559-11564.
109. Li Y, Zhang J, Liu Y, et al. Partially exposed RuP_2 surface in hybrid structure endows its bifunctionality for hydrazine oxidation and hydrogen evolution catalysis. *Sci Adv*. 2020;6(44): abb4197.
110. Chen Q, Wei B, Wei Y, et al. Synergistic effect in ultrafine PtNiP nanowires for highly efficient electrochemical hydrogen evolution in alkaline electrolyte. *Appl Catal B: Environ*. 2022; 301:120754.
111. Zhang W, Jiang X, Dong Z, et al. Porous Pd/$NiFeO_x$ nanosheets enhance the pH-universal overall water splitting. *Adv Funct Mater*. 2021;31(51):2107181.
112. Li L, Ji Y, Luo X, et al. Compressive strain in N-doped palladium/amorphous-cobalt (II) interface facilitates alkaline hydrogen evolution. *Small*. 2021;17(44):2103798.
113. Vanni M, Bellini M, Borsacchi S, et al. Interlayer coordination of Pd-Pd units in exfoliated black phosphorus. *J Am Chem Soc*. 2021;143(27):10088-10098.
114. Zhang D, Zheng X, Qi L, Xue Y, He F, Li Y. Controlled growth of single-crystal Pd quantum dots on 2D carbon for large current density hydrogen evolution. *Adv Funct Mater*. 2022;32:2111501.
115. Zhang G, Wang A, Niu L, et al. Interfacial engineering to construct antioxidative $Pd_4S/Pd_3P_{0.95}$ heterostructure for robust hydrogen production at high current density. *Adv Energy Mater*. 2022;12(11):2103511.
116. Zhan Y, Zhou X, Nie H, et al. Designing Pd/O Co-doped MoS_x for boosting the hydrogen evolution reaction. *J Mater Chem A*. 2019;7(26):15599-15606.
117. Zhang H, Jiang Q, Hadden JHL, Xie F, Riley DJ. Pd ion-exchange and ammonia etching of a prussian blue analogue to produce a high-performance water-splitting catalyst. *Adv Funct Mater*. 2020;31(10):2008989.
118. Li L, Wang B, Zhang G, et al. Electrochemically modifying the electronic structure of IrO_2 nanoparticles for overall electrochemical water splitting with extensive adaptability. *Adv Energy Mater*. 2020;10(30):2001600.
119. Zhu L, Lin H, Li Y, et al. A rhodium/silicon co-electrocatalyst design concept to surpass platinum hydrogen evolution activity at high overpotentials. *Nat Commun*. 2016;7:12272.
120. Zhao Y, Bai J, Wu X-R, et al. Atomically ultrathin RhCo alloy nanosheet aggregates for efficient water electrolysis in broad pH range. *J Mater Chem A*. 2019;7(27):16437-16446.
121. Wang Q, Xu CQ, Liu W, et al. Coordination engineering of iridium nanocluster bifunctional electrocatalyst for highly efficient and pH-universal overall water splitting. *Nat Commun*. 2020;11(1):4246.
122. Meng X, Ma C, Jiang L, et al. Distance synergy of MoS_2-confined rhodium atoms for highly efficient hydrogen evolution. *Angew Chem Int Ed*. 2020;132(26):10588-10593.
123. Xin H, Dai Z, Zhao Y, et al. Recording the Pt-beyond hydrogen production electrocatalysis by dirhodium phosphide with an overpotential of only 4.3 mV in alkaline electrolyte. *Appl Catal B: Environ*. 2021;297:120457.
124. Zhang Y, Li G, Zhao Z, et al. Atomically isolated Rh sites within highly branched Rh_2Sb nanostructures enhance bifunctional hydrogen electrocatalysis. *Adv Mater*. 2021; 33(43):2105049.
125. Kang Y, Jiang B, Malgras V, et al. Heterostructuring mesoporous 2D iridium nanosheets with amorphous nickel boron oxide layers to improve electrolytic water splitting. *Small Methods*. 2021;5(10):2100679.
126. Li J, Hu J, Zhang M, et al. A fundamental viewpoint on the hydrogen spillover phenomenon of electrocatalytic hydrogen evolution. *Nat Commun*. 2021;12(1):3502.
127. Joo J, Jin H, Oh A, et al. An IrRu alloy nanocactus on $Cu_{2-x}S@IrS_y$ as a highly efficient bifunctional electrocatalyst toward overall water splitting in acidic electrolytes. *J Mater Chem A*. 2018;6(33):16130-16138.
128. Feng G, Ning F, Song J, et al. Sub-2 nm ultrasmall high-entropy alloy nanoparticles for extremely superior electrocatalytic hydrogen evolution. *J Am Chem Soc*. 2021;143(41):17117-17127.
129. Chen HY, Jin MX, Zhang L, et al. One-pot aqueous synthesis of two-dimensional porous bimetallic PtPd alloyed nanosheets as highly active and durable electrocatalyst for boosting oxygen reduction and hydrogen evolution. *J Colloid Interface Sci*. 2019;543:1-8.
130. Chen Y, Zheng XX, Huang XY, et al. Trimetallic PtRhCo petal-assembled alloyed nanoflowers as efficient and stable bifunctional electrocatalyst for ethylene glycol oxidation and hydrogen evolution reactions. *J Colloid Interface Sci*. 2020;559: 206-214.
131. Fan J, Wu J, Cui X, et al. Hydrogen stabilized RhPdH 2D bimetallene nanosheets for efficient alkaline hydrogen evolution. *J Am Chem Soc*. 2020;142(7):3645-3651.
132. Chen CH, Wu D, Li Z, et al. Ruthenium-based single-atom alloy with high electrocatalytic activity for hydrogen evolution. *Adv Energy Mater*. 2019;9(20):1803913.
133. Mu X, Gu J, Feng F, et al. RuRh bimetallene nanoring as high-efficiency pH-universal catalyst for hydrogen evolution reaction. *Adv Sci*. 2021;8(2):2002341.
134. Pang B, Liu X, Liu T, et al. Laser-assisted high-performance PtRu alloy for pH-universal hydrogen evolution. *Energ Environ Sci*. 2021;15(1):102-108.
135. Li Z, Fu J-Y, Feng Y, Dong CK, Liu H, du XW. A silver catalyst activated by stacking faults for the hydrogen evolution reaction. *Nat Catal*. 2019;2(12):1107-1114.

136. Yu J, Dai Y, He Q, Cheng C, Shao Z, Ni M. Robust non-Pt noble metal-based nanomaterials for electrocatalytic hydrogen generation. *Appl Phys Rev*. 2020;7(4):041304.
137. Mohammed-Ibrahim J, Sun X. Recent progress on earth abundant electrocatalysts for hydrogen evolution reaction (HER) in alkaline medium to achieve efficient water splitting—a review. *J Energy Chem*. 2019;34:111-160.
138. Vij V, Sultan S, Harzandi AM, et al. Nickel-based electrocatalysts for energy-related applications: oxygen reduction, oxygen evolution, and hydrogen evolution reactions. *ACS Catal*. 2017;7(10):7196-7225.
139. Duan J, Chen S, Ortiz-Ledon CA, Jaroniec M, Qiao SZ. Phosphorus vacancies that boost electrocatalytic hydrogen evolution by two orders of magnitude. *Angew Chem Int Ed*. 2020;59(21):8181-8186.
140. Wang Y, Li X, Zhang M, et al. Lattice-strain engineering of homogeneous $NiS_{0.5}Se_{0.5}$ core-shell nanostructure as a highly efficient and robust electrocatalyst for overall water splitting. *Adv Mater*. 2020;32(40):2000231.
141. Xu Q, Jiang H, Zhang H, Hu Y, Li C. Heterogeneous interface engineered atomic configuration on ultrathin $Ni(OH)_2/Ni_3S_2$ nanoforests for efficient water splitting. *Appl Catal B: Environ*. 2019;242:60-66.
142. Qiu HJ, Ito Y, Cong W, et al. Nanoporous graphene with single-atom nickel dopants: an efficient and stable catalyst for electrochemical hydrogen production. *Angew Chem Int Ed*. 2015;54(47):14031-14035.
143. Menezes PW, Panda C, Loos S, et al. A structurally versatile nickel phosphite acting as a robust bifunctional electrocatalyst for overall water splitting. *Energ Environ Sci*. 2018;11(5):1287-1298.
144. Yin J, Jin J, Zhang H, et al. Atomic arrangement in metal-doped NiS_2 boosts the hydrogen evolution reaction in alkaline media. *Angew Chem Int Ed*. 2019;58(51):18676-18682.
145. Wang F, Li Y, Xu P, Wang Q, He J. Selenium-enriched nickel selenide nanosheets as a robust electrocatalyst for hydrogen production. *Angew Chem Int Ed*. 2016;55(24):6919-6924.
146. Zhang D, Li H, Riaz A, et al. Unconventional direct synthesis of Ni_3N/Ni with N-vacancies for efficient and stable hydrogen evolution. *Energ Environ Sci*. 2021;15(1):185-195.
147. Li Y, Min K-A, Han B, Lee LYS. Ni nanoparticles on active (001) facet-exposed rutile TiO_2 nanopyramid arrays for efficient hydrogen evolution. *Appl Catal B: Environ*. 2021;282:119548.
148. Zhao Y, Ling T, Chen S, et al. Non-metal single-iodine-atom electrocatalysts for the hydrogen evolution reaction. *Angew Chem Int Ed*. 2019;58(35):12252-12257.
149. Gu Y, Xi B, Wei R, Fu Q, Qain Y, Xiong S. Sponge assembled by graphene nanocages with double active sites to accelerate alkaline HER kinetics. *Nano Lett*. 2020;20(11):8375-8383.
150. Wang K, Guo Y, Chen Z, et al. Regulating electronic structure of two-dimensional porous Ni/Ni_3N nanosheets architecture by Co atomic incorporation boosts alkaline water splitting. *InfoMat*. 2021;4(6):e12251.
151. Zang W, Sun T, Yang T, et al. Efficient hydrogen evolution of oxidized Ni-N_3 defective sites for alkaline freshwater and seawater electrolysis. *Adv Mater*. 2021;33(8):2003846.
152. Liu J, Wu H, Li F, Feng X, Zhang P, Gao L. Recent progress in non-precious metal single atomic catalysts for solar and non-solar driven hydrogen evolution reaction. *Adv Sustain Syst*. 2020;4(11):2000151.
153. Zhao G, Rui K, Dou SX, Sun W. Heterostructures for electrochemical hydrogen evolution reaction: a review. *Adv Funct Mater*. 2018;28(43):1803291.
154. You B, Sun Y. Hierarchically porous nickel sulfide multifunctional superstructures. *Adv Energy Mater*. 2016;6(7):1502333.
155. Shang X, Yan KL, Rao Y, et al. In situ cathodic activation of V-incorporated Ni_xS_y nanowires for enhanced hydrogen evolution. *Nanoscale*. 2017;9(34):12353-12363.
156. Li Y, Zhang H, Jiang M, Zhang Q, He P, Sun X. 3D self-supported Fe-doped Ni_2P nanosheet arrays as bifunctional catalysts for overall water splitting. *Adv Funct Mater*. 2017;27(37):1702513.
157. Li J, Yan M, Zhou X, et al. Mechanistic insights on ternary $Ni_{2-x}Co_xP$ for hydrogen evolution and their hybrids with graphene as highly efficient and robust catalysts for overall water splitting. *Adv Funct Mater*. 2016;26(37):6785-6796.
158. Sun Y, Hang L, Shen Q, et al. Mo doped Ni_2P nanowire arrays: an efficient electrocatalyst for the hydrogen evolution reaction with enhanced activity at all pH values. *Nanoscale*. 2017;9(43):16674-16679.
159. Wen L, Yu J, Xing C, et al. Flexible vanadium-doped Ni_2P nanosheet arrays grown on carbon cloth for an efficient hydrogen evolution reaction. *Nanoscale*. 2019;11(10):4198-4203.
160. Chu S, Chen W, Chen G, et al. Holey Ni-Cu phosphide nanosheets as a highly efficient and stable electrocatalyst for hydrogen evolution. *Appl Catal B: Environ*. 2019;243:537-545.
161. Ren JT, Yuan GG, Weng CC, Chen L, Yuan ZY. Uniquely integrated Fe-doped $Ni(OH)_2$ nanosheets for highly efficient oxygen and hydrogen evolution reactions. *Nanoscale*. 2018;10(22):10620-10628.
162. Li Y, Wei B, Yu Z, et al. Bifunctional porous cobalt phosphide foam for high-current-density alkaline water electrolysis with 4000-h long stability. *ACS Sustain Chem Eng*. 2020;8(27):10193-10200.
163. Li J, Xia Z, Xue Q, et al. Insights into the interfacial Lewis acid-base pairs in CeO_2-loaded CoS_2 electrocatalysts for alkaline hydrogen evolution. *Small*. 2021;17(39):2103018.
164. Liu X, Zheng L, Han C, et al. Identifying the activity origin of a cobalt single-atom catalyst for hydrogen evolution using supervised learning. *Adv Funct Mater*. 2021;31(18):2100547.
165. Li J, Xia Z, Zhang M, et al. Ce-doped CoS_2 pyrite with weakened O_2 adsorption suppresses catalyst leaching and stabilizes electrocatalytic H_2 evolution. *J Mater Chem A*. 2019;7(30):17775-17781.
166. Ji P, Yu R, Wang P, et al. Ultra-fast and in-depth reconstruction of transition metal fluorides in electrocatalytic hydrogen evolution processes. *Adv Sci*. 2021;9(3):2103567.
167. Duan J, Chen S, Vasileff A, Qiao SZ. Anion and cation modulation in metal compounds for bifunctional overall water splitting. *ACS Nano*. 2016;10(9):8738-8745.
168. Zhang Y, Hui ZX, Zhou HY, et al. Ga doping enables superior alkaline hydrogen evolution reaction performances of CoP. *Chem Eng J*. 2022;429:132012.
169. Tan Q, Xiao R, Yao X, et al. Non-oxygen anion-regulated in situ cobalt based heterojunctions for active alkaline hydrogen evolution catalysis. *Chem Eng J*. 2021;433:133514.
170. Wu YP, Zhou W, Zhao J, et al. Surfactant-assisted phase-selective synthesis of new cobalt MOFs and their efficient

electrocatalytic hydrogen evolution reaction. *Angew Chem Int Ed*. 2017;56(42):13001-13005.

171. Xu W, Fan G, Zhu S, et al. Electronic structure modulation of nanoporous cobalt phosphide by carbon doping for alkaline hydrogen evolution reaction. *Adv Funct Mater*. 2021;31(48): 2107333.
172. Men Y, Li P, Zhou J, Cheng G, Chen S, Luo W. Tailoring the electronic structure of Co_2P by N doping for boosting hydrogen evolution reaction at all pH values. *ACS Catal*. 2019;9(4): 3744-3752.
173. Liu R, Gong Z, Liu J, et al. Design of aligned porous carbon films with single-atom Co-N-C sites for high-current-density hydrogen generation. *Adv Mater*. 2021;33(41):2103533.
174. Feng JX, Tong SY, Tong YX, Li GR. Pt-like hydrogen evolution electrocatalysis on PANI/CoP hybrid nanowires by weakening the shackles of hydrogen ions on the surfaces of catalysts. *J Am Chem Soc*. 2018;140(15):5118-5126.
175. Sun Y, Mao K, Shen Q, et al. Surface electronic structure modulation of cobalt nitride nanowire arrays via selenium deposition for efficient hydrogen evolution. *Adv Funct Mater*. 2021; 32(9):2109792.
176. Xu R, Jiang T, Fu Z, et al. Ion-exchange controlled surface engineering of cobalt phosphide nanowires for enhanced hydrogen evolution. *Nano Energy*. 2020;78:105347.
177. Huang C, Qin P, Luo Y, et al. Recent progress and perspective of Co-based catalysts for water splitting: design and nanoarchitectonics. *Mater Today Energy*. 2021;23:100911.
178. Cao L, Luo Q, Liu W, et al. Identification of single-atom active sites in carbon-based cobalt catalysts during electrocatalytic hydrogen evolution. *Nat Catal*. 2018;2(2):134-141.
179. Yang Z, Zhao C, Qu Y, et al. Trifunctional self-supporting cobalt-embedded carbon nanotube films for ORR, OER, and HER triggered by solid diffusion from bulk metal. *Adv Mater*. 2019;31(12):1808043.
180. Oh NK, Seo J, Lee S, et al. Highly efficient and robust noble-metal free bifunctional water electrolysis catalyst achieved via complementary charge transfer. *Nat Commun*. 2021;12(1):4606.
181. Liu W, Wang X, Wang F, et al. A durable and pH-universal self-standing MoC-Mo_2C heterojunction electrode for efficient hydrogen evolution reaction. *Nat Commun*. 2021;12(1):6776.
182. Zhu J, Wang Z-C, Dai H, et al. Boundary activated hydrogen evolution reaction on monolayer MoS_2. *Nat Commun*. 2019; 10:1348.
183. Cheng Z, Gao J, Fu Q, et al. Interconnected molybdenum carbide-based nanoribbons for highly efficient and ultrastable hydrogen evolution. *ACS Appl Mater Interfaces*. 2017;9(29): 24608-24615.
184. Jiang H, Yan L, Zhang S, et al. Electrochemical surface restructuring of phosphorus-doped carbon@MoP electrocatalysts for hydrogen evolution. *Nano-Micro Lett*. 2021;13(1):215.
185. Li T, Lu T, Li X, et al. Atomically dispersed Mo sites anchored on multichannel carbon nanofibers toward superior electrocatalytic hydrogen evolution. *ACS Nano*. 2021;15(12):20032-20041.
186. Ge R, Huo J, Liao T, et al. Hierarchical molybdenum phosphide coupled with carbon as a whole pH-range electrocatalyst for hydrogen evolution reaction. *Appl Catal B: Environ*. 2020;260:118196.
187. Hua W, Sun H-H, Xu F, Wang J-G. A review and perspective on molybdenum-based electrocatalysts for hydrogen evolution reaction. *Rare Metals*. 2020;39(4):335-351.
188. Zheng Z, Yu L, Gao M, et al. Boosting hydrogen evolution on MoS_2 via co-confining selenium in surface and cobalt in inner layer. *Nat Commun*. 2020;11(1):3315.
189. Han N, Yang KR, Lu Z, et al. Nitrogen-doped tungsten carbide nanoarray as an efficient bifunctional electrocatalyst for water splitting in acid. *Nat Commun*. 2018;9(1):924.
190. Xie L, Wang L, Zhao W, Liu S, Huang W, Zhao Q. WS_2 moire superlattices derived from mechanical flexibility for hydrogen evolution reaction. *Nat Commun*. 2021;12(1):5070.
191. Zhang X, Cui X, Sun Y, et al. Nanoporous sulfur-doped copper oxide ($Cu_2O_xS_{1-x}$) for overall water splitting. *ACS Appl Mater Interfaces*. 2018;10(1):745-752.
192. Qin Q, Jang H, Li P, Yuan B, Liu X, Cho J. A tannic acid-derived N-, P-codoped carbon-supported iron-based nanocomposite as an advanced trifunctional electrocatalyst for the overall water splitting cells and zinc-air batteries. *Adv Energy Mater*. 2019;9(5):1803312.
193. Zhao X, Zhang Z, Cao X, et al. Elucidating the sources of activity and stability of FeP electrocatalyst for hydrogen evolution reactions in acidic and alkaline media. *Appl Catal B: Environ*. 2020;260:118156.
194. Wu Y, Liu X, Han D, et al. Electron density modulation of $NiCo_2S_4$ nanowires by nitrogen incorporation for highly efficient hydrogen evolution catalysis. *Nat Commun*. 2018;9(1):1425.
195. Liu H, Li X, Chen L, et al. Monolithic Ni-Mo-B bifunctional electrode for large current water splitting. *Adv Funct Mater*. 2021;32(4):2107308.
196. Wu Y, Li G-D, Liu Y, et al. Overall water splitting catalyzed efficiently by an ultrathin nanosheet-built, hollow Ni_3S_2-based electrocatalyst. *Adv Funct Mater*. 2016;26(27):4839-4847.
197. Wang Z, Chen J, Song E, et al. Manipulation on active electronic states of metastable phase β-$NiMoO_4$ for large current density hydrogen evolution. *Nat Commun*. 2021;12(1):5960.
198. Ouyang Q, Lei Z, Li Q, Li M, Yang C. A self-supported $NiCo_2O_4$/Cu_xO nanoforest with electronically modulated interfaces as an efficient electrocatalyst for overall water splitting. *J Mater Chem A*. 2021;9(25):14466-14476.
199. Xu Y, Wang R, Zheng Y, et al. Facile preparation of self-assembled Ni/Co phosphates composite spheres with highly efficient HER electrocatalytic performances. *Appl Surf Sci*. 2020;509:145383.
200. Lv Y, Liu Y, Chen C, Wang T, Zhang M. Octopus tentacles-like WO_3/C@CoO as high property and long life-time electrocatalyst for hydrogen evolution reaction. *Electrochim Acta*. 2018;281:1-8.
201. Gao W, Gou W, Zhou X, Ho JC, Ma Y, Qu Y. Amine-modulated/engineered interfaces of NiMo electrocatalysts for improved hydrogen evolution reaction in alkaline solutions. *ACS Appl Mater Interfaces*. 2018;10(2):1728-1733.
202. Zhang H, Li X, Hähnel A, et al. Bifunctional heterostructure assembly of NiFe LDH nanosheets on NiCoP nanowires for highly efficient and stable overall water splitting. *Adv Funct Mater*. 2018;28(14):1706847.
203. Li Y, Yin J, An L, et al. FeS_2 /CoS_2 interface nanosheets as efficient bifunctional electrocatalyst for overall water splitting. *Small*. 2018;14(26):1801070.
204. Li H, Chen S, Zhang Y, et al. Systematic design of superaerophobic nanotube-array electrode comprised of transition-metal sulfides for overall water splitting. *Nat Commun*. 2018;9(1):2452.
205. Chen Z, Qing H, Wang R, Wu R. Charge pumping enabling Co–NC to outperform benchmark Pt catalyst for pH-universal

hydrogen evolution reaction. *Energ Environ Sci*. 2021;14(5):3160-3173.
206. Huang ZF, Song J, Li K, et al. Hollow cobalt-based bimetallic sulfide polyhedra for efficient all-pH-value electrochemical and photocatalytic hydrogen evolution. *J Am Chem Soc*. 2016;138(4):1359-1365.
207. Yang Y, Zhang K, Lin H, et al. MoS_2–Ni_3S_2 heteronanorods as efficient and stable bifunctional electrocatalysts for overall water splitting. *ACS Catal*. 2017;7(4):2357-2366.
208. Huang H, Cho A, Kim S, et al. Structural design of amorphous $CoMoP_x$ with abundant active sites and synergistic catalysis effect for effective water splitting. *Adv Funct Mater*. 2020;30(43):2003889.
209. Yang Y, Zhang W, Xiao Y, et al. $CoNiSe_2$ heteronanorods decorated with layered-double-hydroxides for efficient hydrogen evolution. *Appl Catal B: Environ*. 2019;242:132-139.
210. Chu H, Feng P, Jin B, et al. In-situ release of phosphorus combined with rapid surface reconstruction for Co–Ni bimetallic phosphides boosting efficient overall water splitting. *Chem Eng J*. 2021;433:133523.
211. Li W, Cheng G, Peng S, et al. Tuning hydrogen binding energy by interfacial charge transfer enables pH-universal hydrogen evolution catalysis of metal phosphides. *Chem Eng J*. 2022;430:132699.
212. Zhang L, Hu M, Li H, et al. Boosting hydrogen evolution reaction via electronic coupling of cerium phosphate with molybdenum phosphide nanobelts. *Small*. 2021;17(40):2102413.
213. Fu HC, Wang XH, Chen XH, Zhang Q, Li NB, Luo HQ. Interfacial engineering of $Ni(OH)_2$ on W_2C for remarkable alkaline hydrogen production. *Appl Catal B: Environ*. 2022;301:120818.
214. Gu M, Deng X, Lin M, et al. Ultrathin NiCo bimetallic molybdate nanosheets coated CuO_x nanotubes: heterostructure and bimetallic synergistic optimization of the active site for highly efficient overall water splitting. *Adv Energy Mater*. 2021;11(41):2102361.
215. Patil SJ, Chodankar NR, Hwang S-K, et al. Co-metal–organic framework derived $CoSe_2$@$MoSe_2$ core–shell structure on carbon cloth as an efficient bifunctional catalyst for overall water splitting. *Chem Eng J*. 2022;429:132379.
216. Ge J, Zhang W, Tu J, Xia T, Chen S, Xie G. Suppressed Jahn-Teller distortion in $MnCo_2O_4$@Ni_2P heterostructures to promote the overall water splitting. *Small*. 2020;16(34):2001856.
217. Li Z, Yang J, Chen Z, et al. V "bridged" Co-O to eliminate charge transfer barriers and drive lattice oxygen oxidation during water-splitting. *Adv Funct Mater*. 2020;31(9):2008822.
218. Xiao Z, Yang M, Wang J, et al. FeNiP/MoO_x integrated electrode grown on monocrystalline $NiMoO_4$ nanorods with multi-interface for accelerating alkaline hydrogen evolution reaction. *Appl Catal B: Environ*. 2022;303:120913.
219. Liu M, Wang JA, Klysubun W, et al. Interfacial electronic structure engineering on molybdenum sulfide for robust dual-pH hydrogen evolution. *Nat Commun*. 2021;12(1):5260.
220. Peng S, Gong F, Li L, et al. Necklace-like multishelled hollow spinel oxides with oxygen vacancies for efficient water electrolysis. *J Am Chem Soc*. 2018;140(42):13644-13653.
221. Sivanantham A, Ganesan P, Shanmugam S. Hierarchical $NiCo_2S_4$ nanowire arrays supported on Ni foam: an efficient and durable bifunctional electrocatalyst for oxygen and hydrogen evolution reactions. *Adv Funct Mater*. 2016;26(26):4661-4672.
222. Shi Q, Liu Q, Ma Y, et al. High-performance trifunctional electrocatalysts based on FeCo/Co_2P hybrid nanoparticles for zinc–air battery and self-powered overall water splitting. *Adv Energy Mater*. 2020;10(10):1903854.
223. Shen Y, Zhou Y, Wang D, Wu X, Li J, Xi J. Nickel-copper alloy encapsulated in graphitic carbon shells as electrocatalysts for hydrogen evolution reaction. *Adv Energy Mater*. 2018;8(2):1701759.
224. McKone JR, Sadtler BF, Werlang CA, Lewis NS, Gray HB. Ni–Mo nanopowders for efficient electrochemical hydrogen evolution. *ACS Catal*. 2013;3(2):166-169.
225. Huang L, Chen D, Luo G, et al. Zirconium-regulation-induced bifunctionality in 3D cobalt-iron oxide nanosheets for overall water splitting. *Adv Mater*. 2019;31(28):1901439.
226. Zhao S, Wang DW, Amal R, Dai L. Carbon-based metal-free catalysts for key reactions involved in energy conversion and storage. *Adv Mater*. 2019;31(9):1801526.
227. Li T, Hu T, Dai L, Li CM. Metal-free photo- and electrocatalysts for hydrogen evolution reaction. *J Mater Chem A*. 2020;8(45):23674-23698.
228. Ito Y, Cong W, Fujita T, Tang Z, Chen M. High catalytic activity of nitrogen and sulfur co-doped nanoporous graphene in the hydrogen evolution reaction. *Angew Chem Int Ed*. 2015;127(7):2159-2164.
229. Hanniet Q, Boussmen M, Bares J, et al. Investigation of polymer-derived Si-(B)-C-N ceramic/reduced graphene oxide composite systems as active catalysts towards the hydrogen evolution reaction. *Sci Rep*. 2020;10(1):22003.
230. Yang M, Zhang Y, Jian J, et al. Donor-acceptor nanocarbon ensembles to boost metal-free all-pH hydrogen evolution catalysis by combined surface and dual electronic modulation. *Angew Chem Int Ed*. 2019;58(45):16217-16222.
231. Xiao F, Chen Z, Wu H, et al. Phytic acid-guided ultra-thin N,P co-doped carbon coated carbon nanotubes for efficient all-pH electrocatalytic hydrogen evolution. *Nanoscale*. 2019;11(47):23027-23034.
232. Gao R, Dai Q, Du F, Yan D, Dai L. C_{60}-adsorbed single-walled carbon nanotubes as metal-free, pH-universal, and multifunctional catalysts for oxygen reduction, oxygen evolution, and hydrogen evolution. *J Am Chem Soc*. 2019;141(29):11658-11666.
233. Zhou J, Qi F, Chen Y, Wang Z, Zheng B, Wang X. CVD-grown three-dimensional sulfur-doped graphene as a binder-free electrocatalytic electrode for highly effective and stable hydrogen evolution reaction. *J Mater Sci*. 2018;53(10):7767-7777.
234. Han G, Hu M, Liu Y, et al. Efficient carbon-based catalyst derived from natural cattail fiber for hydrogen evolution reaction. *J Solid State Chem*. 2019;274:207-214.
235. Tian Y, Mei R, Xue D-Z, Zhang X, Peng W. Enhanced electrocatalytic hydrogen evolution in graphene via defect engineering and heteroatoms Co-doping. *Electrochim Acta*. 2016;219:781-789.
236. Huang S, Meng Y, Cao Y, et al. N-, O- and P-doped hollow carbons: metal-free bifunctional electrocatalysts for hydrogen evolution and oxygen reduction reactions. *Appl Catal B: Environ*. 2019;248:239-248.
237. Chhetri M, Maitra S, Chakraborty H, Waghmare UV, Rao CNR. Superior performance of borocarbonitrides, $B_xC_yN_z$, as stable, low-cost metal-free electrocatalysts for the hydrogen evolution reaction. *Energ Environ Sci*. 2016;9(1):95-101.
238. Tian Y, Ye Y, Wang X, et al. Three-dimensional N-doped, plasma-etched graphene: highly active metal-free catalyst for hydrogen evolution reaction. *Appl Catal A: Gen*. 2017;529:127-133.

239. Jiang H, Gu J, Zheng X, et al. Defect-rich and ultrathin N doped carbon nanosheets as advanced trifunctional metal-free electrocatalysts for the ORR, OER and HER. *Energy Environ Sci*. 2019;12(1):322-333.
240. Jaiswal A, Pal S, Kumar A, Prakash R. Metal free triad from red phosphorous, reduced graphene oxide and graphitic carbon nitride (red P-rGO-g-C_3N_4) as robust electro-catalysts for hydrogen evolution reaction. *Electrochim Acta*. 2020;338:135851.
241. Xu Z, Zhang Q, Li M, et al. One-pot synthesis of multifunctional electrocatalyst for hydrogen evolution, oxygen evolution and oxygen reduction. *ChemCatChem*. 2020;12(21):5534-5539.
242. Zhao Y, Zhao F, Wang X, et al. Graphitic carbon nitride nanoribbons: graphene-assisted formation and synergic function for highly efficient hydrogen evolution. *Angew Chem Int Ed*. 2014;126(50):14154-14159.
243. Duan J, Chen S, Jaroniec M, Qiao SZ. Porous C_3N_4 nanolayers@N-graphene films as catalyst electrodes for highly efficient hydrogen evolution. *ACS Nano*. 2015;9(1):931-940.
244. Shinde SS, Sami A, Lee J-H. Electrocatalytic hydrogen evolution using graphitic carbon nitride coupled with nanoporous graphene co-doped by S and Se. *J Mater Chem A*. 2015;3(24):12810-12819.
245. Odedairo T, Yan X, Gao G, Yao X, du A, Zhu Z. Boosting oxygen reduction and hydrogen evolution at the edge sites of a web-like carbon nanotube-graphene hybrid. *Carbon*. 2016;107:739-746.
246. Zheng Y, Jiao Y, Li LH, et al. Toward design of synergistically active carbon-based catalysts for electrocatalytic hydrogen evolution. *ACS Nano*. 2014;8(5):5090-5296.
247. Liu X, Zhou W, Yang L, et al. Nitrogen and sulfur co-doped porous carbon derived from human hair as highly efficient metal-free electrocatalysts for hydrogen evolution reactions. *J Mater Chem A*. 2015;3(16):8840-8846.

AUTHOR BIOGRAPHIES

Wenfang Zhai received her BS, in School of Materials Science and Engineering from Xi'an Shiyou University in 2014. Now she is a doctoral candidate of Xi'an Jiaotong University, and she is working on bifunctional catalysts for overall water splitting and other new energy applications.

Johnny C. Ho is a professor of Materials Science and Engineering at the City University of Hong Kong. He received his BS degree in chemical engineering and his MS and PhD degrees in materials science and engineering from the University of California, Berkeley, in 2002, 2005, and 2009, respectively. From 2009 to 2010, he was a postdoctoral research fellow in the Nanoscale Synthesis and Characterization Group at Lawrence Livermore National Laboratory. His research interests focus on synthesis, characterization, integration, and device applications of nanoscale materials for various technological applications, including nanoelectronics, sensors, and energy harvesting.

Zhengfei Dai received his PhD from the University of Chinese Academy of Sciences in July 2013. Then, he worked at Korea University, Kyoto University, and Nanyang Technological University as a postdoctoral research fellow. Since December 2017, he joined the School of Material Science and Engineering, Xi'an Jiaotong University as a research professor, and as an adjunct professor of Guilin University of Electronic Technology. His current research interests focus on energy and environmental materials for gas sensors, secondary batteries, and electrocatalysts.

How to cite this article: Zhai W, Ma Y, Chen D, Ho JC, Dai Z, Qu Y. Recent progress on the long-term stability of hydrogen evolution reaction electrocatalysts. *InfoMat*. 2022;4(9):e12357. doi:10.1002/inf2.12357